



Institut für Plasmaphysik

***Automatic reduction of the hydrocarbon  
reaction mechanisms in fusion edge plasmas***

*Alexander Dauwe, Michaël Tytgadt,  
Detlev Reiter, Martine Baelmans*

in collaboration with:

KATHOLIEKE UNIVERSITEIT LEUVEN  
FACULTEIT INGENIEURSWETENSCHAPPEN  
DEPARTEMENT WERKTUIGKUNDE  
AFDELING TOEGEPASTE MECHANICA EN ENERGIECONVERSIE



Promotor :  
Prof. dr. ir. M. Baelmans

TME/2005-2006/06E30

Eindwerk, voorgedragen tot het  
bekomen van de graad van  
Burgerlijk Werktuigkundig-  
Electrotechnisch Ingenieur  
door  
**Alexander Dauwe**  
**Michaël Tytgadt**

Celestijnenlaan 300A  
B-3001 HEVERLEE (BELGIUM)

# Abstract

*For predictions of the tritium inventory in future fusion devices like ITER, the amount of eroded carbon and the hydrogen concentrations in co-deposited hydrocarbon layers have to be predicted quantitatively. Predictions about the locations of co-deposited layers are also necessary in order to design deposition diagnostics and layer removal methods. This requires a detailed physical understanding of the erosion and carbon migration processes, and computer simulations. For accurate simulation the multi-species code EIRENE would require to include over 50 participating species. Because such a calculation is computationally prohibitive current codes are being reduced, typically in an ad hoc fashion. In this work the potential of the mathematically sound method of intrinsic low dimensional manifolds (ILDm) for computational speed-up of the hydrocarbon transport problem simulation is thoroughly investigated. It is basically the Monte Carlo implementation of EIRENE that makes this task so challenging. As the method can substantially ameliorate the results in comparison to the conventional reduction mechanisms a step towards ILDM-reduced kinetics is conceived and tested.*

# Contents

<b>Abstract</b>	<b>iii</b>
<b>Contents</b>	<b>v</b>
<b>List of figures</b>	<b>x</b>
<b>List of tables</b>	<b>xii</b>
<b>Nomenclature</b>	<b>xiv</b>
<b>1 Introduction</b>	<b>1</b>
1.1 Background . . . . .	1
1.2 The problem . . . . .	4
1.3 Proposed solution . . . . .	5
1.4 Outline . . . . .	7
<b>2 Chemistry in the plasma edge</b>	<b>9</b>
2.1 Introduction . . . . .	9
2.2 The hydrocarbon reaction mechanism . . . . .	11
2.2.1 Hydrocarbon reaction channels . . . . .	11
2.2.2 Reaction Rate . . . . .	13
2.2.3 The CH reaction mechanism . . . . .	17
2.2.4 Computational cost of the chemistry in a Monte Carlo code . . . . .	19
2.3 The chemical source term . . . . .	20
2.3.1 Terminology . . . . .	20
2.3.2 The chemical source term of the hydrocarbon reaction mechanism . . . . .	23
2.3.3 Properties of the hydrocarbon Jacobian matrix . . . . .	25
2.3.4 Computational cost of the chemical source term . . . . .	28
2.4 Dynamical response of the hydrocarbon chemistry on perturbations . . . . .	28
2.4.1 Analytical study . . . . .	29
2.4.2 Example . . . . .	30
2.5 Existence of low dimensional manifolds in the composition space . . . . .	32
2.6 Conclusion . . . . .	33
<b>3 Reducing the hydrocarbon reaction mechanism</b>	<b>35</b>
3.1 Introduction . . . . .	35
3.2 Manifold Reduction Technique . . . . .	37

3.2.1	Algebraic equations . . . . .	37
3.2.2	QSSA and ILDM in an analytical example . . . . .	41
3.2.3	The implementation . . . . .	43
3.3	The CH hydrocarbon example . . . . .	46
3.3.1	The QSSA transformation matrix and system . . . . .	46
3.3.2	The ILDM transformation matrix and system . . . . .	47
3.3.3	Illustration of the manifolds . . . . .	47
3.4	Perturbations: projection onto the manifold . . . . .	49
3.4.1	Projection onto the manifold . . . . .	49
3.4.2	Transport as a perturbation of the chemistry . . . . .	51
3.4.3	Example . . . . .	51
3.5	Remarks on the parameters . . . . .	52
3.5.1	The difficulties . . . . .	52
3.5.2	About the choice of the parameter equations . . . . .	53
3.5.3	Non-linear manifold when including the plasma parameters . . . . .	54
3.6	Reducing the Monte Carlo code Eirene . . . . .	55
3.6.1	Localized reaction mechanism . . . . .	55
3.6.2	Strategy for implementation . . . . .	57
3.6.3	Strange effects in the reduced space . . . . .	58
3.7	Conclusion . . . . .	58
<b>4</b>	<b>ADMT Fortran Code</b> . . . . .	<b>61</b>
4.1	Introduction . . . . .	61
4.2	ADMT structure . . . . .	61
4.2.1	Flow chart of the program . . . . .	62
4.2.2	Preprocessing . . . . .	62
4.2.3	Processing . . . . .	63
4.2.4	Postprocessing . . . . .	67
4.3	Validation of ADMT . . . . .	67
4.3.1	Validation of the kinetic coefficients . . . . .	67
4.3.2	Validation of the Jacobian matrix . . . . .	70
4.3.3	Validation of the implicit solvers . . . . .	71
4.3.4	Validation of the reduction techniques . . . . .	73
4.3.5	Validation of the reduction techniques in EIRENE . . . . .	76
4.4	Using ADMT . . . . .	80
4.4.1	Typical Divertor Conditions . . . . .	80
4.4.2	Predicting the results of a closed chemical reactor simulation . . . . .	81
4.4.3	Predicting the results of a plug reactor simulation . . . . .	84
4.5	Conclusion . . . . .	85
<b>5</b>	<b>Results of ADMT</b> . . . . .	<b>87</b>
5.1	Introduction . . . . .	87
5.2	Significance of the Eigenvalues . . . . .	87
5.3	Dimension reduction . . . . .	88
5.4	Stiffness . . . . .	89
5.5	Eigenvalue spectrum . . . . .	91
5.6	Eigenvector analysis . . . . .	93

5.7	Closed chemical reactor . . . . .	94
5.8	Chemical plug reactor . . . . .	96
5.9	Conclusion . . . . .	101
<b>6</b>	<b>Conclusion</b>	<b>103</b>
6.1	Summary . . . . .	103
6.2	Future Work . . . . .	106
	<b>Bibliography</b>	<b>109</b>
<b>A</b>	<b>Comparison ADMT-HYDKIN</b>	<b>111</b>
A.1	The hydrocarbon species . . . . .	111
A.2	Cross Sections . . . . .	112
A.3	Rate Coefficients . . . . .	115
<b>B</b>	<b>Solution methods and stiffness</b>	<b>117</b>
B.1	Numerical solution methods for a system of differential equation . . . . .	117
B.2	Stiffness . . . . .	117

# List of Figures

1.1	Schematic representation of a tokamak reactor JET (2005) and its plasma heating techniques GORISSEN (1995) . . . . .	2
1.2	Divertor configuration and magnetic fields lines . . . . .	3
1.3	Plasma facing plates made of graphite in the divertor FEDERICI et al. (2003)	3
1.4	The transport mechanism of the hydrocarbon particles in the plasma edge . .	4
2.1	Cross sections and rate coefficients of all CH reactions under divertor plasma conditions . . . . .	18
2.2	Cross sections and rate coefficients of all CH <sup>+</sup> reactions under divertor plasma conditions . . . . .	18
2.3	Cross sections and rate coefficients of all C reactions under divertor plasma conditions . . . . .	19
2.4	The time traces of the CH system components. Left: short time behavior, right: long time behavior . . . . .	25
2.5	Left: Dynamical behavior of the concentration of CH <sup>+</sup> for different initial conditions. Right: Dynamical behavior of the perturbations for CH <sup>+</sup> . . . . .	31
2.6	Left: Dynamical behavior of the concentration of CH for different initial conditions. Right: Dynamical behavior of the perturbations for CH . . . . .	31
2.7	Composition curve in a CH-H and a CH <sup>+</sup> -H co-ordinate system for different initial conditions . . . . .	32
3.1	H and C time traces . . . . .	48
3.2	Representation in the composition space (C, CH <sup>+</sup> and CH, $t_{\max} = 1E - 3s$ and the time trace of C up to 2 seconds . . . . .	48
3.3	Representation of the linear manifolds in the C, CH <sup>+</sup> and CH composition space and the orthogonal projection onto the CH <sup>+</sup> – CH plane time is going until 1E-3 s . . . . .	49
3.4	Comparison of the ILDM solution with (left) and without (right) projection for a 1-dimensional plug reactor with a temperature jump in the middle of the domain. More information: see text . . . . .	52
4.1	General flow diagram of ADMT . . . . .	62
4.2	Closed reactor with species up to CH at a plasma temperature of 10eV, a plasma density of 1E13/cm <sup>3</sup> and a species energy of 1eV. Comparison between the solution of the 0D implicit solver and the exact solution for a different number of time-steps . . . . .	72

4.3	Plug reactor with species up to CH at a plasma temperature of $10eV$ , a plasma density of $1E13/cm^3$ and a species energy of $1eV$ . The species move with a constant velocity of $3.8387e5 cm/s$ through a reactor of $19.1935 cm$ . Comparison between the steady state solution of the 1D implicit solver and the scaled exact 0D solution . . . . .	73
4.4	Comparison between the exact and the numerical QSSA solution of the example, for $k_1 = 0.7667/s$ and $k_2 = 3.764/s$ and $\phi_{A0} = 1/cm^3$ . The exact full solution is presented by the dashed lines . . . . .	75
4.5	The QSSA with projection solution of the example, for $k_1 = 0.7667/s$ and $k_2 = 3.764/s$ and $\phi_{A0} = 1/cm^3$ . The exact full solution is presented by the dashed lines . . . . .	75
4.6	Comparison between the exact and the numerical ILDM solution of the example, for $k_1 = 0.7667/s$ and $k_2 = 3.764/s$ and $\phi_{A0} = 1/cm^3$ . The exact full solution is presented by the dashed lines . . . . .	76
4.7	Comparison between the full solution of ADMT and EIRENE, for a plasma temperature of $1eV$ , a plasma density of $1E13/cm^3$ and an influx characterized by a concentration $\phi_{CH}=8.14E10/cm^3$ and a velocity $v=3.8387E5cm/s$ . . . .	77
4.8	Comparison between the QSSA solution of ADMT and EIRENE, for a plasma temperature of $1eV$ , a plasma density of $1E13/cm^3$ and an influx characterized by a concentration $\phi_{CH}=8.14E10/cm^3$ and a velocity $v=3.8387E5cm/s$ . . . .	78
4.9	Comparison between the ILDM solution of ADMT and EIRENE, for a plasma temperature of $1eV$ , a plasma density of $1E13/cm^3$ and an influx characterized by a concentration $\phi_{CH}=8.14E10/cm^3$ and a velocity $v=3.8387E5cm/s$ . . . .	79
4.10	Simulation of the distribution of electron densities in the ITER divertor (REITER and Kotov, 2006) . . . . .	80
4.11	Simulation of the distribution of electron temperature in the ITER divertor (REITER and Kotov, 2006) . . . . .	81
4.12	Time to steady state for plasma conditions $T_{e-}=T_{p+}=E$ and $\phi_{e-}=\phi_{p+}=1E13/cm^3$	82
4.13	Dimension reduction for 5% relative error at a decay time $t_{decay}=1E-5s$ . Left, $\phi_{e-}=\phi_{p+}=1E13/cm^3$ and $E=1eV$ . Right, $T_{p+}=1eV$ , $\phi_{p+}=1E13/cm^3$ and $E=1eV$	83
4.14	Dimension reduction for 5% relative error at a decay time $t_{decay}=1E-6s$ . Left, $\phi_{e-}=\phi_{p+}=1E13/cm^3$ and $E=1eV$ . Right, $T_{p+}=1eV$ , $\phi_{p+}=1E13/cm^3$ and $E=1eV$	83
5.1	Proposed number of fast modes to relax at $T_{p+} = 1eV$ , $\phi_{e-} = \phi_{p+} = 1E13cm^{-3}$ and $E = 1eV$ for 5% error at $\tau = 1E - 05$ . . . . .	88
5.2	Proposed number of fast modes to relax at $T_{p+} = 5eV$ , $\phi_{p+} = 1E14cm^{-3}$ and $E = 1eV$ for 5% error at $\tau = 1E - 07$ or $\tau = 1E - 08$ . . . . .	89
5.3	Stiffness of the full hydrocarbon reaction system in function the temperature of the plasma and the energy of the species, for an electron and proton concentration of $1e13 \frac{1}{cm^3}$ . . . . .	90
5.4	The dependency and grouping of the eigenvalues for plasma concentrations of $1e13 \frac{1}{cm^3}$ . . . . .	90
5.5	Eigenvalue spectrum of the hydrocarbon reaction mechanism, for an electron and proton concentration of $1e13 \frac{1}{cm^3}$ and plasma temperatures being $0.5$ and $3eV$ . . . . .	92
5.6	Eigenvalue spectrum of the hydrocarbon reaction mechanism, for an electron and proton concentration of $1e13 \frac{1}{cm^3}$ . . . . .	92

5.7	Time traces of $\text{CH}_3^+$ and $\text{C}_2\text{H}_3$ for a temperature of 1eV, an energy of 1eV and a background concentration $1e13 \frac{1}{\text{cm}^3}$ . . . . .	95
5.8	Time traces of $\text{C}_2\text{H}_4^+$ and $\text{C}_3\text{H}_8^+$ for a temperature of 1eV, an energy of 1eV and a background concentration $1e13 \frac{1}{\text{cm}^3}$ . . . . .	96
5.9	Left: The spatial behavior of the concentrations of the molecules in the CH-example, for a two cell model, with a temperature jump between both cells from 0.1 to 7 eV. Right: The global concentrations of the molecules of the CH-example for the same conditions. The plasma density is 1E13eV . . . . .	98
5.10	The global concentrations of the molecules of the CH-example for the same conditions, for a two cell model, with a temperature jump between both cells from 0.1 to 7 eV. Left: $L_{\text{Cell}} = 5x_{\text{relax}}$ . Right: $L_{\text{Cell}} = 10x_{\text{relax}}$ . The plasma density is 1E13eV . . . . .	98
5.11	The behavior of the CH-example in a plug reactor with a linear temperature rise, from 8 to 10 eV. The plasma density is 1E13eV . . . . .	99
5.12	The global concentrations of the molecules of the CH-example for the same conditions, for a two cell model, with a linearly increasing temperature from 0.1 to 10 eV. $L_{\text{Grid}} = 10\text{cm}$ and $n_{\text{Cells}} = 19$ . The plasma density is 1E13eV .	100

# List of Tables

1.1	Deuterium-Tritium fusion reaction and its characteristics Wikipedia (2006) . . . . .	2
2.1	The CH reaction scheme, equation types and rate coefficients at $T_{e^-} = T_{p^+} = E = 1eV$ . . . . .	17
2.2	Left eigenvectors corresponding to a 0 eigenvalue for a hydrocarbon system with species up to CH . . . . .	30
2.3	Initial concentrations ( $cm^{-3}$ ) with the same value for the conservation equations . . . . .	31
3.1	The CH reactions and their rates . . . . .	56
4.1	Comparison of the cross sections ( $cm^2$ ) for equation type 5 . . . . .	68
4.2	Comparison of the rate coefficients ( $cm^3/s$ ) for equation type 5 at a species energy $E=0.1eV$ . . . . .	70
4.3	Comparison of the diagonal elements of the Jacobian matrix for a plasma temperature of $1eV$ , a species energy of $1eV$ and a plasma density of $1E13/cm^3$ . . . . .	71
4.4	Exact Full and QSSA solution of the example of RAWLINGS and EKERDT (2004) . . . . .	74
4.5	Implementation of the example of RAWLINGS and EKERDT (2004) in ADMT. The parameters of the reactions are the ones required to calculated the cross sections for reactions of equation type 1 . . . . .	74
4.6	ILDM solution of the example of RAWLINGS and EKERDT (2004) . . . . .	76
5.1	Left eigenvectors of the system at $E_p = E_e = 1eV$ and $E_s = 1eV$ and a plasma concentration of $1e13 \frac{1}{cm^3}$ . . . . .	93
5.2	Jacobian matrices for $T_{pe}=9.420eV$ and $T_{pe}=9.478eV$ , the other background conditions are: $\phi_{pe}=1E13/cm^3$ , $E=1eV$ . Note that the two fastest eigenvalues of the Jacobian matrices cross . . . . .	100
A.1	The 54 species in the hydrocarbon reaction mechanism . . . . .	111
A.2	Comparison of the cross sections ( $cm^2$ ) between ADMT and HYDKIN for equation type 1 . . . . .	112
A.3	Comparison of the cross sections ( $cm^2$ ) between ADMT and HYDKIN for equation type 8 . . . . .	112
A.4	Comparison of the cross sections ( $cm^2$ ) between ADMT and HYDKIN for equation type 5 . . . . .	113
A.5	Comparison of the cross sections ( $cm^2$ ) between ADMT and HYDKIN for equation type 6 . . . . .	113

A.6	Comparison of the cross sections ( $\text{cm}^2$ ) between ADMT and HYDKIN for equation type 2 . . . . .	114
A.7	Comparison of the rate coefficients ( $\text{cm}^3/\text{s}$ ) between ADMT and HYDKIN for equation type 1 . . . . .	115
A.8	Comparison of the rate coefficients ( $\text{cm}^3/\text{s}$ ) for equation type 5 at a species energy $E=0.1\text{eV}$ . . . . .	116
A.9	Comparison of the rate coefficients ( $\text{cm}^3/\text{s}$ ) between ADMT and HYDKIN for equation type 7 . . . . .	116

# Nomenclature

## Latin Letters

ADMT	our program: the initials of our names	-
$E_{\text{pe}}$	plasma energy	J
$\vec{F}$	Chemical source term in the composition space	$\text{s}^{-1}$
$F_{\phi}$	$n_s \times n_s$ Jacobian of the chemical system in the full composition space	$\text{s}^{-1}$
$F'_{\phi}$	$n_s \times n_s$ Jacobian of the reduced chemical system in the full parameter space	$\text{s}^{-1}$
$I_0$	$n_s \times n_s$ dimensional nearly unit matrix	-
ILDMM	Intrinsic Low Dimensional Manifold	-
$m$	dimension of the manifold	-
$n_{\text{reac}}$	dimension of the reaction space	-
$n_c$	number of conservation variables in the Jacobian	-
$n_f$	number of fast timescales to uncouple	-
$n_r$	number of reactions	-
$n_s$	number of species	-
$n_e$	number of elements	-
$\vec{S}$	chemical source term in the state space	-
$P$	$m \times n_s$ dimensional transformation matrix to the reduced parameter space	-
$Q$	$n_f \times n_s$ dimensional matrix containing the reduction equations	-
QSSA	Quasi Steady State Approximation	-
$\vec{r}$	reaction rate vector	$\text{s}^{-1} \text{cm}^{-3}$
$R$	reaction coefficients matrix	-
$T$	$n_s \times n_s$ dimensional transformation matrix to the full parameter space	-
$\vec{u}_i$	eigenvector $i$	-
$U_f^L$	$n_f \times n_s$ matrix containing the fast left eigenvectors	-
$v_{\text{rel}}$	relative collision velocity	$\text{cm s}^{-1}$
$x$	travel length	cm
$x_{\text{mfp}}$	mean free path	cm

## Greek Letters

$\vec{\Gamma}$	physical source term in the state space	-
$\vec{\mu}$	element vector	-
$\vec{\nu}$	reaction vector	-
$\phi_{e^-}$	electron density ( $e^-$ )	$\text{cm}^{-3}$
$\phi_{p^+}$	proton density ( $p^+$ )	$\text{cm}^{-3}$
$\phi_{\text{HC}}$	hydrocarbon density	$\text{cm}^{-3}$
$\phi_{\text{pe}}$	plasma density	$\text{cm}^{-3}$
$\vec{\phi}$	composition vector	$\text{cm}^{-3}$
$\vec{\psi}$	state vector	-
$\langle \sigma v_{\text{rel}} \rangle$	reaction rate coefficient	$\text{s}^{-1}$
$\sigma$	cross section	$\text{cm}^2$
$\vec{\theta}$	parameter vector in the full composition length	$\text{cm}^{-3}$
$\vec{\theta}$	parameter vector with reduced length	$\text{cm}^{-3}$
$\vec{\Xi}$	Transport source term in the composition space	$\text{s}^{-1}$
$\vec{\Xi}'$	On the manifold projected transport source term in the composition space	-
$\vec{\Xi}'$	On the manifold projected transport source term in the parameter space	-

# Chapter 1

## Introduction

This report deals with one of the remaining key design problems for nuclear fusion reactors: the understanding of effects of chemical erosion of high heat flux components of the plasma chamber. This can be of central importance for the availability and maintenance of a future fusion reactor and hence, for example, also be a key parameter determining the cost of electricity from fusion reactors. Specifically: we will be dealing with methods that will allow quantification of transport and chemistry of hydrocarbon molecules in fusion plasmas, which are expected to be released from highly plasma exposed parts of the reactor by so called chemical sputtering. Before describing the particular goal of this report later in this section, let us first briefly summarize the concepts of controlled nuclear fusion research.

### 1.1 Background

The gravitational field of the stars creates the appropriate conditions (“plasma confinement”) in the core to fuse different nuclei together. In the sun, at high densities and temperatures of about 10-15 million Kelvin, hydrogen is converted in this way to helium. Worldwide research programmes are underway to find a way of producing electricity on earth by fusion of deuterium and tritium. The realization of this goal would offer an alternative energy source with significant environmental, safety and supply advantages over the present sources.

Two nuclei lighter than the most stable element iron will release a energy due to the mass defect when melted together. As fusion reactions require to bring two equi-polar ions together, their activation energy is enormous. The Deuterium-Tritium reaction is presently the key candidate process for fusion energy production on earth, because it has comparatively lower activation energy and relatively high probability (reaction cross section). We restrict discussion to this process in the remainder of this report. The concept for a controlled fusion reactor is presented in Table 1.1.

The released neutrons carry 80% of the energy away across the magnetic field lines to the vessel walls and are captured by a lithium blanket outside the vacuum chamber to breed the tritium. The helium ions (the ash of the fusion process) are confined in the plasma and mixed with the fuel (D & T). Three important parameters for the power (stationary burning) or energy (pulsed operation) balance of fusion reactors are:

- Temperature: The activation energy must be available. 100 - 200 million Kelvin
- Density: The density of the fuel ions must be sufficiently large.

- Energy confinement time: ratio of thermal energy in plasma and required input power

They will not be discussed in detail here. But the triple product (“fusion product”) of these three parameters must exceed a certain critical value for a positive power balance of the plasma. This critical value is smallest at plasma temperatures around 10 to 20 keV. In the last 3 decades this achieved value has been doubled about every 1.6 years. Present fusion research is still about a factor 6 away from this goal. More complete information can be found

$$D_{\text{ion}} + T_{\text{ion}} \rightarrow \text{He}_{\text{ion}}^4 + n + 17.6\text{MeV}$$

$\text{He}_{\text{ion}}^4$ :	n:
20% of reaction energy	80% of reaction energy
Magnetically confined	Not confined
Plasma self heating	Energy output and tritium production
3.5 MeV	14.1 MeV
	Radioactive

Table 1.1: Deuterium-Tritium fusion reaction and its characteristics Wikipedia (2006)

on JET (2005) and ITER (2005).

Nowadays the most widespread type of fusion reactor that tries to achieve these requirements is the tokamak. In this toroidal machine the plasma is confined by magnetic fields, which are, in part, generated by large (MAmp) electric current induced in the plasma itself. Basically three different heating techniques are currently used to bring the plasma to fusion conditions. The self heating capacity of the burning plasma by its own plasma current (ohmic heating) is not sufficient. Additionally heating by injection of neutral particle beams or heating by electromagnetic waves are available for plasma heating.

Figure 1.1: Schematic representation of a tokamak reactor JET (2005) and its plasma heating techniques GORISSEN (1995)

Moreover the plasma is isolated by the magnetic fields from the vessel walls, such that it interacts as little as possible with the walls. This “magnetic confinement” reduces convective and conductive heat losses through the vessel and minimizes the release of impurities from the vessel walls back into the plasma. But because the plasma particles collide and cause a displacement of the orbits, the confinement is not perfect and charged particles diffuse across the magnetic field to the plasma edge. This minimal cross field diffusion is typically enhanced significantly by “anomalous” turbulent processes.

Once across the last closed magnetic flux line, the separatrix, plasma flows rapidly (at about ion acoustic speed) along the field lines until the particles are neutralized on a solid structure (“target surface”) that crosses the magnetic field line. This plasma-surface interaction can dislodge impurity atoms from the surface material through a process called sputtering. If no measures are taken, these new ‘neutral’ impurities would first enter the plasma, then be ionized and finally contaminate the plasma. It is thus of primary importance to divert these impurities to a region more remote from the plasma.

### Graphite Divertor

To reduce impurities from reaching the core plasma, a separate structure, called the divertor is often implemented. By additional magnetic fields part of the plasma is systematically diverted away from the central plasmas towards this structure. This is mostly located on the lower part of the tokamak vessel. The hope is to extract or at least control the impurities and meanwhile also to exchange the heat from plasma surface interaction. The divertor is built such that the incoming plasma pushes back the neutral impurities that want to escape back into the main vessel part. Additionally, this neutral gas recycling condition improves the heat load, which

Figure 1.2: Divertor configuration and magnetic fields lines

should be below  $10\text{MW}/\text{m}^2$  for practical reasons. The slow neutral atoms exchange electrons with the hotter ions. The fast atoms can now move unaffected by the magnetic field and dump most of their energy onto the entire divertor surface by thermal conduction. Another way of dissipating the heat to the walls is by locally introducing impurities which will reduce plasma energy by line radiation. Apart from the intrinsic impurities released from the wall (e.g. carbon) noble gases like neon and argon are sometimes deliberately injected for this purpose.

Graphite has often been chosen for the plasma facing components in the divertor for its good thermal properties - good heat conduction, it doesn't melt (it's shape is maintained), high sublimation temperature ( $3825^\circ\text{C}$ ) - . This material can withstand even high transient heat loads beyond the acceptable steady state heat flux.

Figure 1.3: Plasma facing plates made of graphite in the divertor FEDERICI et al. (2003)

### Carbon-deposition and tritium co-deposition

Nevertheless, the major disadvantage of graphite divertor plates, is its rather high erosion rate. In addition to the normal physical sputtering, which is induced by impact of fast ions onto the wall, the carbon plates undergo chemical interaction with the hydrogen ions. This leads to the **formation of hydrocarbons** which are then released into the plasma edge. Erosion itself is not necessarily harmful, because a tokamak is a closed system: It is often exactly where most of the erosion occurs that the plasma flux is the highest. Thus most of the eroded particles come back to the place near where they came from and are redeposited. Ideally we would like to have a local re-deposition probability close to 100% so that the material loss is decreased accordingly. What really happens is that the eroded material is transported over sometimes considerable distances. The erosion, migration and deposition of material in remote areas of the vessel should be understood such that a reliable modelling becomes possible allowing quantitative predictions about the life time of wall components for a given divertor design.

A second, and most serious issue of the graphite divertor plates is the trapping of the radioactive hydrogen isotope tritium in the deposited layers. For example the tritium content of the next step fusion device, the ITER reactor, shouldn't exceed 350g for safety reasons. The carbon set free due to chemical sputtering, or sublimation, is released in form of a wide variety of hydrocarbon species. It is then redeposited at a different location together with the

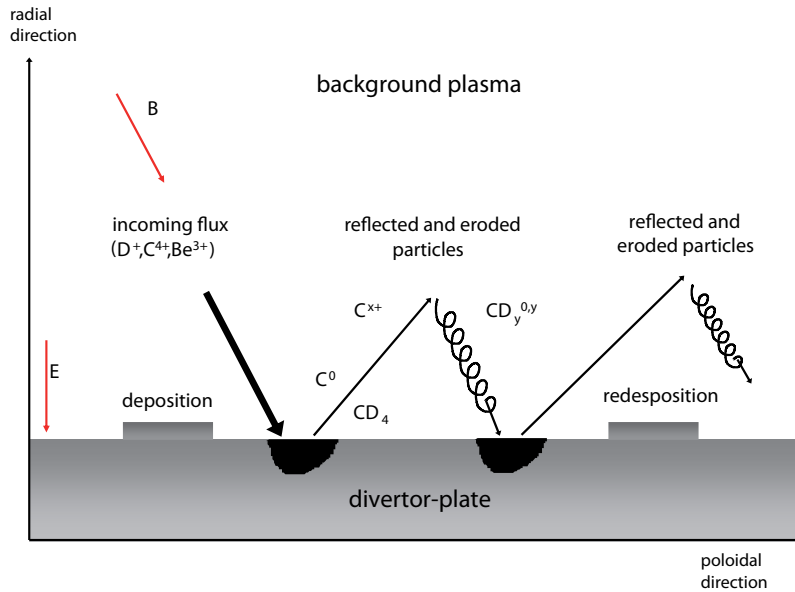


Figure 1.4: The transport mechanism of the hydrocarbon particles in the plasma edge

hydrogen, called co-deposition. In experiments these layers have not only been found in plasma facing components of the machine but also at areas without direct plasma contact. These remote areas can be reached only by the neutral particles and not by the ions, because the particles have to traverse magnetic field lines. Mainly radicals such as  $\text{CH}_3$  and  $\text{C}_2\text{H}_x$  ( $x = 1, 3, 5$ ) seem to contribute to the growth of the hydrocarbon layers. And tritium may be embedded in these poorly accessible layers in intolerable amounts.

Indeed, on JET, operated with tritium, the tritium build up in the machine was found to increase with no sign of saturation. Projecting this finding towards ITER would lead to most pessimistic estimates (between 10 to 200 shots only, before shutdown and tritium removal campaigns) for the operation of ITER. This problem may be so serious as to rule out the use of Carbon, the best known and otherwise most suitable target surface material for fusion. It would be a major setback for fusion research if this problem could not be solved. Before a viable solution can be found, first a quantitative understanding of the basic processes involved is necessary. The present report contributes to this by discussing numerical methods to include efficiently the complex hydrocarbon plasma chemistry into present fusion divertor plasma transport codes.

Alternatives to Carbon have therefore recently gained renewed interest in fusion research. According to a recent article of Samm (SAMM, 2003), Tungsten has a very low erosion rate below its melt temperature of  $3695^\circ\text{C}$ . Therefore, it is a possible alternative for Carbon, if the transient heat loads are limited. Presently it is still very difficult to predict the erosion and deposition processes. A good understanding would lead to better decisions on the optimum use of materials for plasma facing components, but this requires accurate computer simulations.

## 1.2 The problem

The first step towards a good understanding of the hydrocarbon transport processes is a complete inventory of the participating species and the possible reactions as well as the reac-

tion kinetics. A huge amount of experimental and theoretical data about the cross sections, reaction rates and scattering angles have been evaluated, critically assessed and collected by R.K. Janev and D. Reiter. Later the data were fitted into analytical formulas in the reports JANEV and REITER (2002a,b) for further use in computer simulation programs. Also a Monte Carlo transport code, EIRENE (REITER, 2006), was developed by D. Reiter which uses the reaction kinetics database and which combines chemistry and transport by simulating neutral and charged test particles. It also interacts with the plasma simulation code B2 BRAAMS (1986) to provide a full self consistent, two dimensional divertor solution for plasma and gas phase.

EIRENE, until now, can simulate this particle transport and chemistry in the reactor by applying a rather direct Monte Carlo simulation scheme. The computational cost of a Monte Carlo method of solution is difficult to estimate. It scales not only with the number of species and individual collision processes taken into account for the simulation, but is, for example, also strongly influenced by the system size with respect to the collision mean free path, plasma gradients (grid size) and the specific output quantity of interest. Unfortunately at some plasma conditions and geometries, the species of interest are only very seldom produced and it can take days for the Monte Carlo code to get a statistically good prediction of their distribution in the reactor. It would thus be very interesting to reduce the calculation time, without sacrificing accuracy.

There are a number of methods known in literature that achieve this goal by simplifying the reaction kinetics. This present report is discussing these methods and, in particular, for the first time applying the most powerful of these methods, the ILDM method, to the particular problem of hydrocarbon chemistry in fusion divertor plasma conditions.

### 1.3 Proposed solution

In literature a couple of chemistry reduction methods can be found which were developed in combustion science. The main goal of these methods is to reduce the system of differential equations which describes the combustion process. Based on the assumptions that some species are approximated in steady state, hence **Quasi Steady State Approximation**, the oldest of these methods (1906) manages to diminish the number of differential variables. An inconvenience to the method is the necessity of chemical insight in the system. It is the researcher that has to look for potential quasi steady state species, often called radicals in QSSA literature. In the more recent reduction methods it is tried to approach the problem from the more mathematical side. The **Intrinsic Low Dimensional Manifold** method builds, through a spectral decomposition, a subspace defined with fewer variables, called parameters, and on which the reduced solution will evolve. The relation between the parameters and the full state variables is usually tabulated as well as the “effective reaction rates of the parameters”. In this way a solution can be calculated with much less computational effort and simulations can be speeded up. The final goal would be to implement a working ILDM method in the Monte Carlo code EIRENE. It is, at present, not clear if that can ultimately be achieved, because here we are applying the ILDM method, apparently for the first time, to a kinetic problem (Boltzmann equation for distribution both in real and velocity space), whereas all discussions in literature known to us deal with macroscopic (fluid) descriptions of the transport. The kinetic picture is essential for hydrocarbon chemistry in divertors because of the wide range of mean free paths encountered in divertors.

However, the first successful steps have indeed been carried out in this report, and it will also be shown that the current concept employed e.g. by the divertor modelling activities by the international ITER design team to study these processes is obtained as one limiting case of our more general method. Hence we are able at least to provide conditions for the range of validity of the present approach, based on the more general ILDM concept.

The report goes through different subtasks which each achieve partly the main goal:

- Assessment of available literature about chemical (transport) systems and about the different ways to reduce them, including also a comparative study
- A short summary on the Monte Carlo methods, how they work and how they are different from deterministic methods of solution usually applied on chemical systems
- A small program that can simulate a full closed homogeneous chemical system based on the hydrocarbon reaction mechanism database of Janev and Reiter (i.e. neglecting transport). This program has the following features:
  - Ability to read in all the different reactions and the information about the reaction kinetics
  - Automatically recognize the participating species and build a reaction coefficient matrix
  - Calculate the cross sections and reaction rates
  - Build the Jacobian matrix of the system of differential equations
  - Solve this system with an appropriate explicit or implicit method
  - Compare the solution of the program with the one from the HYDKIN program (see: [www.eirene.de](http://www.eirene.de), D. Reiter, B. Küppers, FZ-Jülich) on the internet
- Elaborate the program by incorporating the reduction methods QSSA and ILDM
- Analyse the performance of both methods for different plasma conditions in a closed homogeneous system
  - Show that the methods are correctly implemented and reach the same equilibrium point as the full solution
  - Demonstrate that the accuracy of the ILDM method is higher than the QSSA approach because of its mathematical nature
  - Try to define domains in plasma conditions where a certain reduction can be used for a certain accuracy
- Make a conceptual step towards implementing the ILDM method in a Monte Carlo code: how to interpret the Jacobian of the system

## 1.4 Outline

This section provides an overview about the different chapters of the report.

### **Chapter 2: Collision reaction mechanism and chemical dynamics**

Chapter 2 handles the basic definitions of chemical systems. Starting with a brief explanation on how the database is made up, it is quoted how the Monte Carlo code EIRENE uses the information of the database to simulate the hydrocarbon transport. The reaction scheme is further converted into a system of differential equations which can be solved with a deterministic approach. In this form the properties of the system can quite easily be drawn and it helps to comprehend the dynamical behavior of the system. It should become clear by the end of the chapter that chemical systems contain different lower dimensional subspaces in which the chemical kinetics occur and the conservation of elements are assured. A simple example extracted from the database is used as an illustration for the different concepts introduced here.

### **Chapter 3: Reduction methods and implementation**

In Chapter 3 an overview of the different reduction methods is given. Two of these methods will be worked out more in detail. The reason these two methods were chosen is because one of them, the QSSA technique, is already implemented in EIRENE. The other one, the method of ILDM, is considered to be a more accurate reduction technique. Both are based on the construction of a lower dimensional manifold. Therefore they are exposed together. The appropriate reduction equations are derived in a mathematical way. An analytical example is given for both reduction methods after which a step towards the linear implementation in the deterministic code written for this report, is conceived. The simple hydrocarbon example from Chapter 2 is reviewed and solved with both methods. Next the projection onto the lower dimensional manifold of initial conditions and of the transport term is derived. A section is dedicated to some remarks on the parameter and the manifold projection. To conclude the chapter the implementation in a Monte Carlo code like EIRENE is elaborated.

### **Chapter 4: ADMT-program to investigate the reduction**

Chapter 4 is completely devoted to the ADMT computer program written for the purpose of this report. The program is to some extent identical to the existing Perl code HYDKIN. As it is not yet implemented in EIRENE, HYDKIN also simulates the homogeneous chemistry of the full mechanism. ADMT's structure and functioning is explained at the beginning of the chapter. The correct implementation of the components of ADMT is validated afterwards. This comprises the validation of the integration methods, the calculations of the cross sections and reaction rates, the calculation of the elements in the Jacobian, the reduction methods and the code was compared with an implementation of the reduction methods in EIRENE. To conclude, a section has been added to help the user of ADMT.

### **Chapter 5: Results of the ADMT code for the full reaction mechanism**

The results of certain reductions of the complete reaction mechanism is calculated in Chapter 5. This chapter encloses three sections. The analysis of the Eigenspectrum of the reaction

mechanism offers a good starting point to decide on which dimension reduction to apply. The section about the homogeneous chemical reactor shows the dynamical behavior of certain species, given some initial condition. Many properties of the manifolds can be observed here. The chapter concludes with a model experiment in the form of a chemical plug reactor. This gives the opportunity to test the behavior of grid resolution on the reduction methods.

## Chapter 2

# Chemistry in the plasma edge

### 2.1 Introduction

In the first part of this introduction the origin of the hydrocarbons and the environment in which they react will be discussed. Often these reactions are not so fast, the hydrocarbons are able to travel considerable distances through the plasma edge. For example, the speed of  $\text{CH}_4$  molecules at 0.1 to 1 eV energy is in the range of several  $10^5$  cm/s. The distances to be travelled in a divertor plasma are 1 to 100 cm, hence the transport timescale is  $10^{-3}$  to  $10^{-6}$  sec. For electron densities around  $10^{14}$   $\text{cm}^{-3}$ , plasma temperatures 1 - 10 eV the chemistry timescales for breakup of hydrocarbons are of the order of  $10^{-5}$  to  $10^{-7}$  sec.

This leads to a combined transport-chemistry problem, in which the two aspects cannot be easily separated, at least not for all species involved and not for all relevant plasma conditions.

Most threshold energies for hydrocarbon destruction by electron impact are in the 10 to 15 eV range. The electron temperatures in the near surface area of fusion plasmas can be in the 1 to 30 eV range. Hence, depending upon conditions and details of configuration, the time-scales for these molecular processes can be smaller, comparable and very large compared to the typical transport time scales (free flight of the molecules), all within a single simulation case.

If only a small number of different hydrocarbons and elementary processes is considered, their transport can be directly simulated with the transport codes presented in the second part of this introduction. The goal of this entire work is, therefore, to discuss methods that can reduce a system of many different interacting hydrocarbons and many elementary processes to a model system with fewer “effective species” and “effective processes”. The introduction ends with a motivation and an overview of what will be studied in this chapter.

#### Hydrocarbons in plasma edge

Once the deuterium and the tritium ions from the core plasma cross the separatrix they collide and react with the Carbon wall of the divertor, producing a saturated layer of hydrocarbon isotopes on the carbon wall ( $\text{C}_x\text{D}_y$ ,  $\text{C}_x\text{T}_y$ , and  $\text{C}_x\text{DT}_y$  with  $1 \leq x \leq 3$  and  $1 \leq y \leq 8$ ). As Deuterium (D) and Tritium (T) are hydrogen isotopes they will be replaced by hydrogen (H) in what follows. We do not discuss specific isotope effects in this work, as they are up to now also not treated in the molecular databases used in fusion applications.

The hydrocarbons formed in the wall are then sputtered/released into the divertor region where they undergo subsequent collisions with the plasma electrons and ions, forming a wide

spectrum of  $C_xH_y$  fragments and their ions, with  $0 \leq x' \leq x$  and  $0 \leq y' \leq y$ . Laboratory experiments (JANEV and REITER, 2002a) show that for impact energies typical in a divertor plasma (sub- $eV$  to 10-20  $eV$ ) the main hydrocarbon fluxes into the divertor are due to the chemical sputtering of  $CH_3$ ,  $CH_4$ ,  $C_2H_2$ ,  $C_2H_4$ ,  $C_2H_6$ ,  $C_3H_4$ ,  $C_3H_6$  and  $C_3H_8$ . Inside the divertor but still close to the targets, the plasma temperature ranges from 1-20  $eV$  (from 11605  $^\circ K$  up to 232100  $^\circ K$  closer to the core plasma). Within this temperature range, the hydrocarbon fragmentation to  $C^+$  and  $H^+$  may not be extremely fast, which enables the hydrocarbons to travel through the divertor. Therefore, uncharged hydrocarbons can reach areas that are not influenced by the magnetic field and be deposited there. Indeed, in JET experimental campaigns significant amounts of hydrocarbons have been found in locations without any plasma exposure. To predict which hydrocarbons accumulate in these remote areas and at which rates, simulation codes were developed. To include the hydrocarbon chemistry, these codes require accurate information about the hydrocarbon reaction channels and their rates. In this work the Janev-Reiter reaction database (JANEV and REITER, 2002a,b) is used.

### Modelling

The transport of these hydrocarbons through the divertor can be modelled by two general approaches to numerical modelling, namely the deterministic and the Monte Carlo approach.

**Deterministic codes** are based on a direct numerical interpretation of the system of differential equations built by the reaction mechanism. Such a system can be presented as

$$\begin{aligned} \frac{\partial \vec{\psi}(\vec{r}, t)}{\partial t} &= \vec{S}(\vec{\psi}(\vec{r}, t)) + \vec{\Gamma}(\vec{\psi}(\vec{r}, t), \nabla \vec{\psi}(\vec{r}, t), \Delta \vec{\psi}(\vec{r}, t)) \\ \vec{\psi} &= (T_{e-}, T_{p+}, E, \phi_1, \dots, \phi_{n_s})^T \end{aligned} \quad (2.1)$$

where  $\vec{S}$  represents the rate of change of  $\vec{\psi}$  due to chemical reactions, while  $\vec{\Gamma}$  represents the rate of change due to all other effects such as convection, molecular diffusion etc. The state vector  $\vec{\psi}$  contains the temperature of the plasma particles ( $T_{e-}$ ,  $T_{p+}$ ), the energy of the species ( $E$ ) and the concentrations of both the plasma particles and the hydrocarbons ( $\vec{\phi}$ ).

**A Monte Carlo transport code** simulates the trajectories of thousands of single particles based on stochastic distributions of their travel lengths, their reaction channels and their scattering angles. After this simulation the code averages the residence time of the particles to find the concentrations in the grid cells. A good illustration on how a Monte Carlo transport codes works can be found in an article of Hendricks (HENDRICKS, 1994). It is important to keep in mind the differences with deterministic codes:

MC		Deterministic
single particles	$\leftrightarrow$	concentrations
reaction channels	$\leftrightarrow$	chemical source term $\vec{S}$
travel lengths	$\leftrightarrow$	physical source term $\vec{\Gamma}$

Currently, the transport of the impurity particles (argon, carbon, . . .) through the plasma edge is simulated either by the linear Monte Carlo code EIRENE (REITER, 1995), or by a plasma

fluid model. The EIRENE code uses the plasma edge parameters ( $n_{e^-}$ ,  $n_{p^+}$ ,  $T_{e^-}$  and  $T_{p^+}$ ) given by the deterministic 2-dimensional plasma edge fluid code called B2 (BRAAMS, 1986). Up to now the full hydrocarbon reaction mechanism cannot be included into the EIRENE simulation code because it takes too much time to calculate the entire hydrocarbon chemistry with sufficiently precise statistics. One has to note that on the kinetic level of simulation hydrocarbons alone, up to propane, add 52 species, hence 52 additional 2D or 3D coupled Boltzmann equations, with more than 500 elementary reaction channels to be simulated statistically, in addition to and consistent with the geometrically complex transport in divertor configurations.

### Overview and motivation

As the chemistry of the hydrocarbons takes a huge amount of the computation time on its account, it is useful to disregard the transport and study only the reaction kinetics. In this chapter the chemistry of the 54 hydrocarbon species (including  $e^-$ ,  $p^+$  and up to  $C_3H_8$ ) will be studied in detail. In section 2.2 the hydrocarbon reaction mechanism is discussed by presenting the reaction channels and their corresponding rate equations and by discussing why the mechanism introduces calculation problems in the linear Monte Carlo code EIRENE. As it is our goal to reduce the hydrocarbon reaction mechanism using the ILDM technique, a method which was developed for deterministic transport codes, the chemical source term,  $\vec{S}$  in equation (2.1), will be treated in section 2.3 of this chapter. First it will be build as a function of the state vector ( $\vec{\psi}$ ), then its properties will be presented and finally its computational cost will be discussed. Section 2.4 of this chapter studies the dynamical behavior of the hydrocarbon chemistry on perturbations. We opted to do this analysis in a deterministic way, because the ILDM method was developed for deterministic codes. Before concluding the chapter, an indication of the existence of low dimensional subspaces in the state space will be presented in section 2.5.

## 2.2 The hydrocarbon reaction mechanism

As the hydrocarbons travel through the divertor, they undergo chemical reactions with the background plasma. In section 2.2.1 the different types of reaction channels will be presented. These mechanisms will be categorized on the type of collision partner and on the type of collision reaction. The chance that a collision will happen is related to several factors as the temperature and the density of the background plasma and the energy or velocity of the hydrocarbon. This chance is expressed in cross sections and reaction rates which is the topic of section 2.2.2. Both the reaction channels and their associated chances have been obtained experimentally or by theoretical calculations and are introduced in EIRENE to obtain realistic simulation results. In 2.2.3 a simple example, retrieved from the database, is exposed. This section concludes with a discussion on why the hydrocarbon chemistry is so time consuming in EIRENE.

### 2.2.1 Hydrocarbon reaction channels

Inside the divertor region the concentration of the electrons and the hydrogen ions/protons are a few orders of magnitude higher than the concentration of the impurities<sup>1</sup>. Therefore

---

<sup>1</sup>roughly  $10^2$  and higher

it seems reasonable to assume that the hydrocarbon particles will only interact with the electrons or the protons and not with other hydrocarbons. Based on this assumption Janev and Reiter (JANEV and REITER, 2002a,b) compiled experimentally or theoretically determined individual reaction mechanisms, containing **54 species**, from  $e^-$  up to  $C_3H_8$ , and **706 reaction channels**.

In what follows, first the hydrocarbon-electron and then the hydrocarbon-proton collision reaction channels will be presented. The rate coefficients of these reaction channels will be discussed in the next section.

### Hydrocarbon-electron collision reactions

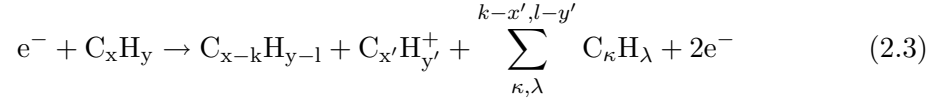
Janev and Reiter divided the electron-impact processes as follows:

Hydrocarbon neutral-electron reactions:

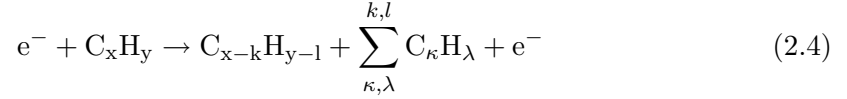
- Direct ionization (I)



- Dissociative ionization (DI)

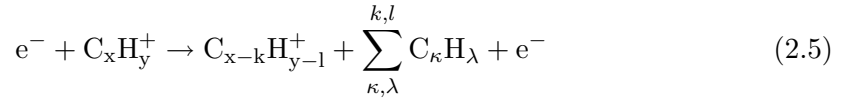


- Dissociative excitation (DE)

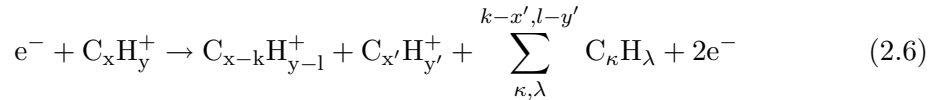


Hydrocarbon ion-electron reactions:

- Dissociative excitation (DE)



- Dissociative ionization (DI)



- Dissociative recombination (DR)

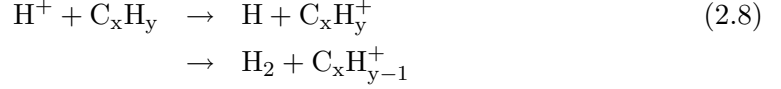


Because each dissociative channel has a different number of products and/or a different type of products, it is impossible to represent all hydrocarbon reactions mathematically. Therefore the summations in equations (2.3)-(2.7) cover all dissociative channels and their boundaries only point out that the C- and H-balance of the reactions is conserved.

### Hydrocarbon-proton collision reactions

Because of the ‘low’ divertor energies and the equal charge, the repulsive force between the hydrocarbon ions and the protons will be strong enough to prevent “chemical” proton-ion collision reactions. Therefore only the neutral hydrocarbons will chemically react with the protons:

- Charge exchange and particle rearrangement (CX)



The first reaction in equation (2.8) represents charge exchange and the second represents particle rearrangement. Elastic processes are not considered in this work, as their effects may be regarded as being part of the transport part of the problem.

### 2.2.2 Reaction Rate

Beside the stoichiometry of the reaction channels, the probability at which they occur is also important in the Monte Carlo code. The code uses these probabilities to select one reaction channel among all the possible ones, each time the particle reacts. The chance that a particle reacts determines its travel length. In this section we will illustrate that the probability at which a reaction occurs is equivalent to the product of the rate coefficient of the reaction with the plasma density and that the probability at which a particle reacts is equivalent to the sum of the probabilities of all possible reactions for that particle.

#### Rate coefficients and probabilities

In the plasma edge, the hydrocarbons are struck by plasma particles with a Maxwellian energy distribution. In this text we will assume that the hydrocarbons have a fixed energy ( $E$ ), their speed being  $V = \sqrt{2E/M}$ , with  $M$  being the mass of the particular hydrocarbon molecule. The frequency at which reaction  $l$  occurs is defined as the Reaction Rate (LAMARSH and BARATTA, 2001):

$$\text{RR}_l \left[ \frac{\# \text{ of times reaction } l \text{ happens}}{\text{sec} \cdot \text{cm}^3} \right] = \langle \sigma v_{\text{rel}} \rangle_l \cdot \phi_{\text{pe}} \cdot \phi_{\text{HC}} \quad (2.9)$$

with  $\phi_{\text{pe}}$  being the density of the reacting plasma particles, which can be either the density of the protons or the electrons,  $\phi_{\text{HC}}$  being the density of the reacting hydrocarbon species,  $\sigma$  being the cross section of reaction  $l$  and  $v_{\text{rel}}$  being the relative speed of the hydrocarbon species and the plasma particle. The **rate coefficient** of reaction  $l$ ,  $\langle \sigma_l v_{\text{rel}} \rangle$ , is the average of the reaction’s cross section over the Maxwellian energy distribution of the plasma particles. Thus, in general the rate coefficient is a non-linear function of the *plasma temperature* and the energy of the reacting hydrocarbon.

Although expression (2.9) can be directly used in deterministic codes, as will be seen in section 2.3.1, it must be adopted when used in a Monte Carlo code. When observing only a single hydrocarbon particle, equation (2.9) changes into:

$$\text{SF}_l \left[ \frac{\# \text{ of times reaction } l \text{ happens}}{\text{sec}} \right] = \langle \sigma v_{\text{rel}} \rangle_l \cdot \phi_{\text{pe}}$$

with  $SF_l$  being the Species collision Frequency for reaction  $l$ , which is the reciprocal of mean time that the reacting hydrocarbon particle has, before it undergoes a reaction of type  $l$ .

The total species collision frequency of that particle is obtained by summing this frequency for all reactions  $l$ , between that hydrocarbon particle and the background particles. If we split up the electron and the proton reactions, the total cross sections found in the database can be used for this purpose. We then obtain something very similar to the total reaction rate for that species which is used later in section 2.3. The total species collision frequency is then given by:

$$\begin{aligned} SF_{\text{total}} &= \sum_{e^- \text{-reacs}} \langle \sigma_l v_{\text{rel}} \rangle \cdot \phi_{e^-} + \sum_{p^+ \text{-reacs}} \langle \sigma_l v_{\text{rel}} \rangle \cdot \phi_{p^+} \\ &= \langle \sigma_{\text{tot},e^-} v_{\text{rel}} \rangle \cdot \phi_{e^-} + \langle \sigma_{\text{tot},p^+} v_{\text{rel}} \rangle \cdot \phi_{p^+} \end{aligned} \quad (2.10)$$

with  $\phi_{e^-}$  and  $\phi_{p^+}$  being the concentration of the electrons and the protons respectively. Together with the speed of the reacting hydrocarbon particle ( $V$ ), the total species collision frequency allows the calculation of the **mean free path** ( $x_{mfp}$ ):

$$x_{mfp} = \frac{V}{SF_{\text{total}}}$$

When running the simulation the travel length  $x$  of each particle is generated in the Monte-Carlo code by picking a random length according to the Poisson distribution. This **probability density function** has the following form:

$$\text{pdf}(x) = x_{mfp}^{-1} \exp\left(-\frac{x}{x_{mfp}}\right)$$

When the hydrocarbon particle has travelled a length  $x$ , the Monte Carlo code generates a random number to select a reaction channel for the particle. The chance that precisely reaction  $l$  is picked, is given by:

$$\text{chance } l = \frac{SF_l}{SF_{\text{total}}} \quad (2.11)$$

The scattering angles and the velocities of the reaction products are generated in a similar way, but are of no importance here, as in later examples all particles are supposed to move in 1-dimension at a constant speed, based on  $E$ .

In what follows first the expressions for the cross sections and the rate coefficients of the hydrocarbon reaction mechanism will be subsequently presented. The formulas correspond to the Janev-Reiter database (JANEV and REITER, 2002a,b).

### Cross Section formulas

For each collision reaction, Janev and Reiter deduced analytic fittings for the cross sections in function of the **plasma energy** ( $E_{pe}$ ), which is the energy of the electrons ( $E_{e^-}$ ) or the energy of the protons ( $E_{p^+}$ ) depending on the collision reaction. They divided the reaction mechanism into 7 groups, based on the physical nature of the process. The numbers of the equation type correspond to the ones used in (JANEV and REITER, 2002a,b):

**Equationtype 1** The cross section of direct and dissociative ionization reactions of neutral hydrocarbons  $\text{CH}_y, y = 0, \dots, 4$ ,  $\text{C}_2\text{H}_y, y = 0, \dots, 6$  and  $\text{C}_3\text{H}_8$  (equations (2.2),(2.3)), are calculated with the following formula in the Janev-Reiter database:

$$\sigma_1 = \frac{10^{-13}}{E_{e^-} \cdot I_c} \left[ A_1 \ln \left( \frac{E_{e^-}}{I_c} \right) + \sum_{j=2}^N A_j \left( 1 - \frac{I_c}{E_{e^-}} \right)^{j-1} \right]$$

with  $A_1, \dots, A_N$  being coefficients and  $I_c$  being the threshold energy depending on the reaction.

**Equationtype 2** The cross section of dissociative ionization reactions of charged hydrocarbons (equation (2.6)) and dissociative excitation reactions of charged and uncharged hydrocarbons (equation (2.4),(2.5)) are calculated with the following formula in the Janev-Reiter database:

$$\sigma_2 = R \cdot p_0 (p_1 + p_2 (y - p_3)) \left( 1 - \frac{E_{th}}{E_{e^-}} \right)^{p_4} \frac{1}{E_{e^-}} \ln (e + p_5 E_{e^-}) \cdot 10^{-16}$$

with  $p_0, \dots, p_5$  being the parameters,  $R$  being the contribution to the total cross sections,  $E_{th}$  being the threshold energy depending on the reaction.

**Equationtype 3** Equationtype 3 is used to calculate the total dissociative recombination cross section of  $\text{C}_x\text{H}_y^+$ , with  $x = 1, 2, 3; y = 1, \dots, 2x + 2$ . The formula for the total cross section is:

$$\sigma_3 = \frac{A}{E_{e^-}^\alpha \cdot (1 + aE_{e^-})^\gamma} \cdot 10^{-16}$$

with  $a, A, \alpha$  and  $\gamma$  being the parameters depending on the  $y$ .

**Equationtype 4** The total cross section of charge exchange and particle rearrangement reactions of neutral hydrocarbons, are calculated with the following formula in the Janev-Reiter database:

$$\sigma_4 = \left( \frac{a_1 e^{-a_2/E_{p^+} + a_3}}{a_4 E_{p^+}^{a_5} + a_6 E_{p^+}^{a_7}} + \frac{b_1 e^{-b_2/E_{p^+} + b_3}}{E_{p^+}^{b_4} + b_5 E_{p^+}^{b_6} + b_7 E_{p^+}^{b_8} + b_9 E_{p^+}^{b_{10}}} \right) \cdot 10^{-16}$$

with  $a_1, \dots, a_7$  and  $b_1, \dots, b_{10}$  being the parameters depending on the reacting hydrocarbon. This expression unifies the different expressions given in the original database into one single formula for all charge exchange processes, with the energy now always consistently given in eV.

**Equationtype 5** The cross section of charge exchange and particle rearrangement reactions of neutral hydrocarbons (equation (2.8)), are calculated with the following formula in the Janev-Reiter database:

$$\begin{aligned} \sigma_{CX}^{(a)} &= \sigma_4 - \sum \sigma_{CX}^{(b)} \\ \sigma_{CX}^{(b)} &= 7.26 \cdot \frac{R_{CX}^{(b)} \cdot K_{CX}^{tot}}{E_{p^+}^{1/2} (1 + \alpha E_{p^+}^\beta)} \cdot 10^{-16} \end{aligned}$$

with the product  $R_{CX}^{(b)} \cdot K_{CX}^{tot}$  representing the thermal particle rearrangement rate coefficient and  $\alpha$  and  $\beta$  being the parameters depending on the reaction. Channel  $a$  is “true” charge exchange, and channel  $b$  is particle rearrangement.

**Equationtype 6** The partial cross section of direct and dissociative recombination reactions of charged hydrocarbons of  $\text{CH}_y^+$ , with  $x = 1, 2, 3; y = 1, \dots, 2x + 2$  (equation (2.7)), are calculated with the following formula in the Janev-Reiter database:

$$\sigma_6 = R_{DR} \cdot \frac{A}{E_{e^-}^{-\alpha} \cdot (1 + aE_{e^-})^\gamma} \cdot 10^{-16}$$

with  $A, a, \alpha$  and  $\gamma$  being the parameters to calculate the total cross section and the branching ratio  $R_{DR}$  being the contribution to the total cross section depending on the reaction.

**Equationtype 7** The equationtype no. 7 was used in the original database for those dissociative recombination processes, for which only fits for rate coefficients but not for the cross sections have been available. In the meantime all missing cross section have been obtained from the rate coefficients by an implicit fitting procedure, so that this equationtype has become redundant. All dissociative recombination processes are now treated by equationtype 3.

**Equationtype 8** The cross section of direct and dissociative ionization reactions of  $\text{C}_3\text{H}_y$ ,  $y = 0 \dots 7$  hydrocarbons (equation (2.2),(2.3)), are calculated with the following formula in the Janev-Reiter database:

$$\sigma_8 = R \cdot 84.0 (a_0 + a_1 y) \cdot \left(1 - \frac{E_{thmin}}{E_{e^-}}\right)^3 \cdot \frac{1}{E_{e^-}} \cdot \ln(e + 0.09E_{e^-}) \cdot 10^{-16}$$

with  $a_0$  and  $a_1$  being parameters,  $R$  being the contribution to the total cross section and  $E_{thmin}$  being the minimal threshold energy based on the dissociative ionization reactions of the same hydrocarbon molecule, depending on the reaction.

### Rate coefficient formulas

Depending on the plasma particles and the hydrocarbon molecules, the rate coefficient  $\langle \sigma v \rangle$  can be determined as follows:

**Electron impact reactions** Because the electrons are so light and consequently usually move very fast, the speed of the hydrocarbon particle can be neglected. The rate coefficient of electron impact reactions is calculated by averaging the cross section of a reaction over the Maxwellian velocity distribution of electrons. For the units  $m_e = 1, k_B = 1, k_B$  being the Boltzmann constant, the formula to calculate the rate coefficient of reaction  $l$  is:

$$\langle \sigma v \rangle_l = \frac{4}{\pi^{1/2} u^3} \int_{v_{th}}^{\infty} v^3 \sigma_l(v) e^{-\frac{v^2}{u^2}} \cdot dv \quad (2.12)$$

where  $u = (2T_{e^-})^{1/2}$ ,  $T_{e^-}$  is the electron temperature,  $v$  is the electron collision velocity and  $v_{th}$  is the velocity corresponding to the threshold energy ( $v_{th} = (2E_{th}^{1/2})$ ) of reaction  $l$ .

**Proton impact reactions** We assume the protons to have a Maxwellian velocity distribution that is characterized by a temperature  $T_{p^+} = m_p u^2/2$  and the hydrocarbons to have certain kinetic energy  $E = MV^2/2$ . The rate coefficient of a charge exchange reaction  $l$  is then defined as:

$$\langle \sigma v \rangle_l = \frac{1}{\pi^{1/2} u V} \int_0^\infty v_{\text{rel}}^2 \sigma_l(v_{\text{rel}}) \left( e^{-\frac{(v_{\text{rel}}-V)^2}{u^2}} - e^{-\frac{(v_{\text{rel}}+V)^2}{u^2}} \right) \cdot dv_{\text{rel}} \quad (2.13)$$

where  $v_{\text{rel}} = |\vec{u} - \vec{V}|$  is the relative collision velocity.

### 2.2.3 The CH reaction mechanism

To illustrate the **reaction channels** together with their cross sections and rate coefficients, a simple example is extracted from the Janev-Reiter database. Only 9 species up to CH are retained as well as the 12 reactions they are involved in. This reaction mechanism will be used throughout this report to clarify the different definitions and theoretical concepts that are introduced. The reaction scheme can be found in table (2.1).

#	Reactions						Eq. Type	$\langle \sigma v \rangle_l$			
1	C	+	e <sup>-</sup>	→	C <sup>+</sup>	+	2e <sup>-</sup>	1-I	1.34E-13		
2	C	+	H <sup>+</sup>	→	C <sup>+</sup>	+	H	5-CXa	1.03E-15		
3	CH <sup>+</sup>	+	e <sup>-</sup>	→	C <sup>+</sup>	+	H	+	e <sup>-</sup>	2-DE	4.03E-12
4	CH <sup>+</sup>	+	e <sup>-</sup>	→	C	+	H <sup>+</sup>	+	e <sup>-</sup>	2-DE	1.01E-21
5	CH <sup>+</sup>	+	e <sup>-</sup>	→	C <sup>+</sup>	+	H <sup>+</sup>	+	2e <sup>-</sup>	2-DI	1.67E-08
6	CH <sup>+</sup>	+	e <sup>-</sup>	→	C	+	H			6-DR	5.14E-11
7	CH	+	e <sup>-</sup>	→	C	+	H	+	e <sup>-</sup>	2-DE	1.94E-11
8	CH	+	e <sup>-</sup>	→	CH <sup>+</sup>	+	2e <sup>-</sup>			1-I	7.67E-14
9	CH	+	e <sup>-</sup>	→	C <sup>+</sup>	+	H	+	2e <sup>-</sup>	1-DI	2.05E-16
10	CH	+	e <sup>-</sup>	→	C	+	H <sup>+</sup>	+	2e <sup>-</sup>	1-DI	7.71E-18
11	CH	+	H <sup>+</sup>	→	CH <sup>+</sup>	+	H			5-CXa	6.58E-10
12	CH	+	H <sup>+</sup>	→	C <sup>+</sup>	+	H <sub>2</sub>			5-CXb	6.20E-10

Table 2.1: The CH reaction scheme, equation types and rate coefficients at  $T_{e^-} = T_{p^+} = E = 1\text{eV}$

The behavior of the **cross sections and the rate coefficients** as function of the plasma energy and the plasma temperature is plotted in figures 2.1 to 2.3 for all reactions of respectively CH, CH<sup>+</sup> and C. As the reaction database does not contain reactions with the background plasma for the other species, these species are only formed by the presented reactions. In figures 2.1 to 2.3 the energy of the hydrocarbon species equals  $E = 1\text{eV}$ . The cross sections and reaction rates are plotted for equal proton and electron energy ( $E_{\text{pe}} = E_{e^-} = E_{p^+}$ ) and temperature ( $T_{\text{pe}} = T_{e^-} = T_{p^+}$ ), respectively.

Because the cross section of a reaction is equivalent to the chance that the reaction will happen if stationary C, CH or CH<sup>+</sup> are struck by a mono-energetic beam of plasma particles (energy of the beam =  $E_{\text{pe}}$ ) (LAMARSH and BARATTA, 2001), one can see that at low plasma energies only charge exchange reactions (CX) will occur for CH and C (figures 2.1 and 2.3 left) and only dissociative recombination reactions (DR) for CH<sup>+</sup> (figure 2.2 left). As the energy rises above the threshold energies, also the other reactions start contributing to

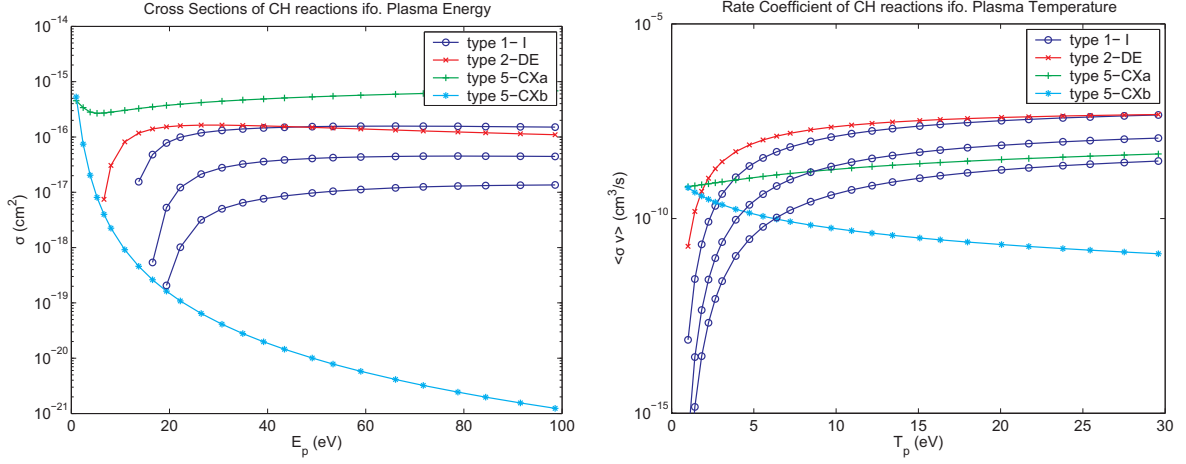


Figure 2.1: Cross sections and rate coefficients of all CH reactions under divertor plasma conditions

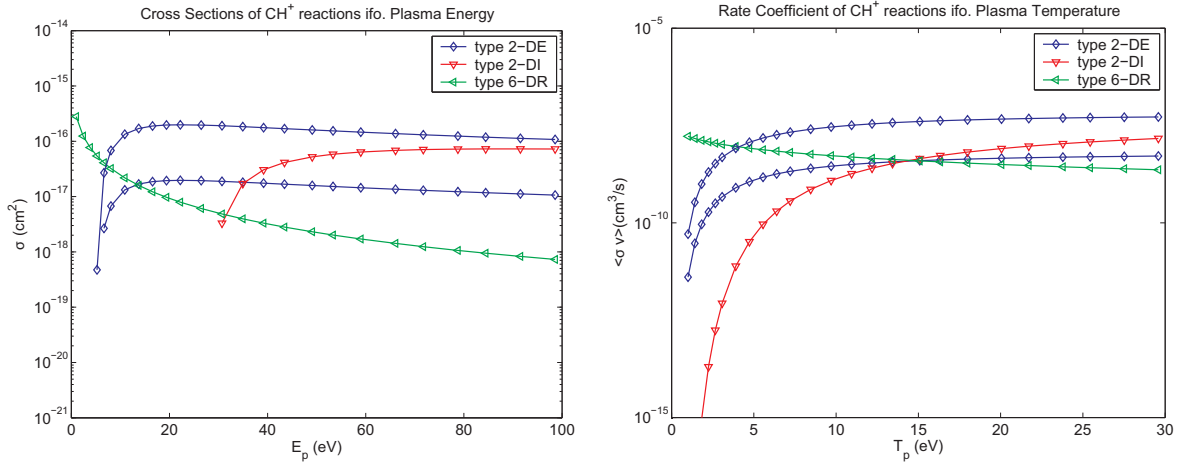


Figure 2.2: Cross sections and rate coefficients of all  $\text{CH}^+$  reactions under divertor plasma conditions

the total cross section of C, CH and  $\text{CH}^+$ . At high plasma energies CX reactions of type b for CH and DR reactions for  $\text{CH}^+$  lose their importance.

Averaging the product of the cross section and the relative speed over the Maxwellian energy distribution of the plasma, the rate coefficients of the C, the CH and the  $\text{CH}^+$  reactions are obtained. In contrast to cross sections, rate coefficients are never zero, because they are averages. The same reactions as for the cross sections contribute to the total reaction rate in the different ranges of plasma temperatures. To conclude which one of the species C, CH or  $\text{CH}^+$ , will collide and react faster, the sum of the product of the rate coefficients with the plasma density must be made for each species as in equation (2.10). Using this knowledge and figures 2.1 to 2.3, it is easy to see that the C-reactions are much slower, especially at low temperatures.

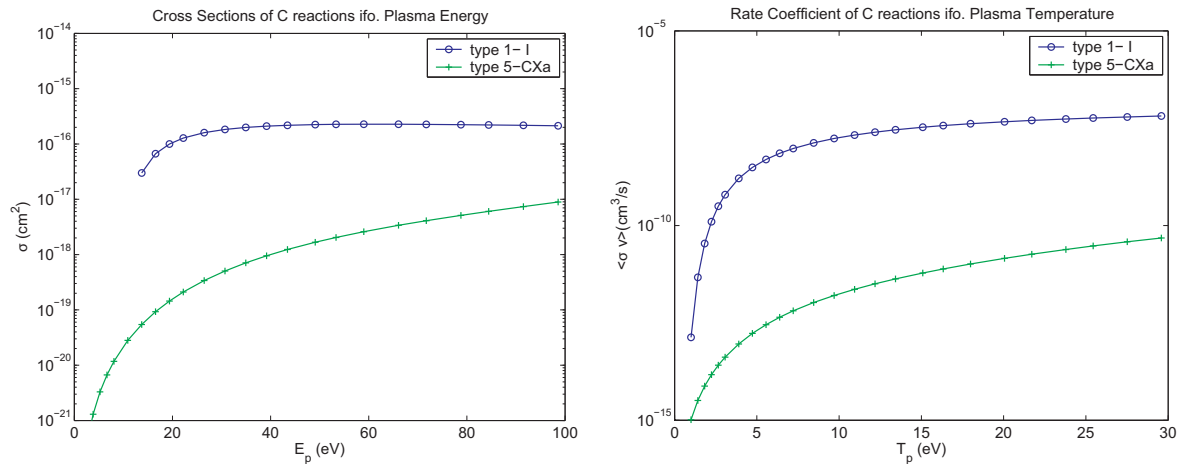


Figure 2.3: Cross sections and rate coefficients of all C reactions under divertor plasma conditions

## 2.2.4 Computational cost of the chemistry in a Monte Carlo code

In a direct Monte Carlo simulation of particle transport and chemistry each individual process is simulated with random numbers, and the particle trajectories are computed from the birth-place (e.g. the divertor target surfaces) until either the trajectory escapes from the system (pumping entrance) or is finally absorbed by the plasma: in our case for example: ionization of the final products C and H into the main plasma components  $C^+$  and  $H^+$ .

The computational cost of a Monte Carlo code is determined by the statistical noise level achieved in a given computing time. Excluding overhead for pre- and post processing the product of statistical variance  $\sigma^2$  and cpu-time is a constant.

It is obvious that the numerical value for this figure of merit depends sensitively on a large number of parameters, such as:

- geometrical complexity of algorithm, grid size,
- complexity of trajectories (long vs. short trajectories, many vs. few collisions per trajectory)
- method of estimating the mean values from particle trajectories (counting collisions or counting flight distances)
- number of non-zero contributions to the final estimates (frequent vs. rare events)
- number of species which interact with each other
- number of individual collision processes to be simulated.

The goal of the present work is to discuss approximate procedures to reduce the number of species and of individual collision processes, which achieve a maximum reduction at a minimum loss of accuracy. The principle of such a model reduction has been already studied with the EIRENE code in a first proto-typical test application. As will be shown below in this (very simple) case a drastic improvement has been achieved, namely by resulting in a Monte Carlo procedure without any statistical noise: the ILDM procedure results here in a

method, in which all test particles give exactly identical contributions to the final result, and this result coincides with the analytical solution. All the labor went into setting up the ILDM equations, and nothing was left for the Monte Carlo procedure. Of course this is only a proof of principle, and more realistic models, with a more complex geometry and collision kinetics, will reduce the Monte Carlo cost only by a finite amount. But still significant savings can be expected even in more complex model situations.

## 2.3 The chemical source term

In combustion science, mechanism reduction methods have been developed to reduce the general deterministic reactive transport equation, presented in equation (2.1). These methods will be thoroughly explained in chapter 3, but we can already say that all techniques are based on a study of the chemical source term  $\vec{S}$  to reduce the whole transport equation. Before adapting the existing methods to work in the Monte Carlo code, we first want to examine the potential of these methods for the specific reactions under investigation. Therefore these methods are applied to a deterministic model of the hydrocarbon reaction system.

In the first part of this section three concepts will be explained. First the independent variables of the chemical source term will be gathered in the *state vector*. Then the reaction channels and their rates will be grouped in a constant *reaction coefficient matrix* and in a *reaction rate vector* respectively. In the second part of this section the chemical source term of the hydrocarbon reaction mechanism will be constructed. Depending on the other processes present in the system, the chemistry can be fully represented either in the state space, the composition space or in the reaction space. In the composition space, the properties specific to the hydrocarbon reaction mechanism allow the chemical source term to be linearized. This section is concluded by discussing the calculation cost of the hydrocarbon chemical source term.

### 2.3.1 Terminology

#### State vector

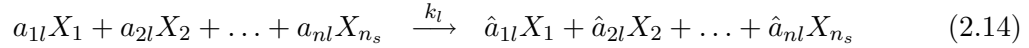
Macroscopically the state of a chemical mixture is normally represented by 2 intensive variables (e.g.  $T$  and  $p$  of the mixture) and the concentration of the species which defines the composition. In the case of the hydrocarbon system it is a little more tricky. The plasma parameters: electron temperature  $T_{e^-}$ , proton temperature  $T_{p^+}$ , electron densities  $\phi_{e^-}$  and proton density  $\phi_{p^+}$  have to be looked at as macroscopic variables while the energies of the hydrocarbons are to be treated microscopically. For simplicity we assume that all hydrocarbons have the same energy  $E$ . The macroscopic approach now requires to work with the density ( $\phi_i$ ) of a certain hydrocarbon instead of considering just one particle. The state of the chemical hydrocarbon mixture will be represented in the state space vector:

$$\vec{\psi} = (T_{e^-}, T_{p^+}, E, \phi_1, \dots, \phi_{n_s})^T$$

where  $(\phi_1, \dots, \phi_{n_s}) = (\phi_{e^-}, \phi_{p^+}, \phi_3, \dots, \phi_{n_s}) = \vec{\phi}$  is the local composition of the mixture. For the full hydrocarbon system, the dimension of the **state space** is  $54 + 3 = 57$ , being the number of species involved in the full system plus the temperature of the electrons, the protons and the energy of the hydrocarbon particle. The unit of this vector is eV for the first three components and  $\frac{\#\text{particles}}{\text{cm}^3}$  for the others.

### Reaction coefficient matrix

The chemical reactions of the database can be represented by a vector, called the **reaction vector**. Say a chemical reaction  $l$  has species  $X_i$  and stoichiometric coefficients  $a_{il}, \hat{a}_{il}$ :



$$\sum_{i=1}^{n_s} (\hat{a}_{il} - a_{il})X_i = 0 \quad (2.15)$$

with  $\nu_{il} = a_{il} - \hat{a}_{il}$  being the reaction coefficient of species  $i$  for reaction  $l$  and  $n_r$  being the number of reactions. The reaction vector of reaction  $l$  is now defined as:  $\vec{\nu}_l = (\nu_{1l}, \nu_{2l}, \dots, \nu_{nl})^T$ . The vectors for all reaction channels can be assembled in the dimensionless **reaction matrix**  $R$ :

$$R = \begin{pmatrix} | & | & & | \\ \vec{\nu}_1 & \vec{\nu}_2 & \dots & \vec{\nu}_{n_r} \\ | & | & & | \end{pmatrix} \quad (2.16)$$

It is obvious that  $R$  is constant and independent from  $T_{e^-}, T_{p^+}, E, \phi_{e^-}, \phi_{p^+}$  because it arises directly from the reaction stoichiometry. For the full hydrocarbon reaction mechanism  $R$  is a  $n_s \times n_r = 54 \times 706$  matrix, with 51 being the highest possible rank because all reactions conserve mass (H- and C-atoms) and charge ( $e^-$ ). This can be mathematically checked with the help of the element vectors which will later appear to be conservation equations. Let  $\mu_{ji}$  be the number of atoms of element  $j$  in the species  $i$ . The element vector of element  $j$  is then written as

$$\vec{\mu}_j = (\mu_{j1}, \mu_{j2}, \dots, \mu_{jn})^T \quad (2.17)$$

for example in the complete chemical system:

	$e^-$	$H^+$	$\dots$	$C_3H_8$		$e^-$	$H^+$	$\dots$	$C_3H_8^+$	$C_3H_8$
$C$	$\mu_{1,1}$	$\mu_{1,2}$	$\dots$	$\mu_{1,54}$	$C$	0	0	$\dots$	3	3
$H$	$\mu_{2,1}$	$\mu_{2,2}$	$\dots$	$\mu_{2,54}$	$H$	0	1	$\dots$	8	8
$Charge$	$\mu_{3,1}$	$\mu_{3,2}$	$\dots$	$\mu_{3,54}$	$Charge$	-1	1	$\dots$	1	0

For simplicity of writing and because charge is also conserved by the chemical reactions we consider the charge to be an element. Therefore the hydrocarbon reaction mechanism has three elements, namely the H-atom, the C-atom and charge. Because elements are neither formed nor destroyed by chemical reactions, their numbers must stay equal before and after the reaction has occurred. Mathematically this means that the element vectors and the reaction vectors are orthogonal (scalar product is zero):

$$\vec{\nu}_l \cdot \vec{\mu}_j^T = \vec{\mu}_j \cdot \vec{\nu}_l^T = 0 \quad \text{for} \quad l = 1, \dots, n_r \quad j = 1, \dots, n_e$$

These mathematical relationships did not only help to identify some errors in the original reaction text files, which have now been removed, but they also demonstrate that the dimension of the chemical dynamics can be lowered with 3.

### Reaction rate vector

The **reaction rate coefficient**  $k_l$  in (2.14) is usually a function of the intensive parameters pressure and temperature as widely found in literature under the name Arrhenius equation.

It is applicable for rather narrow temperature ranges. However here this coefficient is calculated as described in section 2.2, because of the typically much wider temperature range in fusion plasma applications. Similar to combustion science the reaction rate coefficient for the hydrocarbon reactions is defined as a non-linear function of the plasma temperature and the energy of the colliding hydrocarbon. To obtain the **reaction rate** the coefficient still has to be multiplied with the density of the reactants ( $\phi_{\text{pr}}$  and  $\phi_{\text{HC}}$ ). For the total reaction mechanism up to  $\text{C}_3\text{H}_8$  the reaction rate vector groups all the rates into a vector of size  $n_r = 706$ . The units of this vector are  $\frac{\#\text{reactions}}{\text{cm}^3\text{s}}$

$$\vec{r} = \begin{pmatrix} \langle \sigma v \rangle_1 \cdot (\phi_{\text{pe}} \cdot \phi_{\text{HC}})_1 \\ \langle \sigma v \rangle_2 \cdot (\phi_{\text{pe}} \cdot \phi_{\text{HC}})_2 \\ \vdots \\ \langle \sigma v \rangle_{n_r} \cdot (\phi_{\text{pe}} \cdot \phi_{\text{HC}})_{n_r} \end{pmatrix}$$

### Example for the CH reaction scheme

The reaction matrix and the reaction rate vector for the CH reaction scheme, see table 2.1, are presented below.

$$R = \begin{pmatrix} 1 & 0 & 0 & 0 & 1 & -1 & 0 & 1 & 1 & 1 & 0 & 0 \\ 0 & -1 & 0 & 1 & 1 & 0 & 0 & 0 & 0 & 1 & -1 & -1 \\ 0 & 1 & 1 & 0 & 0 & 1 & 1 & 0 & 1 & 0 & 1 & 0 \\ 0 & 0 & 0 & 0 & 0 & 0 & 0 & 0 & 0 & 0 & 0 & 0 \\ 0 & 0 & 0 & 0 & 0 & 0 & 0 & 0 & 0 & 0 & 0 & 1 \\ 1 & 1 & 1 & 0 & 1 & 0 & 0 & 0 & 1 & 0 & 0 & 1 \\ -1 & -1 & 0 & 1 & 0 & 1 & 1 & 0 & 0 & 1 & 0 & 0 \\ 0 & 0 & -1 & -1 & -1 & -1 & 0 & 1 & 0 & 0 & 1 & 0 \\ 0 & 0 & 0 & 0 & 0 & 0 & -1 & -1 & -1 & -1 & -1 & -1 \end{pmatrix} \quad \text{and} \quad \vec{r} = \begin{pmatrix} 1,34E+00 \\ 1,03E-02 \\ 4,03E+01 \\ 1,01E-08 \\ 1,67E+05 \\ 5,14E+02 \\ 7,67E-01 \\ 2,05E-03 \\ 7,71E-05 \\ 1,94E+02 \\ 6,58E+03 \\ 6,20E+03 \\ 2,05E-03 \\ 7,71E-05 \end{pmatrix}$$

The dimension of  $\vec{r}$  is  $\left[ \frac{\#\text{reactions}}{\text{cm}^3\text{s}} \right]$ . As the reaction rates are non-linearly dependent on the state of the mixture they have to be evaluated in a point of the state space. For the reaction rates above the following values were chosen:

$$\vec{\psi}_0 = (T_{e^-}, T_{p^+}, E, \phi_{e^-}, \phi_{H^+}, \phi_H, \phi_{H_2^+}, \phi_{H_2}, \phi_{C^+}, \phi_C, \phi_{CH^+}, \phi_{CH})^T$$

$$\vec{\psi}_0 = (1\text{eV}, 1\text{eV}, 1\text{eV}, 1\text{e}13/\text{cm}^3, 1\text{e}13/\text{cm}^3, 1/\text{cm}^3, 1/\text{cm}^3, 1/\text{cm}^3, 1/\text{cm}^3, 1/\text{cm}^3, 1/\text{cm}^3, 1/\text{cm}^3)^T$$

Due to the linearity of this particular reaction scheme (no collisions amongst the hydrocarbons themselves) the choice of the last 7 entries in this vector is irrelevant. The first 5 entries have to be set to physically meaningful values, however.

It is clear also that multiplying the reaction vectors found in the columns of the reaction matrix above, with the element vectors presented below gives always zero.

	$e^-$	$H^+$	H	$H_2^+$	$H_2$	$C^+$	C	$CH^+$	CH	
$e^-$	( 1	-1	0	-1	0	-1	0	-1	0	) <sup>T</sup>
H	( 0	1	1	2	2	0	0	0	0	) <sup>T</sup>
C	( 0	0	0	0	0	1	1	1	1	) <sup>T</sup>

### 2.3.2 The chemical source term of the hydrocarbon reaction mechanism

As we are primarily interested in the chemistry of the reactions we choose to model an isothermal ( $T_{e^-}$  and  $T_{p^+}$  are constant) and iso-energetic ( $E$  is constant) system. In this closed homogeneous system it is possible to study the effect of chemistry, because only the chemical reactions can change the state of the system. In the first part of this section the homogenous system will be presented mathematically, then the non-linear effect of the chemical reactions will be elaborated. To conclude we will show that it is in our case reasonable to linearize the hydrocarbon system around the point  $\vec{\psi} = (T_{e^-}, T_{p^+}, E, \phi_{e^-}, \phi_{p^+}, 0, \dots, 0)$  to study its behavior.

#### Homogeneous chemical system and its composition space

If only chemistry influences movements in the state space, the transport equation (2.1) becomes:

$$\frac{\partial \vec{\psi}(t)}{\partial t} = \vec{S}(\vec{\psi}(t))$$

In an isothermal and iso-energetic system  $\vec{S}(\vec{\psi}(t))$  is specified by:

$$\begin{aligned} \frac{\partial T_{e^-}}{\partial t} &= 0 \\ \frac{\partial T_{p^+}}{\partial t} &= 0 \\ \frac{\partial E}{\partial t} &= 0 \\ \frac{\partial \vec{\phi}}{\partial t} &= \vec{F}(T_{e^-}, T_{p^+}, E, \vec{\phi}) \end{aligned} \quad (2.18)$$

In this equation  $T_{e^-}$ ,  $T_{p^+}$  and  $E$  are conserved variables and they can be determined by the initial conditions,  $T_{e^-0}$ ,  $T_{p^+0}$  and  $E_0$ . This system is called a homogeneous chemical system. We introduce a new source term here.  $\vec{F}$  is a  $n_s$  dimensional vector function of the state vector that represents the changes in composition due to the chemical reactions. It exactly contains the lower  $n_s$  components of  $\vec{S}$ . From now on to study only the isothermal, iso-energetic homogeneous closed system we will disregard the  $T_{e^-}$ ,  $T_{p^+}$  and  $E$  dependency of  $\vec{F}$  and it will be only dependent on the **composition vector**  $\vec{\phi}$ . So we write:  $\vec{F}(\vec{\phi})$ . The transport  $\vec{\Gamma}$  also has a counterpart in the composition space. We call it  $\vec{\Xi}$ .

#### Species production rate

The most general form of the source term from which (2.9) was derived, is given below. The species production rate for a homogeneous chemical system (2.14) is:

$$\frac{\partial \phi_i}{\partial t} = \sum_{l=1}^{n_r} \nu_{il} \langle \sigma v \rangle_l \prod_{j_l} (\phi_j)^{a_j}$$

$j_l$  covers all indices of the reactants of reaction  $l$ . Since we are dealing with collisions between only two particles the exponents  $a_j$  being the left side reaction coefficient of species  $j$  have

been found to be always 1. Moreover only 2 factors arise from the product sign. The chemical source term is thus best represented as:

$$\frac{\partial \vec{\phi}}{\partial t} = \vec{F}(\vec{\phi}) = \sum_{l=1}^{n_r} \vec{\nu}_l \langle \sigma v \rangle_l \phi_{\text{pe}} \phi_{\text{HC}} \equiv R \vec{r} \quad (2.19)$$

The indices **pe** (proton or electron) and **HC** (HydroCarbon) refer respectively to the plasma and the hydrocarbon particle involved in the collision reaction  $l$ .

Equation (2.19) is the **general non-linear homogeneous chemical system** of the hydrocarbon reaction mechanism that has to be solved by the deterministic code. We will now show that this system can be further simplified.

### Linearizing the homogeneous system

The source term (2.19) is dependent only on the product of two species concentrations. If we had considered the non-homogeneous system it also would have been dependent on the rate coefficient (thus on  $T_{e^-}$ ,  $T_{p^+}$ ,  $E$ ). One could simply extrapolate for the other case himself. The concentration of the electrons and the protons inside the divertor is usually at least 2 orders of magnitude higher than the concentration of the hydrocarbons ( $\phi_{e^-}$  and  $\phi_{p^+} \gg \mathbf{N}_i$ ), the influence of the collision reaction channels on the concentration of the plasma is negligible and the plasma concentration can be supposed constant. Therefore it is reasonable to **linearize** equation (2.19) **around** the point  $\vec{\phi}_0 = (\phi_{e^-}, \phi_{p^+}, \mathbf{0}, \dots, \mathbf{0})^T$ :

$$\frac{\partial \vec{\phi}}{\partial t} = \vec{F}(\vec{\phi}_0) + F_{\vec{\phi}}|_{\vec{\phi}_0} (\vec{\phi} - \vec{\phi}_0) + O((\vec{\phi} - \vec{\phi}_0)^2) \quad (2.20)$$

with  $F_{\vec{\phi}}|_{\vec{\phi}_0}$  being the Jacobian of equation (2.19) evaluated in the point  $\vec{\phi}_0$ . The Jacobian is defined as:

$$F_{\vec{\phi}} = \begin{pmatrix} \frac{\partial F_1}{\partial \phi_1} & \frac{\partial F_1}{\partial \phi_2} & \dots & \frac{\partial F_1}{\partial \phi_{n_s}} \\ \frac{\partial F_2}{\partial \phi_1} & \frac{\partial F_2}{\partial \phi_2} & \dots & \frac{\partial F_2}{\partial \phi_{n_s}} \\ \vdots & \vdots & \ddots & \vdots \\ \frac{\partial F_{n_s}}{\partial \phi_1} & \frac{\partial F_{n_s}}{\partial \phi_2} & \dots & \frac{\partial F_{n_s}}{\partial \phi_{n_s}} \end{pmatrix} \quad (2.21)$$

Linearizing equation (2.19) around the point  $\vec{\phi}_0$  has important consequences on the system that we are going to use. It can be checked that in  $\vec{\phi}_0$ :

$$\vec{F}(\vec{\phi}_0) = \vec{0} \quad (2.22)$$

$$F_{\vec{\phi}}|_{\vec{\phi}_0} \vec{\phi}_0 = \vec{0} \quad (2.23)$$

Substitution in equation (2.20) leads to the following equation system for the **chemical source term** of the isothermal and iso-energetic homogenous **hydrocarbon system**:

$$\boxed{\frac{\partial}{\partial t}(\vec{\phi}) = F_{\vec{\phi}}|_{\vec{\phi}_0} \vec{\phi}} \quad (2.24)$$

### The chemical source term of the CH-example

The chemical behavior of the CH system can be modelled by the following system of linear differential equation:

$$\begin{pmatrix} \partial[e^-]/\partial t \\ \partial[H^+]/\partial t \\ \partial[H]/\partial t \\ \partial[H_2^+]/\partial t \\ \partial[H_2]/\partial t \\ \partial[C^+]/\partial t \\ \partial[C]/\partial t \\ \partial[CH^+]/\partial t \\ \partial[CH]/\partial t \end{pmatrix} = \begin{pmatrix} 0 & 0 & 0 & 0 & 0 & 0 & 1.34E+00 & -1.67E+05 & 7.69E-01 \\ 0 & 0 & 0 & 0 & 0 & 0 & -1.03E-02 & 5.14E+02 & -1.28E+04 \\ 0 & 0 & 0 & 0 & 0 & 0 & 1.03E-02 & 1.67E+05 & 6.78E+03 \\ 0 & 0 & 0 & 0 & 0 & 0 & 0 & 0 & 0 \\ 0 & 0 & 0 & 0 & 0 & 0 & 0 & 0 & 6.20E+03 \\ 0 & 0 & 0 & 0 & 0 & 0 & 1.35E+00 & 4.03E+01 & 6.20E+03 \\ 0 & 0 & 0 & 0 & 0 & 0 & -1.35E+00 & 1.68E+05 & 1.94E+02 \\ 0 & 0 & 0 & 0 & 0 & 0 & 0 & -1.68E+05 & 6.58E+03 \\ 0 & 0 & 0 & 0 & 0 & 0 & 0 & 0 & -1.30E+04 \end{pmatrix} \begin{pmatrix} [e^-] \\ [H^+] \\ [H] \\ [H_2^+] \\ [H_2] \\ [C^+] \\ [C] \\ [CH^+] \\ [CH] \end{pmatrix} \quad (2.25)$$

Remember this system was linearized around the point  $\psi_0 = (T_{e^-}, T_{e^-}, E, \phi_{e^-}, \phi_{p^+}, 0, \dots, 0)^T = (1eV, 1eV, 1eV, 1e13/cm^3, 1e13/cm^3, 0, \dots, 0)^T$ .

The solution of this system is presented in figure 2.4. It should be noted that at a plasma temperature of 1eV, as considered in this example, the evolution of C and C<sup>+</sup> is much slower than the evolution of the other species. This is a consequence of the small rate coefficients of the C-reactions at this temperature, which can be seen in figure 2.3.

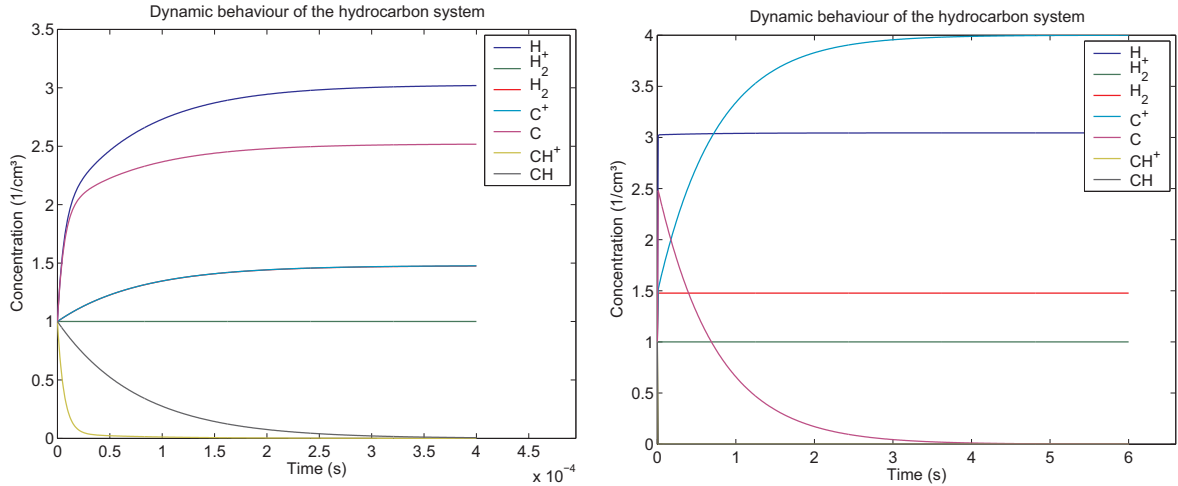


Figure 2.4: The time traces of the CH system components. Left: short time behavior, right: long time behavior

### 2.3.3 Properties of the hydrocarbon Jacobian matrix

As can be seen in equation (2.24) it is the Jacobian matrix  $F_{\vec{\psi}}|_{\vec{\psi}_0}$  that determines the behavior of the hydrocarbon chemistry. In this section the properties of the Jacobian matrix of the hydrocarbon system will be studied. First its dependencies will be discussed, then its structure and next its eigenvalues/eigenvectors. We end this section by analyzing the rank of the Jacobian matrix.

### Dependencies

As the chemical source term is linearized around the point  $\vec{\psi}_0 = (T_{e-}, T_{p+}, E, \phi_{e-}, \phi_{p+}, 0, \dots, 0)^T$  the dependencies of the Jacobian matrix are given by:

$$F_{\vec{\phi}}|_{\vec{\phi}_0} = f(T_{e-}, T_{p+}, E, \phi_{e-}, \phi_{p+}) \quad (2.26)$$

These dependencies are important for deterministic models with transport, because then the plasma conditions in every grid cell can be different.

### Zero columns in the Jacobian

Because of the linearization around  $\vec{\phi}_0$  the first two columns of the Jacobian in the composition space are zero. This arises from the zero concentration of the hydrocarbons. On the other hand hydrocarbons that do not interact with the plasma induce extra zero columns in the Jacobian. It will become clear later that all the zero columns result in conservation variables in the system.

### Upper triangular structure of the Jacobian matrix

The hydrocarbon reaction database only contains fragmentation collision reactions, which means that the mass of the formed hydrocarbons is always lower than the mass of the reacting hydrocarbon species. If the species in  $\vec{\phi}$  are ordered by mass, with  $\phi_1$  being the concentration of the electrons and  $\phi_{54}$  being the concentration of  $C_3H_8$ , the Jacobian matrix will have an upper triangular structure:

$$F_{\vec{\phi}}|_{\vec{\phi}_0} = \begin{pmatrix} 0 & 0 & F_{13} & \dots & F_{1n_s} \\ 0 & 0 & F_{23} & \dots & F_{2n_s} \\ 0 & 0 & F_{33} & \dots & F_{3n_s} \\ \vdots & \vdots & \vdots & \ddots & \vdots \\ 0 & 0 & 0 & \dots & F_{n_s n_s} \end{pmatrix}$$

with  $F_{ij}$  being the elements of the Jacobian in row  $i$  and column  $j$ :

$$F_{ij} = \begin{cases} \sum_{l_j} \nu_{il} \langle \sigma v \rangle_l \cdot \phi_{pe} & \text{for } i = 1, \dots, n_s \text{ and } 3 \leq j \leq i \\ 0 & \text{for all other indices} \end{cases} \quad (2.27)$$

where the sum contains all the reactions  $l_j$  between species  $j$  and the background particles.

This structure has interesting properties:

- The eigenvalues of an upper triangular matrix lie on its diagonal. Consequently they are real.
- The eigenvectors of a real upper triangular matrix with real eigenvalues are real.

As the ILDM analysis will be built on an eigenvalue/eigenvector analysis of the Jacobian matrix, these properties will introduce computational advantages.

### All non-zero eigenvalues are negative

The diagonal elements of the Jacobian matrix are given by equation (2.27):

$$F_{ii} = \sum_{l_i} \nu_{il} \langle \sigma v \rangle_l \cdot \phi_{pe} \quad \text{for } i > 2$$

with  $l_i$  being every reaction between species  $i$  and the background plasma. As it is the species  $i$  that reacts, its coefficient  $\nu_{il}$  is negative for each reaction  $l$ , which makes  $F_{ii}$  negative for all species  $i$ . If  $i \leq 2$  or if species  $i$  doesn't react with the background plasma  $F_{ii} = 0$ . As the diagonal elements are also the eigenvalues of an upper triangular matrix:

$$\lambda_i \leq 0 \quad i = 1, \dots, n_s$$

### Rank of the Jacobian matrix

In a closed homogeneous reaction system only the chemical reactions can change the composition. As these reactions obey certain conservation laws, the evolution of the composition can be modelled in a lower dimensional subspace of the composition space. In this section we will show that the rank of the Jacobian matrix determines the dimension of this subspace, which will be called the **reaction space**.

To determine the rank of the Jacobian matrix, the number of zero rows in its row reduced echelon form  $J$  can be used. Suppose  $T$  is the matrix to transform the Jacobian matrix to its row reduced echelon form, then:

$$T \cdot F_{\vec{\phi}}|_{\vec{\phi}_0} = J = \begin{pmatrix} - & J_1 & - \\ - & 0 & - \end{pmatrix}$$

with  $J_1$  being the nonzero rows and 0 being the  $n_c$  zero rows in  $J$ . By definition, the rank of the Jacobian is  $n_s - n_c$ . To demonstrate that it also determines the dimension of the reaction space, one can use  $T$  to transform the chemical source term:

$$T \cdot \frac{\partial \vec{\phi}}{\partial t} = \frac{\partial T \cdot \vec{\phi}}{\partial t} = T \cdot F_{\vec{\phi}}|_{\vec{\phi}_0} \vec{\phi} \\ \begin{pmatrix} \frac{\partial T_1 \cdot \vec{\phi}}{\partial t} \\ \frac{\partial T_2 \cdot \vec{\phi}}{\partial t} \end{pmatrix} = \begin{pmatrix} - & J_1 & - \\ - & 0 & - \end{pmatrix} \vec{\phi}$$

with  $T_2$  being the last  $n_c$  rows of  $T$  and  $(T_2 \cdot \vec{\phi})$  being a vector with size  $n_c$ , containing the linear combinations of species which do not change in time. These  $n_c$  linear equations are called the **conservation equations** and their value is determined by the initial conditions:

$$\frac{\partial T_2 \cdot \vec{\phi}}{\partial t} = 0 \\ T_2 \cdot \vec{\phi} = T_2 \cdot \vec{\phi}_{t=0} \quad (2.28)$$

By introducing these  $n_c$  algebraic equations into the system and leaving out some differential equations a system of  $n_s - n_c$  differential equations can be kept to calculate the chemical dynamics. The algebraic equations are then needed to reconstruct the full composition space at each time step. Therefore the dimension of the reaction space equals the rank of the Jacobian matrix.

For the hydrocarbon reaction mechanism the rank of the Jacobian is not equal to its size because:

- The first two columns of the Jacobian matrix are 0 (we linearized in  $\psi_0$ )
- Each species  $i$  that doesn't react with the background plasma introduces a zero column
- The chemical reactions conserve elements, a property which is also present in the reaction matrix  $R$ .

The total number of dependencies in the Jacobian matrix is not equal to the sum of the presented dependencies, because the first two items introduce column dependencies while the last item introduces row dependencies. For the full mechanism, the Jacobian matrix has 13 zero columns and all other columns are independent because of its upper triangular structure. Therefore the hydrocarbon reaction mechanism, characterized by  $T_{e^-}$ ,  $T_{p^+}$ ,  $E$  and 54 species, has 13 conservation equations ( $n_c = 13$ ). The reaction space has dimension ( $n_{reac} = n_s - n_c = 41$ ).

Similarly, since the Jacobian matrix of the CH-hydrocarbon system has 6 zero columns, it has 6 conservation equations and its reaction space has dimension  $9-6=3$ .

A last important note: The conservation equations of the Jacobian can be retrieved from the left eigenvectors of the zero eigenvalues. See section 2.4.1 for the explanation.

### 2.3.4 Computational cost of the chemical source term

To calculate the evolution of the composition due to chemistry a set of Ordinary Differential Equations (ODE) needs to be numerically integrated. In our case the system is represented by equation (2.24):

$$\frac{\partial \vec{\phi}}{\partial t} = F_{\vec{\phi}}|_{\vec{\phi}_0} \vec{\phi}$$

The computational cost of solving this system consists of the computational cost of the solver and the computational cost of  $F_{\vec{\phi}}|_{\vec{\phi}_0}$ . The stiffness (SAJDA, 2001) of the system requires the use of an implicit solver to solve the system. Its cost scales normally scales as  $(n_s)^3$ , because it requires to solve a system of 'linear' equations:

$$\begin{pmatrix} 1 - F_{11}\Delta t & -F_{12}\Delta t & \cdots & -F_{1n_s}\Delta t \\ -F_{21}\Delta t & 1 - F_{22}\Delta t & \cdots & -F_{2n_s}\Delta t \\ \vdots & \cdots & \ddots & \vdots \\ -F_{n_s1}\Delta t & \cdots & -F_{n_s n_s - 1}\Delta t & 1 - F_{n_s n_s}\Delta t \end{pmatrix} \vec{\phi}_t = \vec{\phi}_{t-1} \quad (2.29)$$

with  $F_{ij}$  being element  $ij$  of  $F_{\vec{\phi}}|_{\vec{\phi}_0}$ . Because of the structure of the Jacobian  $F_{ij} = 0$  if  $i > j$ , the equations can be solved with backward substitution, a process which computational cost scales with  $(n_s) \times (n_s + 1)/2$ .

The computation of the Jacobian matrix requires  $n_s$  evaluations of  $\vec{F}$  to calculate the finite-differences. To evaluate  $\vec{F}$ ,  $n_r$  rate coefficients must be calculated. The cost of the chemical source term thus roughly scales with  $(n_s) \times (n_s + 1)/2 + (n_s) \times (n_r)$  per time step.

## 2.4 Dynamical response of the hydrocarbon chemistry on perturbations

As we have seen in sections 2.2 and 2.3, the chemistry of the hydrocarbon reaction mechanism can be simulated in both a Monte Carlo and a deterministic way. In this section the dynamical

response of the hydrocarbon chemistry on small perturbations will be studied by solving the chemical source term. In what follows first the dynamical response of the hydrocarbon chemistry will be derived mathematically and then it will be applied on an example.

### 2.4.1 Analytical study

Imagine a small perturbation  $\vec{\epsilon}_0$  moves  $\vec{\phi}(t=0)$  to a new point  $\vec{\phi}_\epsilon(t=0)$ . What we want to study, is how the error  $\vec{\epsilon}(t)$  behaves in time: if the error becomes smaller, if it stays the same or if it enlarges in time. In the point  $\vec{\phi}_\epsilon$  the systems behavior is modelled by the following system of differential equations:

$$\frac{\partial \vec{\phi}_\epsilon}{\partial t} = F_{\vec{\phi}}|_{\vec{\phi}_\epsilon} \vec{\phi}_\epsilon \quad \vec{\phi}_\epsilon(t=0) = \vec{\phi}(t=0) + \vec{\epsilon}_0$$

Subtracting the behavior of  $\vec{\phi}_\epsilon$  and  $\vec{\phi}$ , the dynamics of the perturbation  $\vec{\epsilon} = \vec{\phi}_\epsilon - \vec{\phi}$  are written as:

$$\begin{aligned} \frac{\partial}{\partial t} (\vec{\phi}_\epsilon - \vec{\phi}) &= F_{\vec{\phi}}|_{\vec{\phi}_\epsilon} (\vec{\phi}_\epsilon - \vec{\phi}) \\ \frac{\partial \vec{\epsilon}}{\partial t} &= F_{\vec{\phi}}|_{\vec{\phi}_\epsilon} \vec{\epsilon} \quad \vec{\epsilon}(t=0) = \vec{\epsilon}_0 \end{aligned}$$

In the eigenvector space of the Jacobian matrix it is possible to solve this system analytically, because the Jacobian matrix has a diagonal form in this space:

$$F_{\vec{\phi}}|_{\vec{\phi}_\epsilon} = U D U^{-1}$$

with  $U = [U_1 \ U_2 \ \dots \ U_{n_s}]$  being a matrix built by the eigenvectors  $U_i$  of the Jacobian, corresponding to the eigenvalues  $\lambda_i$  and  $D$  being a diagonal matrix with the eigenvalues  $\lambda_i$  on its diagonal. Transforming the system from state space to eigenvector space ( $\vec{\epsilon} = U \hat{\vec{\epsilon}}$  and  $\hat{\vec{\epsilon}} = U^{-1} \vec{\epsilon}$ ) introduces the diagonal matrix  $D$  into the system:

$$\frac{\partial \hat{\vec{\epsilon}}}{\partial t} = D \hat{\vec{\epsilon}}$$

because matrix  $D$  is a diagonal matrix containing the eigenvalues  $\lambda_i$  on its diagonal, the system can be decoupled:

$$\frac{\partial \hat{\epsilon}_i}{\partial t} = \lambda_i \hat{\epsilon}_i \quad i = 1, \dots, n_s$$

In the space spanned by the eigenvectors, the analytical solution of this equation is given by:

$$\hat{\epsilon}_i(t) = \hat{\epsilon}_{i,0} \exp(\lambda_i t) \quad i = 1, \dots, n_s$$

with  $\hat{\epsilon}_{i,0}$  being the amplitude of  $\vec{\epsilon}_0$  in the direction of eigenvector  $i$  ( $\hat{\epsilon}_0 = U^{-1} \vec{\epsilon}_0$ ). The solution in the state space can be found by transforming back:

$$\vec{\epsilon}(t) = U \hat{\vec{\epsilon}}(t) \tag{2.30}$$

Keeping in mind the eigenvalues of the chemical source term are always real and negative or zero (see section 2.3.3) this analysis leads to the following conclusions:

- Perturbations in the direction of an eigenvector  $i$  with a negative eigenvalue will relax to zero with a relaxation time  $\tau = -1/\lambda_i$ . These eigenvectors span the reaction space.
- Perturbations in the direction of an eigenvector  $i$  with eigenvalue zero will not relax but stay constant. These eigenvectors represent the conservation equations which give us the conservation variables:  $\vec{T}_i \cdot \vec{\phi} = \vec{u}_i \cdot \vec{\phi}$  (equation (2.28)).
- If the system is only perturbed in the direction of the eigenvectors that have negative eigenvalues, the system will still reach the same equilibrium point. So, different initial conditions will end up in the same equilibrium point if they have the same value for the conservation equations.

These conclusions are important because transport can be interpreted as a dynamical perturbation of the chemical reaction mechanism. As long as the hydrocarbon transport doesn't change the conservation variables, the chemical system can fully absorb the perturbations if their timescales are a lot larger than the chemical timescales.

## 2.4.2 Example

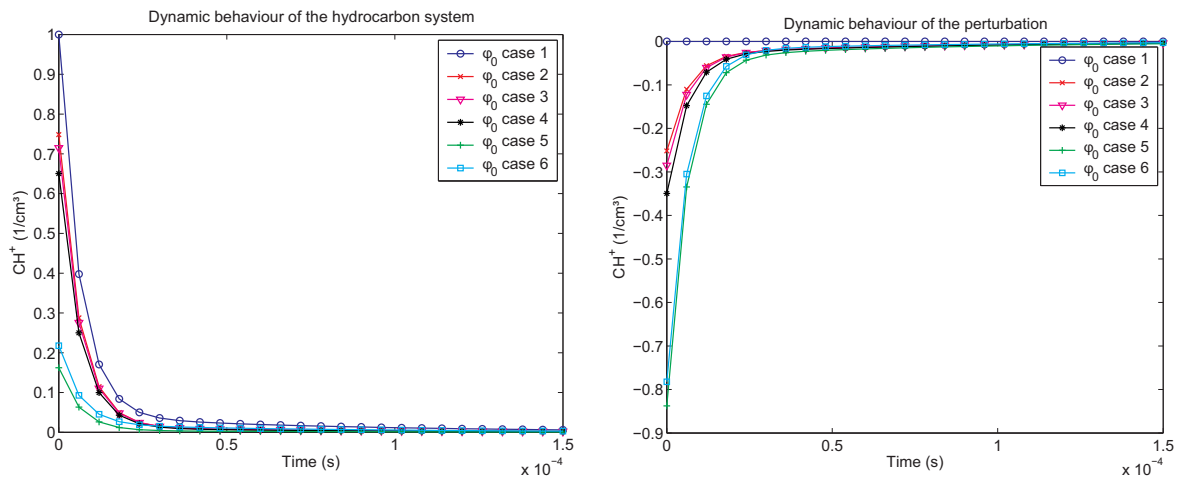
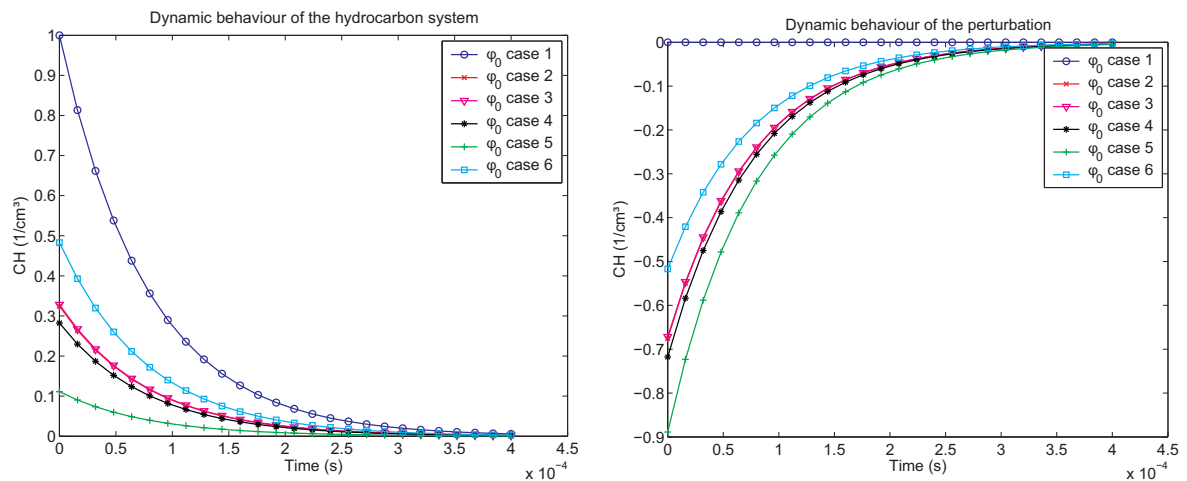
In what follows the dynamical behavior of the isothermal and iso-energetic hydrocarbon reaction systems with 9 species, from  $e^-$  up to CH, will be illustrated. Because the plasma temperatures ( $T_{e^-}, T_{p^+}$ ), the plasma densities ( $n_{e^-}, n_{p^+}$ ) and the species energy ( $E$ ) are constant, the system only shows dynamic behavior in the reaction space. The system is studied for a plasma temperature of  $T_{e^-} = T_{p^+} = 10eV$  and a hydrocarbon energy of  $E = 1eV$ . An eigenvalue/eigenvector analysis of the Jacobian matrix leads to the discovery of six zero eigenvalues. Their corresponding left eigenvectors are exposed in table 2.2.

	$e^-$	$H^+$	H	$H_2^+$	$H_2$	$C^+$	C	$CH^+$	CH
$\vec{U}_1^L$	1	0	0	0	0	0	1	0.79	1.25
$\vec{U}_2^L$	0	1	0	0	0	0	-9.7e-5	0.79	0.25
$\vec{U}_3^L$	0	0	1	0	0	0	9.7e-5	0.21	0.75
$\vec{U}_4^L$	0	0	0	1	0	0	0	0	0
$\vec{U}_5^L$	0	0	0	0	1	0	0	0	0.00
$\vec{U}_6^L$	0	0	0	0	0	1	1	1	1

Table 2.2: Left eigenvectors corresponding to a 0 eigenvalue for a hydrocarbon system with species up to CH

Because their eigenvalue is 0, the product of these left eigenvectors and the composition ( $\vec{\phi}$ ) does not change through time ( $\vec{U}_{\lambda=0}^L \cdot \vec{\phi}(t) = cte$ ). Looking carefully at table 2.2, one can discover that left eigenvector 6 represents the element vector of the C-atoms. Making a linear combination of the eigenvectors it is also possible to reconstruct the element vector of the H-atoms ( $U_2 + U_3 + 2 \cdot U_4 + 2 \cdot U_5$ ) and the element vector of charge ( $-U_1 + U_2 + U_4 + U_6$ ). The remaining vectors arise from species that do not react. The theory presented in section 2.4.1 states that if different initial conditions have the same value for the conservation equations ( $\vec{U}_{\lambda=0}^L \cdot \vec{\phi} = cte$ ), the system will end up in the same equilibrium point. Figures 2.5 and 2.6 illustrate this statement for the following initial conditions:

$1/cm^3$	$e^-$	$H^+$	$H$	$H_2^+$	$H_2$	$C^+$	$C$	$CH^+$	$CH$
$\phi_0$ case 1	1e+13	1e+13	1	1	1	1	1	1	1
$\phi_0$ case 2	1e+13	1e+13	1.55	1	1.00	2.19	0.73	0.75	0.32
$\phi_0$ case 3	1e+13	1e+13	1.56	1	1.00	2.91	0.05	0.71	0.33
$\phi_0$ case 4	1e+13	1e+13	1.61	1	1.00	3.06	0.01	0.65	0.28
$\phi_0$ case 5	1e+13	1e+13	1.83	1	1.00	3.57	0.16	0.16	0.11
$\phi_0$ case 6	1e+13	1e+13	1.55	1	1.00	3.14	0.16	0.22	0.48

Table 2.3: Initial concentrations ( $cm^{-3}$ ) with the same value for the conservation equationsFigure 2.5: Left: Dynamical behavior of the concentration of  $CH^+$  for different initial conditions. Right: Dynamical behavior of the perturbations for  $CH^+$ Figure 2.6: Left: Dynamical behavior of the concentration of  $CH$  for different initial conditions. Right: Dynamical behavior of the perturbations for  $CH$ 

The initial conditions presented in table 2.3 have the same value for the conservation equations characterized in table 2.2. Cases 2 to 6 can be seen as perturbations of case 1. As the

perturbations are not in the direction of the eigenvectors with eigenvalue 0, they will be in the direction of the three remaining eigenvectors with a negative eigenvalue. Therefore the dynamics of the perturbation should be a linear combination of these three eigenvalues ( $-1.82 \cdot 10^5$ ,  $-3.93 \cdot 10^5$  and  $-4.06 \cdot 10^5$ ), see equation (2.30):

$$\vec{\epsilon}_j = a_{7j} \exp(-1.82 \cdot 10^5 \cdot t) \vec{u}_7 + a_{8j} \exp(-3.93 \cdot 10^5 \cdot t) \vec{u}_8 + a_{9j} \exp(-4.06 \cdot 10^5 \cdot t) \vec{u}_9$$

$j = 1, \dots, 5$  being the number of the perturbation and  $a_i$  with  $i = 7, 8$  or  $9$  being the amplitude of the perturbation in the direction of the eigenvector  $\vec{u}_i$  determined by equation (2.30). The exponential decay of the perturbation can also be verified in figures 2.5 and 2.6 for the hydrocarbon species  $\text{CH}^+$  and  $\text{CH}$ .

## 2.5 Existence of low dimensional manifolds in the composition space

In this section it is our goal to illustrate, that as time increases, the solutions for different initial conditions which have the same conservation variables, are attracted towards consecutive smaller subspaces of the composition space until the composition ends up in the equilibrium point or one could say the zero dimensional subspace. Such subspaces are called **manifolds**. One can observe this behavior very clearly when looking at a representation of the trace in a composition window. Two dimensional projections of the  $n_s = 9$ -dimensional curve are plotted in figure 2.7 to demonstrate the existence of the manifolds in the  $\text{CH}$ -example (2.2.3). In the plots of figure 2.7 the concentrations of  $\text{CH}$  and  $\text{CH}^+$  are set out in function of the concentration of  $\text{H}$ . Each dot on a trace represents the composition at a certain moment in

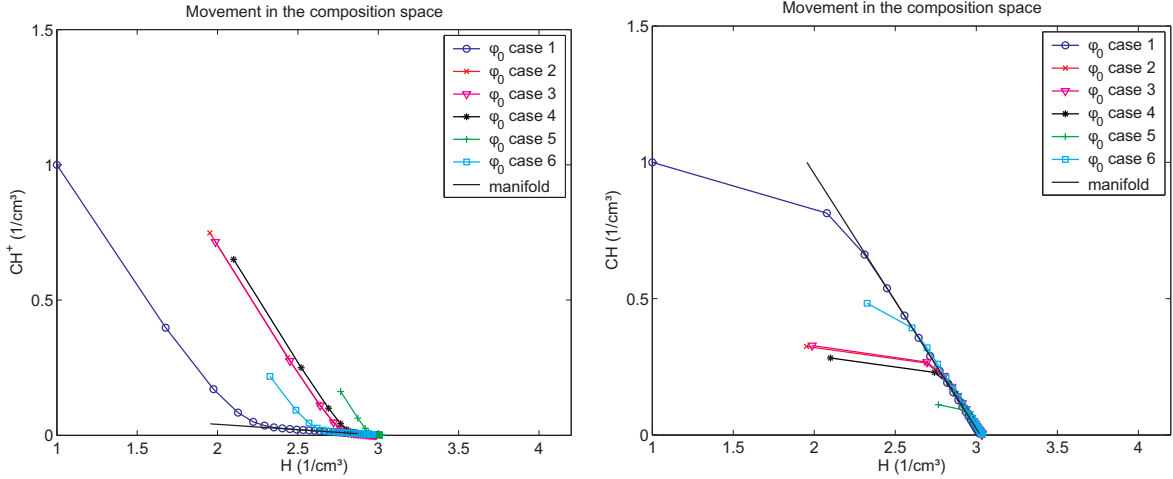


Figure 2.7: Composition curve in a  $\text{CH}$ - $\text{H}$  and a  $\text{CH}^+$ - $\text{H}$  co-ordinate system for different initial conditions

time. A closer look shows that the solutions do not only reach the equilibrium point, but they do so from the same angle. It is therefore possible to draw a tangent line, which is in this case a manifold, in the figure. Notice also that the manifold is reached quite rapidly compared to the time spent on the manifold to reach equilibrium. Less than 7 out of 25 equidistant time-steps are needed to converge with the manifold. The  $\text{CH}$  system contains only 3 independent

variables ( $n_{\text{reac}} = n_s - n_c$ ). This means the system starts on a 3-dimensional manifold and as it evolves it gradually lowers its dimension until it reaches the 0-D manifold. From this last section it should be clear that manifolds exist, which are intrinsic to the chemical system, whereas in the next chapter it will become clear how to calculate them.

## 2.6 Conclusion

To model the Carbon chemistry and transport in the plasma edge realistically an accurate database containing the cross sections and reaction rates of the participating species at different plasma temperatures and densities are available. The Janev-Reiter database used in this work contains up to now (2006 A.D.) 706 reactions and 54 species from  $e^-$  up to  $C_3H_8$ . In order to understand how this mechanism can be reduced it is important to know how the Monte Carlo code EIRENE uses the data for simulations.

A link to the deterministic method of solution was necessary for several reasons.

- First, the non-linear system was simplified to a homogeneous linear system of differential equations. The Jacobian of the linear system has such simple structure that the eigenvalues can be retrieved without calculation. At the same time it can be proved that the system is stable.
- Secondly, for the deterministic system the computational cost is known.
- Finally, it is possible to acquire insight in the dynamical behavior of the chemical system. The existence of different subspaces in which the chemical and physical dynamics are occurring is the basis for the reduction methods used in our work.

Though it should be kept in mind that the two approaches are fundamentally different: the reduction methods for macroscopic models proposed in the next chapter will have to be translated towards the microscopic (kinetic) Monte Carlo scheme.



## Chapter 3

# Reducing the hydrocarbon reaction mechanism

### 3.1 Introduction

The multi-species transport codes developed in the last 20 years to simulate the transport of the impurity particles in the plasma edge, are too time consuming to satisfy the desired accuracy for certain species of interest in the remote areas of the reactor. Therefore several attempts to reduce the computational cost have been made so far. We want to mention two of them. The ions, being very reactive species, can be assumed in quasi steady state. This approach has already been implemented in EIRENE (REITER, 2006) and reduces computation time. The ITER design team further reduced the computational effort by limiting the reaction mechanism to species up to C, to simulate the transport of the hydrocarbons. The question remains to what extent both approaches are justified.

#### Overview and motivation

The main goal of this chapter is to develop an automatic technique to create a simplified reaction mechanism, which can be implemented in EIRENE. To be successful we need to construct new elementary reactions for fewer species, with corresponding rates. Combustion researchers have already developed mathematical techniques to reduce the transport equation, which models similar problems as EIRENE. This introduction will be concluded with an overview of existing reduction methods widely found in literature. In this chapter we will discuss if the ILDM technique provides a viable way to reduce the hydrocarbon chemistry. This will be accomplished in a number of steps. In section 3.2 both the ILDM and the QSSA techniques will be elaborated in detail. As these methods are purely based on the chemistry of the problem, they will first be used to reduce the hydrocarbon chemical source term. Next, in section 3.4, they will be used to reduce the full transport equation. Finally the ILDM technique will be interpreted for its implementation in EIRENE.

### Reducing a reaction mechanism in combustion science

At present a number of techniques to reduce the calculation time for the solution of the reactive transport equations exist:

$$\begin{aligned}\frac{\partial \vec{\psi}(\vec{r}, t)}{\partial t} &= \vec{S}(\vec{\psi}(\vec{r}, t)) + \vec{\Gamma}(\vec{\psi}(\vec{r}, t), \nabla \vec{\psi}(\vec{r}, t), \Delta \vec{\psi}(\vec{r}, t)) \\ \vec{\psi} &= (T_{e^-}, T_{p^+}, E, \phi_1, \dots, \phi_{n_s})^T\end{aligned}\quad (3.1)$$

In the composition space (dimension  $n_s$ ) equation (2.1) can be reduced to:

$$\frac{\partial \vec{\phi}(\vec{r}, t)}{\partial t} = \vec{F}(\vec{\phi}(\vec{r}, t)) + \vec{\Xi}(\vec{\phi}(\vec{r}, t), \nabla \vec{\phi}(\vec{r}, t), \Delta \vec{\phi}(\vec{r}, t))\quad (3.2)$$

To lower the computational effort of the chemical source term of this equation ( $\vec{F}$ ), several things can be done:

1. Shortening the list of species which decreases the size of  $\vec{F}$ .
2. Shortening the list of reactions which decreases the calculation time of  $\vec{F}$ .
3. Decreasing the stiffness of the system  $\vec{F}$  which enables faster explicit solvers due to an increase in time step.

In combustion problems, some of the chemical processes ( $\vec{F}$ ) are much faster than the fluid dynamic processes ( $\vec{\Xi}$ ). So, if one is only interested in computing the behavior on the scale of the fluid processes, the fast chemical processes will already have equilibrated. Therefore this information is used to develop techniques which detect and use these fast equilibrating processes to reduce the transport equation. Initially timescale-based reduction techniques like QSSA and PE required the insight of the chemist. More recent methods like ILDM, CSP and MIM are based on a fully mathematical approach. This allows them to reduce the transport equation automatically, thus no longer requiring the chemists intuition to detect the fast species and/or fast reactions. Although the latter techniques provide better results, they are significantly more complicated to implement. A short qualitative discussion of these reduction techniques follows.

**QSSA** In the famous method of the Quasi-Steady State Approximation (BODENSTEIN and LIND, 1906; ROUSSEL and FRASER, 1991) it is the researcher's task to point out the fast equilibrating species. Assuming these species are in equilibrium, their rates are zero. From these assumptions result algebraic equations, which are then used to eliminate the fast equilibrating species from the system, decreasing the size of  $\vec{S}$ .

**PE** In the Partial Equilibrium technique (LAM and GOUSSIS, 1992), the researcher has to detect the reactions that equilibrate fast. Assuming these reactions are at equilibrium, their overall rate is zero. The algebraic equations that are formed in this way can be used to eliminate the fast equilibrating reactions, shortening the list of reactions.

**ILDM** The Intrinsic Low Dimensional Manifold method (MAAS and POPE, 1992b,a) explicitly computes a low-dimensional subspace/manifold of the state space (decrease in size of  $\vec{S}$ ) on which the slow chemical processes evolve (decrease in stiffness). By projecting the physical processes in this subspace, a new transport equation can be built, with the dimension of the subspace.

**CSP** The Computational Singular Perturbation method (LAM and GOUSSIS, 1988, 1992; LAM, 1993) is similar to the ILDM method as it also uses a transformation of the system basis vectors. In contrast with ILDM the new basis is used to automatically compute the optimum steady state and partial equilibrium relationships.

**MIM** The Method of Invariant Manifold (GORBAN and KARLIN, 1992b,a) is similar to the ILDM method as it also explicitly computes a low-dimensional manifold of the state space. In contrast with the ILDM, the IM is invariant. This means that once an individual trajectory has started on the manifold it will stay on it.

## 3.2 Manifold Reduction Technique

In general the QSSA technique does not explicitly calculate the manifold because it is not necessary, but we will present it in this way, to emphasize the similarities and differences between ILDM and QSSA.

In this section both the QSSA and the ILDM method will be presented as belonging to a group of reduction methods that transform the chemical source term onto a new basis in which one can separate the fast from the slow processes. The main goal of this section is to reduce the chemical source term of the hydrocarbon reaction mechanism which was defined in section 2.3:

$$\frac{\partial \vec{\phi}}{\partial t} = \vec{F}(\vec{\phi})$$

The linearised system is:

$$\frac{\partial \vec{\phi}}{\partial t} = F_{\vec{\phi}}|_{\vec{\psi}_0} \vec{\phi}$$

### 3.2.1 Algebraic equations

The two reduction techniques exposed below both use the chemical source term to determine algebraic relations between the species concentrations. The user specifies a certain number  $m$  of variables to be relaxed. With respect to the method used, these relaxed variables are certain local combinations of the state space variables. This can be written explicitly as

$$\phi_i = f_i(\vec{\theta}) \quad i = 1, \dots, n_s \quad (3.3)$$

$\vec{\theta}$  having length  $m$ . These combinations can be seen as algebraic equations that restrict the movement of the chemical kinetics in the reaction space, so the dynamics of the reduced system can be calculated with less degrees of freedom. It is exactly these algebraic equations that define the manifold. The theoretical background of these equations will now be exposed.

### QSSA-algorithm

**Literature** The QSSA method was pioneered by Bodenstein in 1913 to reduce systems in order to get an analytical solution. It was not before Chen (1988) and Fraser (1988) that it was applied for reducing the stiffness of a chemical system. More information on the method, its properties and its error are by DEUFLHARD and HEROTH (1995) and Turanyi and Philling (1993). It should be mentioned that several versions of the method have been invented ever since and that it has been applied with different levels of success on various reactive systems.

**Assumptions** The quasi steady state approximation splits the list of species in two groups: the slow basic and the fast intermediate (radicals, etc.). Likewise the concentration vectors of both groups are accordingly  $\vec{\phi}_s$  and  $\vec{\phi}_f$ . The total vector is  $\vec{\phi} = \vec{\phi}_s + \vec{\phi}_f$ . If the subsystem relaxes to a stationary state at fixed values of  $\vec{\phi}_s$ ,  $\vec{\phi}_f \rightarrow \vec{\phi}_f^{qss}(\vec{\phi}_s)$ , then the assumption  $\vec{\phi}_f = \vec{\phi}_f^{qss}(\vec{\phi}_s)$  is precisely the QSS assumption. The system to be solved now is:

$$\begin{aligned} \frac{\partial \vec{\phi}}{\partial t} &= \vec{F}(\vec{\phi}_s + \vec{\phi}_f), \quad \vec{\phi}_s = \text{const}; \quad \vec{\phi}_f \rightarrow \vec{\phi}_f^{qss}(\vec{\phi}_s); \\ \frac{\partial \vec{\phi}}{\partial t} &= \vec{F}(\vec{\phi}_s + \vec{\phi}_f^{qss}(\vec{\phi}_s)) \end{aligned} \quad (3.4)$$

For the species assumed in quasi steady state the differential equations are transformed in algebraic equations of state. In the general non-linear case the manifold is defined by setting the component of the chemical source term  $F_i$  to zero for the quasi steady state species  $f$ .

$$\boxed{F_i(\vec{\phi}) = 0} \quad i \in f = \text{set of fast qss-species}$$

These algebraic equations define the quasi steady state approximation manifold. From these equations one can retrieve the concentration of the fast species as a function of the concentration of slow species.

**Linear equations** The equations of quasi steady state are easily derived from the linear chemical system. Be  $\vec{F}_i$  the rows of the Jacobian  $F_{\vec{\phi}}|_{\vec{\phi}_0}$  and  $f$  the indices of the species in quasi steady state. The algebraic equations for the system are then:

$$\vec{F}_i \cdot \vec{\phi} = 0 \quad i \in f \quad (3.5)$$

The remaining differential equations for the slow species  $s$  are

$$\frac{\partial \phi_i}{\partial t} = \vec{F}_i \cdot \vec{\phi} \quad i \in s = \text{set of slow species} \quad (3.6)$$

At every time step the concentration of  $\vec{\phi}_f$  has to be calculated from the new value of  $\vec{\phi}_s$  with the algebraic equations. One could also fill in the explicit form of equations (3.5) into the reduced differential equation system of (3.6). The practical implementation follows later.

**Closing remarks** The quasi steady-state approximation is more restrictive and less robust than for example the quasi-equilibrium approximation and the ILDM. In addition it is, just like quasi-equilibrium, very sensitive to the initial conditions! A slight change in composition makes the approximations invalid. In general if no measures are taken one will observe loss of conservation. This can be seen in the results of Tzafirri and Edelman (1993). The “chemists intuition” plays an even more important role than for QE in the choice of stationary species. To overcome this, the theory of singularly perturbed systems of ordinary differential equations is used to provide a mathematical background for the QSS approximation. This has successfully been worked out in the CSP-method by LAM and GOUSSIS (1988). Until now it remains, in general, unclear what is the parameter that separates the intermediate (fast) species from the basic (slow). Unlike in the case of quasi-equilibrium, the reaction rate constant cannot be such a parameter. Indeed, intermediate species participate in the same reactions as the basic species. It is therefore incorrect to state that  $\vec{\phi}_f$  evolves faster than  $\vec{\phi}_s$ .

### ILDM-algorithm

**Literature** The general non-linear derivation of the ILDM can be widely found in literature. The first to implement the scheme were Maas and Pope describing the method in their articles (MAAS and POPE, 1992a,b). For a work regrouping most of one has to know about ILDM we refer to SCHMIDT (1995). One can find in this German text a mathematical derivation of the method, an alternative basis for the eigenvectors, the properties of the intrinsic low dimensional manifold, the numerical calculation and tabulation of the manifold as well as a how to project perturbed state vectors back onto the manifold. For a practical implementation on a small very illustrative example we recommend Glassmaker (1999). Even though a complete picture of the ILDM method would be very useful for analyzing the results of the method, we will stick to a brief mathematical derivation for the homogeneous linear problem and refer to the literature for more information.

$$\frac{\partial \vec{\phi}}{\partial t} = F_{\vec{\phi}}|_{\vec{\phi}_0} \vec{\phi}$$

**Decoupling** In contrast with QSSA, the ILDM technique transforms the chemical system to a new basis, created by the eigenvectors of the Jacobian matrix of the chemical source term, where the variables are decoupled. This means that their rate is not dependent on the concentrations of the other variables. Therefore it is easy in this space to detect the fast and the slow variables. Transforming the composition space coordinates  $\vec{\phi}$  to a new equivalent one with variables  $\vec{\xi}$ . The transformation to this space is done in the following way:

$$\vec{\xi} = U^L \cdot \vec{\phi} \quad \text{and} \quad \vec{\phi} = U \cdot \vec{\xi}$$

The columns of  $U$  are the ‘right’ eigenvectors  $\vec{u}_i$  of the Jacobian matrix  $F_{\vec{\phi}}|_{\vec{\phi}_0}$  of the chemical source term.  $U^L = U^{-1}$  is the inverse and contains the left eigenvectors in the rows. Using these transformations to manipulate the system leads to the new system:

$$\begin{aligned} U^L \cdot \frac{\partial \vec{\phi}}{\partial t} &= U^L \cdot F_{\psi}|_{\vec{\psi}_0} \cdot U \cdot \vec{\xi} \\ \frac{\partial \vec{\xi}}{\partial t} &= D \cdot \vec{\xi} \end{aligned} \tag{3.7}$$

with  $D$  being a diagonal matrix containing the eigenvalues on the diagonal. It can be demonstrated that in the general case of complex or degenerated eigenvalues a solution still exists (SCHMIDT, 1995). In the eigenvector basis, the system of differential equations is thus completely decoupled. As the eigenvalues of the Jacobian are always real (see section 2.3.3) the decay of every component of  $\vec{\xi}(t)$  can be solved separately:

$$\frac{\partial \xi_i}{\partial t} = \lambda_i \xi_i \quad i = 1, \dots, n_s \quad (3.8)$$

The analytical solution of this decoupled system shows why the eigenvalues provide a ground to determine the fast and slow processes:

$$\xi_i = \xi_{i0} \exp(\lambda_i t) \quad \xi_{i0} = \xi_i(t=0) \quad i = 1, \dots, n$$

If  $\lambda_i$  is big and negative,  $\xi_i$  will decay in a very short timescale  $\tau_i = \frac{-1}{\lambda_i}$ . For example the influence of eigenvector  $\vec{u}_i$  on the full solution is reduced to  $0.0498 \cdot \xi_{i0}$  after a time  $t = 3 \cdot \tau_i$ . Therefore  $\xi_i$  can be assumed in quasi steady state if its timescale is fast enough so its influence can be neglected in the full solution.

As input of the ILDM-method, the user provided the full chemical reaction kinetics and the dimension of the Invariant Low Dimensional Subspace. The dimension of the subspace is  $m = n_s - n_f$ , with  $n_f$  the number of eigenvalues that are assumed to be fast, and thus relaxed on the manifold. In linear system an alternative definition to determine the number of relaxed timescale, could be a cut-off timescale. For example the fastest of the transport timescales could be used here. However this technique would result in a changing dimension of the ILDM during calculation, because in general non-linear systems have changing eigenvalues.

**Manifold** The dimension, provided by the user, separates the eigenvector space into  $n_f$  fast directions and  $m = n_s - n_f$  slow directions. So, chemical reactions change the composition rapidly in the direction of the eigenvectors with the most negative eigenvalues. Splitting transformed coordinates, the inverted eigenvalues and the diagonal matrix into a fast and a slow part:

$$\vec{\xi} = \begin{pmatrix} \vec{\xi}_s \\ \vec{\xi}_f \end{pmatrix} \quad U^{-1} = \begin{pmatrix} - & U_s^L & - \\ - & U_f^L & - \end{pmatrix} \quad D = \begin{pmatrix} D_s & 0 \\ 0 & D_f \end{pmatrix}$$

System (3.7) can then be divided into its slow and its fast components and the corresponding initial conditions can be calculated:

$$\frac{\partial \vec{\xi}_s}{\partial t} = D_s \vec{\xi}_s \quad \vec{\xi}_{s0} = U_s^L \vec{\phi}_0 \quad (3.9a)$$

$$\frac{\partial \vec{\xi}_f}{\partial t} = D_f \vec{\xi}_f \quad \vec{\xi}_{f0} = U_f^L \vec{\phi}_0 \quad (3.9b)$$

The indices  $s$  and  $f$  refer to respectively the slow and the fast (local) processes or one could call them eigenmodes. The ILDM-assumption is now that  $n_f$  fastest processes  $\frac{\partial \xi_i}{\partial t}$  for  $i = m + 1, \dots, n$  immediately relax to zero:

$$\begin{aligned} \frac{\partial \vec{\xi}_f}{\partial t} &= 0 \\ U_f^L \frac{\partial \vec{\psi}}{\partial t} &= 0 \end{aligned}$$

For the homogeneous system linearized in  $\vec{\psi}_0$  this can be written as:

$$U_f^L F_{\vec{\phi}}|_{\vec{\psi}_0} \vec{\phi} = 0 \tag{3.10}$$

This can now be extrapolated for the case of the non-linear system. Note that for the left eigenvectors one now has to keep in mind the dependency on the plasma conditions  $(\phi_{e-}, \phi_{p+}, T_{e-}, T_{p+})$ . In a nonlinear system the ILDM equations around point  $\vec{\psi}_0$  are given by:

$$\boxed{U_f^L \vec{F}(\phi) = 0} \tag{3.11}$$

Possible interpretations of this equation are:

- There is no movement of the system in the direction of the  $n_f$  fastest eigenvectors.
- The chemical source term  $\vec{F}$  disappears in the direction of the fast timescales  $\vec{u}_{m+1}, \dots, \vec{u}_n$ .
- The system evolves in direction orthogonal to the fast processes.
- The system moves in a low dimensional space spanned by the slow eigenvectors.

The dynamics of the chemical system are limited to changes in the directions of the slow eigenvectors, characterised by the local eigenvalues  $\lambda_1 \dots \lambda_m$ . In every point of the reaction space, it is possible to calculate the Jacobian of the system and subject it to an eigenvalue analysis in order to determine the ILDM-equations. Because  $n_f$  additional algebraic equations are provided for the reaction space, the dimension of the space in which the system moves, can be further reduced to  $n_r - n_f$ . As said before,  $n_f$  should be given by the user.

**Closing remarks** In contrast with PE or QSSA the ILDM technique distinguishes automatically the fast from the slow processes. This gives ILDM a big advantage over QSSA. The so called ‘chemist’s intuition’ is no more required and the mathematical foundation of this method is beneficial for the approximation of the full solution. The method has proved its strength throughout the many validations on combustion models. One of the most important properties of the ILDM is that it is an attractive manifold. This means that points lying away from the manifold will through the chemical kinetics evolve towards the manifold. Computational errors or processes that disturb the evolution and move it away from the manifold will automatically be corrected and decay until it falls onto the manifold again. This makes the ILDM-technique very robust in calculations. The method has also the advantage to be applicable in every case. Even when the eigenvalues are degenerated and/or complex. Though in this case it is recommended to use instead of the eigenvector basis the real Schur decomposition which offers an alternative basis for the eigenvectors and is numerically better conditioned (MAAS and POPE 1992a and SCHMIDT 1995).

### 3.2.2 QSSA and ILDM in an analytical example

Take the following system with the variable column vector  $\vec{y}(t) = (y_1(t), y_2(t), y_3(t))^T$ :

$$\frac{d\vec{y}}{dt} = \begin{pmatrix} -1 & 1 & 0 \\ 1 & -1 & 0 \\ 0 & 1 & -1 \end{pmatrix} \vec{y}(t)$$

One can see easily that row 1 and 2 are dependent from each other. The conservation equation is thus:

$$\begin{pmatrix} 1 & 1 & 0 \end{pmatrix} \frac{d\vec{y}(t)}{dt} = 0 \quad \text{or} \quad y_1 + y_2 = \text{constant}$$

The equilibrium point (at time  $t_\infty$ ) can be calculated upon imposing the condition:

$$\frac{d\vec{y}(t_\infty)}{dt} = \vec{0} \quad (3.12)$$

Imposing zero derivatives results in only two independent equations from the full system matrix:

$$\begin{pmatrix} -1 & 1 & 0 \\ 0 & 1 & -1 \end{pmatrix} \vec{y}(t_\infty) = 0$$

Moreover the conservation should be fulfilled with the initial conditions at  $t_0$ :

$$\begin{pmatrix} 1 & 1 & 0 \end{pmatrix} \vec{y}(t_\infty) = \begin{pmatrix} 1 & 1 & 0 \end{pmatrix} \vec{y}(t_0)$$

The equilibrium is:

$$\vec{y}(t_\infty) = \begin{pmatrix} \frac{y_{10} + y_{20}}{2} \\ \frac{y_{10} + y_{20}}{2} \\ \frac{y_{10} + y_{20}}{2} \end{pmatrix}$$

The QSSA assumption is given in the algebraic equation:

$$\frac{d\vec{y}_1}{dt} = \begin{pmatrix} -1 & 1 & 0 \end{pmatrix} \vec{y}(t) = 0$$

With the usual parameter choice (see later at section 3.5) the system is reduced to:

$$\begin{aligned} \frac{dy_2}{dt} &= 0 \\ \frac{dy_3}{dt} &= y_2 - y_3 \end{aligned}$$

It is clear that  $y_2$  will not evolve and will remain as in the initial condition. Imposing the condition of (3.12) the equilibrium of this reduced system is:

$$\begin{aligned} y_2(t_\infty) &= y_{20} \\ y_1(t_\infty) &= y_{20} \\ y_3(t_\infty) &= y_{20} \end{aligned}$$

Clearly the conservation laws have been violated.

The opposite can be demonstrated for ILDM. With the known eigenvalues 0,-1,-2 and eigenvectors the solution can be written analytically as:

$$\vec{y}(t) = c_1 e^{0t} \begin{pmatrix} 1 \\ 1 \\ 1 \end{pmatrix} + c_2 e^{-t} \begin{pmatrix} 0 \\ 0 \\ 1.7321 \end{pmatrix} + c_3 e^{-2t} \begin{pmatrix} 1 \\ -1 \\ 1 \end{pmatrix}$$

The terms are sorted according to increasing magnitude of the eigenvalue. In ILDM the choice to eliminate the third term is made automatically as this is associated with the fastest

time scale. The number of timescales neglected can never exceed the number of dynamical variables ( $n_s - m \geq n_c$ ). The first term in the equation is now exactly the conserved one. Because its eigenvalue is zero. It is no surprise that in the matrix of inverse eigenvectors one can recognize the conservation equation in the first row.

$$U^{-1} = \begin{pmatrix} 1/2 & 1/2 & 0 \\ -0.5774 & 0 & 0.5774 \\ 1/2 & -1/2 & 0 \end{pmatrix}$$

Obviously for  $t \rightarrow t_\infty$  the equilibrium point becomes:

$$\vec{y}(t) = c_1 \begin{pmatrix} 1 \\ 1 \\ 1 \end{pmatrix} + 0 \begin{pmatrix} 0 \\ 0 \\ 1.7321 \end{pmatrix} + 0 \begin{pmatrix} 1 \\ -1 \\ 1 \end{pmatrix}$$

And as the  $c$ 's were defined by the initial conditions the same equilibrium is attained.

### 3.2.3 The implementation

In ILDM simulations the equations presented above are usually used to tabulate the manifold in advance. The manifold reduces the space from  $n_s$  variables down to  $m$  variables. For tabulation it is thus necessary to define  $m$  parameters. These can be a linear combination of species concentrations. For a range of parameter values inside the domain of manifold existence, the complete composition as well as the rates are calculated and stored in the table. At any time, knowing the parameter values, the complete composition can be retrieved from the table. The table is used in this way during the calculations to know the concentrations of the species and the associated rates. More generally, if the kinetics depend on the intensive variables such as  $T_{e-}$  and  $T_{p+}$ , they should also be included as parameters in the table. For improved tabulation techniques we refer to POPE (1997). As we are simplifying the Carbon reaction system to a linear form we opted for a different approach. This doesn't eliminate the option to tabulate the manifold for the final implementation in EIRENE. But because they are easy to handle, the implementation is basically done with matrices. This section explains how we constructed the manifolds. As there is a similarity between QSSA and ILDM, they can be worked out together and differentiated only when necessary.

#### Parameters

Now for a **fixed background temperature and density** let's concentrate only on the chemistry and assume a linear system in the composition space with no influence of background temperature and density on the rates:

$$\frac{d\vec{\phi}}{dt} = F_\phi \vec{\phi} \quad (3.13)$$

The  $F_\phi$ -matrix is then called the Jacobian of the system and is constant in this case. The reduced space or parameter space of dimension  $m = n - n_f$  is represented by the  $n$  dimensional

vector

$$\vec{\theta} = \begin{pmatrix} \vec{\theta} \\ \vec{0} \end{pmatrix} = \begin{pmatrix} \theta_1 \\ \theta_2 \\ \vdots \\ \theta_m \\ 0 \\ \vdots \\ 0 \end{pmatrix}$$

with chosen structure for purposes that will become clear later. The first  $m$  components contained in  $\vec{\theta}$  are the effective parameters that evolve with the reduced dynamics. One could call them the *manifold parameters*. The added zeros can be seen as the result of the reduction. These parameters have to be zero at all time. They are produced by the equations of the assumption, be it QSSA- or ILDM-equations:  $\hat{\theta}_i = \vec{q}_i \vec{\phi}$  for  $i = m + 1, \dots, n$ . Therefore we call them the *assumption parameters* ( $\vec{\theta}_q$ ). The reduced system is

$$\frac{d\vec{\theta}}{dt} = F'_\phi \vec{\theta} \quad (3.14)$$

Where the  $n \times n$  matrix  $F'_\phi$  is the Jacobian of the reduced system. The structure of the new Jacobian can be deduced from the applied transformation. First as we are dealing with a linear system the tabulation of the manifold can be simplified. Indeed the manifold in the composition space is, according to its dimension, a line, plane or hyperplane for the given energy and density. This means we can find a linear transformation  $n \times n$  matrix  $T$  which projects the points, lying on the manifold  $\vec{\phi}_m^1$ , onto the vector  $\vec{\theta}$  described above. This matrix is constructed as

$$T = \begin{pmatrix} P_{m \times n} \\ Q_{n_f \times n} \end{pmatrix} \quad (3.15)$$

with

$$P = \begin{pmatrix} - & \vec{p}_1 & - \\ - & \vec{p}_2 & - \\ & \vdots & \\ - & \vec{p}_m & - \end{pmatrix} \text{ and the reduction equations } Q = \begin{pmatrix} - & \vec{q}_{m+1} & - \\ - & \vec{q}_{m+2} & - \\ & \vdots & \\ - & \vec{q}_n & - \end{pmatrix}$$

being the parameter equations  $\vec{p}_i$  and the  $n_f$  equations  $\vec{q}_i$  defining the lower dimensional manifold. The  $\vec{p}_i$  can be freely chosen quite by the user as long as they are **linearly independent** from the  $\vec{q}_i$  and from each other such that  $T$  is an alternative basis for the complete composition space. Remember that a parametrization means selecting a set of differential equations which will be the driving force for the reduced system dynamics. Experimenting with the ILDM reduction one notices that the choice of parameter equations doesn't influence the solution of the ILDM simulations, though a good choice of parameters can facilitate computations and ameliorate accuracy (POPE, 1997). On the other hand one will experience that doing a consistent choice is more tricky in the QSSA situation. See section 3.5.  $Q$ , containing the manifold equations, makes the lower  $n_f$  vector components of  $\vec{\theta}$  zero if and

<sup>1</sup>Subscript  $m$  is in this case not the dimension of the manifold but is used here to indicate that the point lies on the manifold. It should be clear from the context what  $m$  refers to.

only if  $\vec{\phi}$  is a point on the manifold. Furthermore the inverse of the projection matrix  $T$  can now be calculated:

$$T^{-1} = T^L = \left( \begin{array}{cc} P^L & Q^L \end{array} \right)$$

with

$$P^L = \left( \begin{array}{c|c|c|c} \left| \right. & \left| \right. & \dots & \left| \right. \\ \left. \left. \begin{array}{c} \vec{p}_1^L \\ \vec{p}_2^L \\ \dots \\ \vec{p}_m^L \end{array} \right. \right. & & & \end{array} \right) \text{ and the reduction equations } Q^L = \left( \begin{array}{c|c|c|c} \left| \right. & \left| \right. & \dots & \left| \right. \\ \left. \left. \begin{array}{c} \vec{q}_{m+1}^L \\ \vec{q}_{m+2}^L \\ \dots \\ \vec{q}_n^L \end{array} \right. \right. & & & \end{array} \right)$$

With both  $T$  and  $T^{-1}$  the transformations from parameter space to composition space and vice versa is done as:

$$T\vec{\phi} = \vec{\theta} \quad \text{and} \quad T^{-1}\vec{\theta} = \vec{\phi} \quad (3.16)$$

using (3.16) to transform equation (3.13) into (3.14) leads to the deduction of  $F'_\phi$

$$T \frac{d(T^{-1}\vec{\theta})}{dt} = T F_\phi T^{-1}\vec{\theta} = \frac{d\vec{\theta}}{dt} = F'_\theta \vec{\theta} \Rightarrow F'_\theta = T F_\phi T^{-1} \quad (3.17)$$

Although  $F'_\phi$  has dimension  $n \times n$  the useful part is only the upper left  $m \times m$  block matrix. The equations to fill in sub-matrix  $Q$  according to the manifold we want to use follow.

**The ILDM subspace:** The intrinsic lower dimensional subspace was defined earlier by the equations:

$$U_f^L \vec{F}(\vec{\phi}) = U_f^L F_\phi \vec{\phi} = Q\vec{\phi} = 0$$

The transformation matrix for the parametrization of the ILDM subspace:

$$Q = U_f^L F_\phi = \left( \begin{array}{ccc} - & \vec{u}_{m+1}^L F_\phi & - \\ - & \vec{u}_{m+2}^L F_\phi & - \\ & \vdots & \\ - & \vec{u}_n^L F_\phi & - \end{array} \right) \quad (3.18)$$

One is able to choose freely the parameter equations in  $P$ . This doesn't alter the result.

Note that the ILDM equations are equivalent to  $U_f^L \vec{\phi} = 0$ . This can be shown by

$$U^L F_\phi \vec{\phi} = U^L U D U^L \vec{\phi} = D U^L \vec{\phi}$$

The matrix  $D$  is a diagonal matrix. This means the fast eigenvectors are separately set equal to zero because only the scaling factor  $\lambda_i$  in  $D$  is multiplied with each vector, hence the equivalence is proved.

**The QSSA subspace:** The quasi steady state lower dimensional subspace was defined by the equations:

$$\vec{F}_{\phi,i} \vec{\phi} = \vec{q}_i \vec{\phi} = 0, \quad \forall i_{QSSA}$$

$\vec{F}_{\phi,i}$  are the rows of  $F_\phi$  and  $i_{QSSA}$  the index of the QSS-species. We write

$$Q = F_\phi^f = \left( \begin{array}{ccc} - & \vec{F}_{\phi,m+1} & - \\ - & \vec{F}_{\phi,m+2} & - \\ & \vdots & \\ - & \vec{F}_{\phi,n} & - \end{array} \right) \quad (3.19)$$

For the QSSA subspace  $P$  has to be chosen with more precaution (see section 3.5)!

### 3.3 The CH hydrocarbon example

Let's take a look again at the CH mechanism from chapter 2. This to give an idea of the matrices one encounters when working with the hydrocarbon system. The conditions are still the same:  $1E13\text{cm}^{-3}$  plasma densities,  $0.1\text{eV}$  plasma temperature,  $1\text{eV}$  particle energy and an initial condition of  $1\text{cm}^{-3}$ . As the system has 9 species, one expects to find 9 variables. Because of the 6 conservation equations, 6 conservation variables, being combinations of species concentrations, are fixed for a closed homogeneous system. Thus only 3 degrees of freedom remain. The chemistry moves the state inside the 3-dimensional reaction space. Consequently the system can chemically be reduced by maximum 3 dimensions. Let's suppose now that a reduction of 1 variable is desired. The spectral decomposition will be given first because a lot of information, among which the conservation equations, can be retrieved from it. The eigenvalues, eigenvectors and inverse (left) eigenvectors have been calculated and sorted according to increasing absolute value of the eigenvalues:

$$F_\phi = UDU^L = \begin{pmatrix} 1 & 0 & 0 & 0 & 0 & 0 & 5.74E-01 & -2.68E-01 & 4.99E-01 \\ 0 & 1 & 0 & 0 & 0 & 0 & -4.39E-03 & -4.80E-01 & -1.54E-03 \\ 0 & 0 & 1 & 0 & 0 & 0 & 4.39E-03 & 5.23E-01 & -4.99E-01 \\ 0 & 0 & 0 & 1 & 0 & 0 & 0 & 0 & 0 \\ 0 & 0 & 0 & 0 & 1 & 0 & 0 & 2.33E-01 & 0 \\ 0 & 0 & 0 & 0 & 0 & 1 & 5.79E-01 & 2.33E-01 & -1.16E-04 \\ 0 & 0 & 0 & 0 & 0 & 0 & -5.79E-01 & 2.76E-01 & -5.01E-01 \\ 0 & 0 & 0 & 0 & 0 & 0 & 0 & -2.08E-02 & 5.01E-01 \\ 0 & 0 & 0 & 0 & 0 & 0 & 0 & -4.88E-01 & 0 \end{pmatrix}$$

$$\begin{pmatrix} 0 & 0 & 0 & 0 & 0 & 0 & 0 & 0 & 0 \\ 0 & 0 & 0 & 0 & 0 & 0 & 0 & 0 & 0 \\ 0 & 0 & 0 & 0 & 0 & 0 & 0 & 0 & 0 \\ 0 & 0 & 0 & 0 & 0 & 0 & 0 & 0 & 0 \\ 0 & 0 & 0 & 0 & 0 & 0 & 0 & 0 & 0 \\ 0 & 0 & 0 & 0 & 0 & 0 & 0 & 0 & 0 \\ 0 & 0 & 0 & 0 & 0 & 0 & -1.35E+00 & 0 & 0 \\ 0 & 0 & 0 & 0 & 0 & 0 & 0 & -1.30E+04 & 0 \\ 0 & 0 & 0 & 0 & 0 & 0 & 0 & 0 & -1.68E+05 \end{pmatrix}$$

$$\begin{pmatrix} 1 & 0 & 0 & 0 & 0 & 0 & 9.92E-01 & -4.53E-03 & 1.26E-02 \\ 0 & 1 & 0 & 0 & 0 & 0 & -7.60E-03 & -4.53E-03 & -9.87E-01 \\ 0 & 0 & 1 & 0 & 0 & 0 & 7.60E-03 & 1.00E+00 & 1.03E+00 \\ 0 & 0 & 0 & 1 & 0 & 0 & 0 & 0 & 0 \\ 0 & 0 & 0 & 0 & 1 & 0 & 0 & 0 & 4.78E-01 \\ 0 & 0 & 0 & 0 & 0 & 1 & 1 & 1 & 1.00E+00 \\ 0 & 0 & 0 & 0 & 0 & 0 & -1.73E+00 & -1.73E+00 & -9.02E-01 \\ 0 & 0 & 0 & 0 & 0 & 0 & 0 & 0 & -2.05E+00 \\ 0 & 0 & 0 & 0 & 0 & 0 & 0 & 2.00E+00 & -8.49E-02 \end{pmatrix}$$

#### 3.3.1 The QSSA transformation matrix and system

The QSSA parameter transformation matrix is very simply constructed with from top to bottom respectively the 6 conservation equations which can be found in  $U^L$ , 2 self chosen parameter equations which cannot be the QSS species and 1 QSSA equation retrieved directly from the Jacobian (2.25).

$$\vec{\theta} = \begin{pmatrix} 1 & 0 & 0 & 0 & 0 & 0 & 9.92E-01 & -4.53E-03 & 1.26E-01 \\ 0 & 1 & 0 & 0 & 0 & 0 & -7.60E-03 & -4.53E-03 & -9.87E-01 \\ 0 & 0 & 1 & 0 & 0 & 0 & 7.60E-03 & 1.00E+00 & 1.03E+00 \\ 0 & 0 & 0 & 1 & 0 & 0 & 0 & 0 & 0 \\ 0 & 0 & 0 & 0 & 1 & 0 & 0 & 0 & 4.78E-01 \\ 0 & 0 & 0 & 0 & 0 & 1 & 1 & 1 & 1.00E+00 \\ 0 & 0 & 0 & 0 & 0 & 0 & 1 & 0 & 0 \\ 0 & 0 & 0 & 0 & 0 & 0 & 0 & 0 & 1 \\ 0 & 0 & 0 & 0 & 0 & 0 & 0 & -1.68E+05 & 6.58E+03 \end{pmatrix} \cdot \vec{\phi} \quad (3.20)$$

The reduced QSSA Jacobian contains 6 zero rows thanks to the conservation equations:

$$\frac{\partial \vec{\theta}}{\partial t} = \begin{pmatrix} 0 & 0 & 0 & 0 & 0 & 0 & 0 & 0 \\ 0 & 0 & 0 & 0 & 0 & 0 & 0 & 0 \\ 0 & 0 & 0 & 0 & 0 & 0 & 0 & 0 \\ 0 & 0 & 0 & 0 & 0 & 0 & 0 & 0 \\ 0 & 0 & 0 & 0 & 0 & 0 & 0 & 0 \\ 0 & 0 & 0 & 0 & 0 & 0 & 0 & 0 \\ 0 & 0 & 0 & 0 & 0 & 0 & -1.35E+00 & 6.78E+03 \\ 0 & 0 & 0 & 0 & 0 & 0 & 0 & -1.30E+04 \end{pmatrix} \vec{\theta}$$

### 3.3.2 The ILDM transformation matrix and system

As parametrization for the ILDM manifold usual parameters can be used (row 1-8). We can take for example with the ILDM-equation at the end:

$$\vec{\theta} = \begin{pmatrix} 1 & 0 & 0 & 0 & 0 & 0 & 0 & 0 \\ 0 & 1 & 0 & 0 & 0 & 0 & 0 & 0 \\ 0 & 0 & 1 & 0 & 0 & 0 & 0 & 0 \\ 0 & 0 & 0 & 1 & 0 & 0 & 0 & 0 \\ 0 & 0 & 0 & 0 & 1 & 0 & 0 & 0 \\ 0 & 0 & 0 & 0 & 0 & 1 & 0 & 0 \\ 0 & 0 & 0 & 0 & 0 & 0 & 1 & 0 \\ 0 & 0 & 0 & 0 & 0 & 0 & 0 & 1 \\ 0 & 0 & 0 & 0 & 0 & 0 & 2.00E+00 & -8.49E+00 \end{pmatrix} \cdot \vec{\phi} \quad (3.21)$$

The reduced ILDM Jacobian becomes:

$$\frac{\partial \vec{\theta}}{\partial t} = \begin{pmatrix} 0 & 0 & 0 & 0 & 0 & 0 & 1.34E+00 & -1.67E+05 \\ 0 & 0 & 0 & 0 & 0 & 0 & -1.03E-02 & -3.00E+05 \\ 0 & 0 & 0 & 0 & 0 & 0 & 1.03E-02 & 3.27E+05 \\ 0 & 0 & 0 & 0 & 0 & 0 & 0 & 0 \\ 0 & 0 & 0 & 0 & 0 & 0 & 0 & 1.46E+05 \\ 0 & 0 & 0 & 0 & 0 & 0 & 1.35E+00 & 1.46E+05 \\ 0 & 0 & 0 & 0 & 0 & 0 & -1.35E+00 & 1.72E+05 \\ 0 & 0 & 0 & 0 & 0 & 0 & 0 & -1.30E+04 \end{pmatrix} \vec{\theta}$$

The trick of using conservation equations as parameters can also be used here with the ILDM technique. Or one could even use the slow eigenvector space as a parameter space. This would induce conservation parameters which do have a fixed value in the closed homogeneous system. These can then be removed from the Monte Carlo simulation, because some of these variables are exactly conserved even in different plasma conditions. They only depend on the initial conditions. However analyzing to what extent this reduction can be integrated is beyond the scope of this work. We just point out the possibility and might use it ourselves to accelerate our calculations for the localized reaction mechanism.

### 3.3.3 Illustration of the manifolds

The solution of the system is presented in the figures 3.1, 3.2 and 3.3. In 3.1 the time traces of a fast, reactive species (H) and a slow species (C) are given. The ILDM traces seem to be very good approximations for the complete system. The QSSA has no problem with the slow species but seems incorrect for the more stable C's. In the left figure of 3.2 the system's dynamics are plotted in the 3 dimensional composition space C – CH<sup>+</sup> – CH.

This full solution is repeated in the graphics 3.3. They are only plotted starting from the fifth time step in order to take a closer look at the manifolds. The true initial condition was

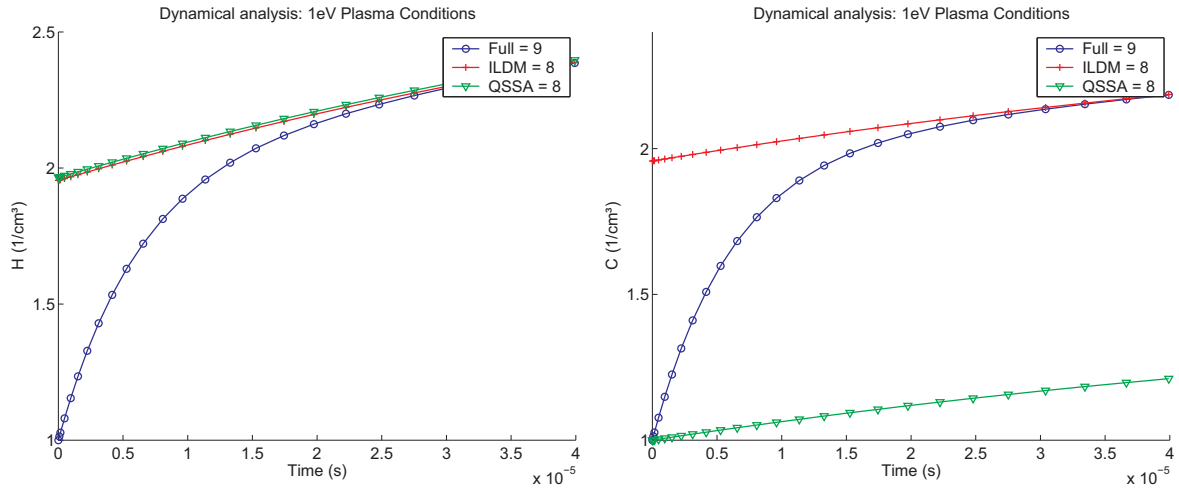


Figure 3.1: H and C time traces

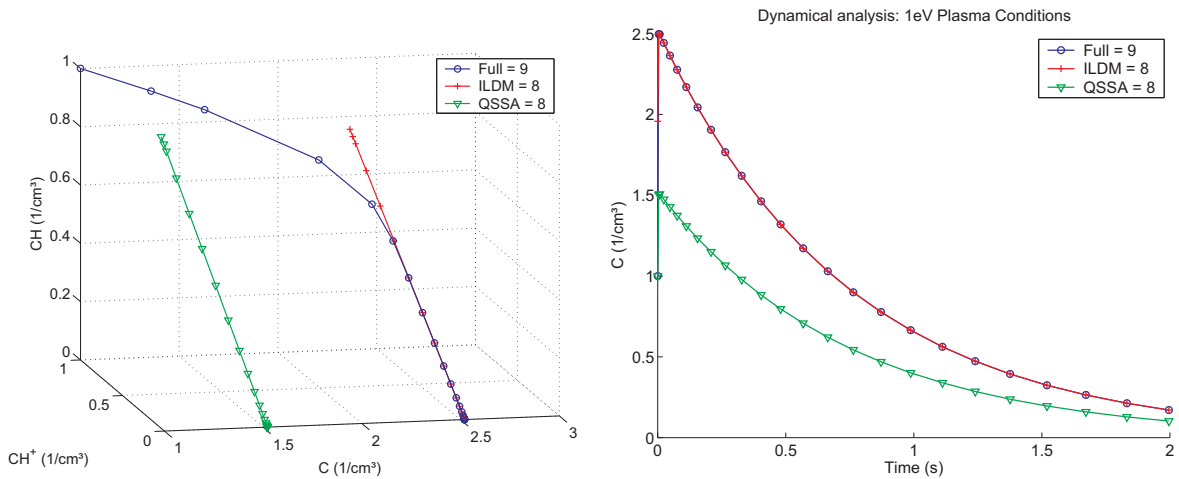


Figure 3.2: Representation in the composition space ( $C$ ,  $CH^+$  and  $CH$ ,  $t_{\max} = 1E - 3s$  and the time trace of  $C$  up to 2 seconds

$\phi_0 = (1E + 13, 1E + 13, 1, 1, 1, 1, 1, 1)^T$ . The initial points of the ILDM and QSSA solutions have been projected onto their respective manifolds. This will be explained in section 3.4.

The QSSA and ILDM manifolds are linear and are thus represented by planes in the composition space. The planes have also been rendered in the plots. One can easily see that the  $C$ -axis is contained in both of the manifolds. This follows from the equations on the last row of the transformation matrices (3.20) and (3.21). No  $C$  coefficient is to be found in the vectors. The left graph of 3.3 is a projection parallel to the  $C$  axis. So the 2 planes are represented by lines here. Under this angle the QSSA approximation is not much different from the ILDM. The full solution comes from its initial point nearly perpendicularly towards the planes and turns to adopt a motion in the ILDM plane and approximately parallel with the QSSA because both planes lie close together.

However in 3.3 left it can be seen that the QSSA solution stays away from the ILDM and

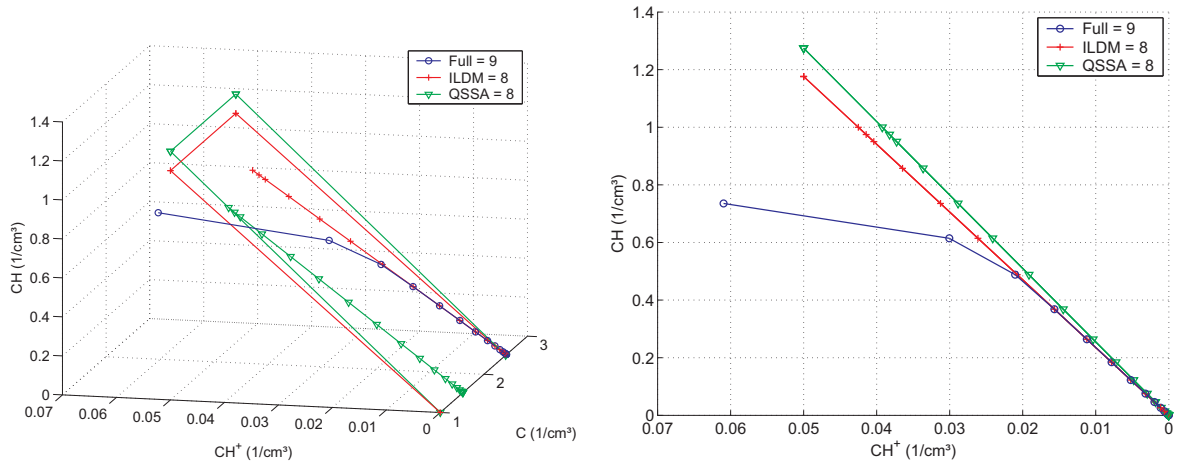


Figure 3.3: Representation of the linear manifolds in the C, CH<sup>+</sup> and CH composition space and the orthogonal projection onto the CH<sup>+</sup> – CH plane time is going until 1E-3 s

the full solution. The time traces of C (figure 3.1) and C<sup>+</sup> do not seem to converge with the full solution. The reason is that the diagonal element of CH<sup>+</sup> and CH in the Jacobian are very big, respectively  $-1.68\text{E}+05$  1/s and  $-1.30\text{E}+04$  1/s, while the C has a small value ( $-1.35\text{E}+00$  1/s). This is only so because the timescale is too small ( $4\text{E}-05$  s). In figure 3.2 right the time scale was increased to 2 seconds and the convergence becomes clear. This results from the use of conservation equations in matrix (3.20).

### 3.4 Perturbations: projection onto the manifold

#### 3.4.1 Projection onto the manifold

**Introduction** When simulating a random physical problem, the initial conditions ( $\vec{\phi}_0$ ) or boundary conditions could be a state outside the manifold. In order to calculate with less variables ( $\vec{\theta}$ ) in the reduced space these conditions should be projected on the manifold. Nevertheless there is more than one point on the manifold on which we could project. Should this point lie then as close as possible to the original one? The answer is no, not necessarily. It is obvious that doing so requires agreement with the conservation equations. Otherwise the system would not relax to the same equilibrium. Moreover the projection onto the manifold should be such that a same lapse of time is necessary to relax the new system to the equilibrium point. In the ILDM-method these requirements are achieved by a projection perpendicular to the slow left eigenvectors which indicate the direction where the reduced system wants to evolve.

**In general** however the derivative of the slow variables should be fixed to zero while one lets the fast variables relax onto the manifold. Then only when the projection has been effectuated correctly and the point lies on the manifold, the simulation can be started letting the slow variables evolve and imposing the conservation of the fast ones. We shall proceed now with a mathematical derivation of the projection for the linear case.

**Projection on the ILD Manifold** The projection of an arbitrary point  $\vec{\phi}_0$  on the intrinsic lower dimensional manifold manifold point  $\vec{\phi}_{0,m}$ <sup>2</sup> can be done in the following way. The new point  $\vec{\phi}_{0,m}$  should meet the following requirements:

1.  $\vec{\phi}_{0,m}$  doesn't alter the conservation variables of  $\vec{\phi}_0$  otherwise the same equilibrium state as for  $\vec{\phi}_0$  cannot be reached. Note that the first  $n_c$  left eigenvectors, with eigenvalue 0, are perfectly equivalent to the conservation equations. They span the same space.

$$\vec{c}_i \cdot (\vec{\phi}_{0,m} - \vec{\phi}_0) = 0 \quad i = 1, \dots, n_c$$

2.  $\vec{\phi}_0$  is projected perpendicularly onto the manifold in the point  $\vec{\phi}_{0,m}$  and thus perpendicular to the slow left eigenvectors which are tangential to the manifold:

$$\vec{u}_i^L \cdot (\vec{\phi}_{0,m} - \vec{\phi}_0) = 0 \quad \text{for } i = n_c + 1, \dots, m$$

3. Finally  $\vec{\phi}_{0,m}$  fulfills the ILDM-equations.

$$\vec{q}_i \cdot \vec{\phi}_{0,m} = 0 \quad \text{for } i = m + 1, \dots, n_s$$

It was already discussed in 3.2.3 that  $\vec{u}_i^L$  are equivalent vectors for  $\vec{q}_i$ .

The alternative vectors proposed imply that one can use the inverse eigenvector matrix  $U^L$  to project the point. This is what MAAS and POPE (1992b) and SCHMIDT (1995) use for the projection of the convection velocity vectors onto the manifold as we will also briefly explain in section 3.4.2. A nearly unit matrix is introduced to calculate the projection:

$$\vec{\phi}_{0,m} = U \begin{pmatrix} I_{m \times m} & 0_{m \times n_f} \\ 0_{n_f \times m} & 0_{n_f \times n_f} \end{pmatrix} U^L \quad \vec{\phi}_0 = U I_0 U^L \vec{\phi}_0 \quad (3.22)$$

To get the initial conditions in the parameter space one still needs to multiply with the transformation matrix:

$$\vec{\theta}_0 = T \vec{\phi}_{0,m}$$

Notice that if one would choose  $T = U^L$  the projection onto the manifold expressed in the parameter space becomes extremely simple:

$$\vec{\theta}_{0,m} = I_0 T \vec{\phi}_0$$

**Projection on the QSSA Manifold** The QSSA doesn't require projection. Not projecting induces errors. Normally it is not needed anyway to project the initial conditions onto the QSSA manifold. In combustion science this is often realistic because the radicals appear only at the higher temperatures and disappear as the temperature drops again. The fast species are thus seldom present in the initial conditions or boundary fluxes. This is also true for the hydrocarbon reaction mechanism. Nevertheless to start the reduced simulations it is needed to project the point onto the parameter space. This will be done directly with the parameter projection matrix ( $T$ ) from the previous section. Remember that this matrix contains the conservation equations.

$$\vec{\theta}_{0,m} = I_0 T \vec{\phi}_0$$

---

<sup>2</sup>subscript  $m$  indicates the point lies on the manifold

### 3.4.2 Transport as a perturbation of the chemistry

Just like an initial condition that doesn't lie on the manifold, the transport term can be seen as a motion that can make a point to leave the manifold. It is therefore necessary to project this movement onto the manifold. Recall that the full equation system, including transport, reads:

$$\frac{\partial \vec{\phi}(\vec{r}, t)}{\partial t} = \vec{F}(\vec{\phi}(\vec{r}, t)) + \vec{\Xi}(\vec{\phi}(\vec{r}, t)) \quad (3.23)$$

The vector  $\vec{\Xi}$  representing the influence of transport on the concentration derivatives. One can show that in this macroscopic approach convective transport cannot move the point away from the manifold as it only changes the conservation variables. This can be easily understood when a Lagrange transformation is applied for the convective processes. Consider a volume element moving with the fluid, convection indeed changes the position of the volume, but not its composition. Consequently convection doesn't influence the chemical kinetics. This reasoning is probably extendable for the Monte Carlo simulations. On the contrary when non-linear diffusion processes are considered, they do tend to push the composition away from the manifold. But if equal diffusivity is assumed for all species, only the movement tangential to the manifold will remain and the diffusion will have no influence on the chemical kinetics. For Monte Carlo transport codes these problems are not really applicable due to the direct simulation of single particles. In the 1-dimensional test grid presented in the results part of this report transport is present and has to be projected. Therefore we briefly explain how to project them. The projected transport term in the composition space is represented by  $\vec{\Xi}'$

$$\vec{\Xi}'(\vec{\phi}) = U \begin{pmatrix} I & 0 \\ 0 & 0 \end{pmatrix} U^L \vec{\Xi}(\vec{\phi}) = U I_0 U^L \vec{\Xi}(\vec{\phi}) \quad (3.24)$$

This term should still be projected onto the parameter space:

$$\vec{\Xi}'(\vec{\phi}) \xrightarrow{T} \vec{\Xi}'(\vec{\theta})$$

A more complete explanation on the mathematical background and how to handle the transport term in the ILDM-method can be found in SCHMIDT (1995) p. 56–62.

### 3.4.3 Example

The projection can be tested in a 1-dimensional test case. This model has been used once by applying the projection in figure 3.4 left,  $\phi_{m2} = U_2 I_0 U_2^L \phi_{m1}$ <sup>3</sup>, and once by neglecting the projection in figure 3.4 right, thus assuming the composition at the entrance of cell 2  $\phi_{m2}$  is the same as the composition  $\phi_{m1}$  leaving the previous cell. The red lines on the plots is the temperature step of 2.9eV between the first half (0.1eV) of the grid and the second half 2.8eV. The vertical temperature axis is however not given. It is obvious that when the temperature changes the composition lying on the cell with background conditions 1 the linear manifold is different than the one in cell 2 where new conditions have been imposed. The composition will have to be projected from manifold 1 onto manifold 2 even though no chemistry could occur in the mean time. This projection is however not effectuated in the ILDM method as described

<sup>3</sup>the index 2 refers to the next grid cell in which the particles enter

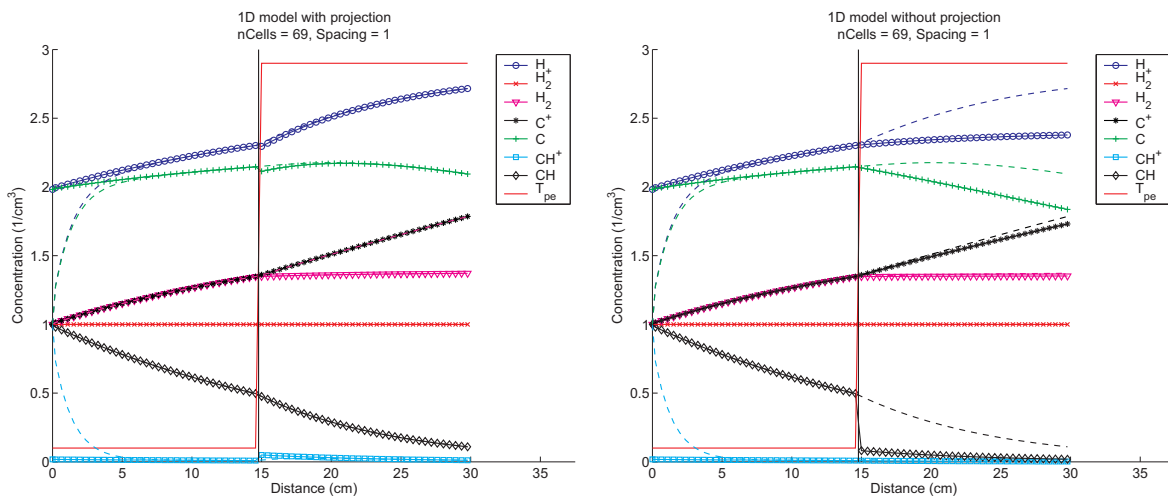


Figure 3.4: Comparison of the ILDM solution with (left) and without (right) projection for a 1-dimensional plug reactor with a temperature jump in the middle of the domain. More information: see text

and applied by MAAS and POPE (1992a). In their model the temperature parameter would simply be set to the new value. This implies however a loss in the convergence between the full solution and the ILDM solution. We compared the behavior of the system with and without the projection to check whether the solution converges to the full solution or not. The full solution is given in dashed lines. In the left figure of 3.4 one notices very clearly that a jump in composition space exists because of the projection from one manifold to another. This jump is quite small compared to the enforced energy jump of about a factor 30. The ILDM solution however converges perfectly with the full solution within a few grid cells. In the right figure of 3.4 the same system was implemented, but the projection was not done. This means the parameters from the first half were used as the initial conditions in the second half of the grid although a new manifold is to be used here. This gives no jumps in the solution of the parameters. Because the first eight species were chosen as parameters they do not show jumps. Note that for more randomly chosen parameters all species could show jumps. The CH species which is not taken as a parameter shows this discontinuity at the temperature jump. It is clear from the figure that omitting the projection results in loss of equilibrium. The projections at the cell boundaries are however very time consuming. It is then also the question whether a low calculation cost projection can be implemented in such methods.

### 3.5 Remarks on the parameters

#### 3.5.1 The difficulties

Until now it has been described how the manifold is parameterized and how initial conditions or transport terms are projected onto the manifold. There are two problems that will be discussed in this section. Firstly in a QSSA reduction the space spanned by the parameter vectors has repercussions on the outcome of the reduced simulation. However, this phenomenon is not observed in ILDM simulations. In this present work we suggest a choice of parameter equations which is different from the classical QSSA implementation. This choice

is founded in the first part of this section. The second issue is related to the dependency of these projection matrices ( $T, T^{-1}, U$  and  $U^L$ ) on the plasma conditions and species energy. In non-homogeneous conditions this results in the necessity to project the composition vector at the cell boundaries. Therefore the option to tabulate the manifold as a non-linear function of plasma conditions will be examined in the second part of this section. This whole section arises from problems encountered during the implementation and validation process of the program. They incited us to think forward towards a holistic implementation for EIRENE.

### 3.5.2 About the choice of the parameter equations

**General** At this point we consider it important to deal with the question how to choose the parameter vectors in  $P$  for the reduced system. We have already stated that they should be chosen linearly independent from each other and from the reduction vectors. In other words, together with the QSSA or respectively ILDM equations they span the whole composition space. But we experienced non consistent results between different parameterizations of the QSSA manifold. So arguably one cannot choose freely in every case.

**ILDM** For the ILDM method we found that one can choose freely the parameters. This follows from the fact that the system has been totally decoupled when transformed to the eigenvector space. It has been exploited by some authors and used to their advantage by finding a locally adapted and thus locally optimized parametrization (POPE, 1997).

**QSSA** With QSSA on the other hand different results were obtained for different parameterizations. An explanation is that the algebraic equations retrieved from the Jacobian are used to calculate the concentrations of the species assumed to be in quasi steady state. These equations contain the slow species as well as the QSS-species. Of course the slow ones vary through time as described by the reduced differential equation system. Consequently the concentrations of the QSS species have to evolve with them too. The assumptions first made  $\frac{\partial \phi_i}{\partial t} = 0, \forall i \in f$ , yet do not seem to be fulfilled anymore. As a result, when species were used as parameters, conservation was lost and the equilibrium state of the reduced system differed from the exact solution. It seems intrinsic to the QSSA method and is probably due to the fact that the system was not decoupled and the species were chosen by the user. The QSSA method appears to be very sensitive on the conditions in which it is applied. For good conditions were the assumptions are more or less valid, this discrepancy is not perceptible. In conditions not appropriate for the QSSA assumptions (often in low temperature ranges) or for bad choices of QSS species the results get really poor.

How is QSSA then normally applied? It cannot be found in literature that the QSSA manifold is parameterized in a special way. The many authors that use the method for reducing their system just take the *slow species as parameters*. The equations take the form  $\vec{p}_j = (0, \dots, 0, 1, 0, \dots, 0)$  with a 1 at the position of the species we want to take as a parameter. The differential equations to be solved are in this case equations of the slow species where the fast species have been replaced by a function of the slow ones. These functions are exactly the QSSA assumptions. Even though this approach seems logical at first sight, it is very sensitive to the conditions in which it is applied. But in nearly all cases it can be noticed that conservation is lost and that another equilibrium is obtained. Remember the analytical example 3.2.2 and the results in literature (Tzafiriri and Edelman, 1993). This loss is illustrated there with a clarifying analytical example.

This is very much in contrast with the QSSA-approaches applied in the *Monte Carlo* code EIRENE. This can be understood easily. When a species is assumed in quasi steady state it is short circuited. The chance or frequency to form that species remains. Its travel time is retained for a correct averaging of the concentrations after the Monte Carlo game, but its travel distance is assumed zero. When it is formed the code picks a product of the possible reactions it can undergo. So at the point of formation of that quasi steady state species another species is produced according to the chance distribution between the products of the QSS species. Because it only states that ions react on the spot, the conservation is maintained in the reactions and by extension also in the local Jacobian. Beside this most used QSSA-approach, there are other implementations of QSSA available in EIRENE. For these implementations tables have been made to simulate with reduced chemistry and retrieve the QSS-species concentrations from the tabulated QSSA relations. For us it is only important to remember that this second implementation also has the property to conserve.

To compare the QSSA method implemented in EIRENE we thus have to implement a QSSA that conserves the same *conservation* variables as from the full system. This can easily be done by ensuring that the space spanned by the conservation equations is contained in the space spanned by the parameter equations. This is achieved by introducing the conservation equations as parameter equations. The choice of the remaining parameter equations will of course still influence the results, though in practice the changes are negligible. This is the closest implementation to the QSSA in EIRENE. It has been validated by comparison to an EIRENE QSSA simulation for the closed homogeneous system.

**Note** Beside the problem of conservation, it is obvious that QSS-species cannot be chosen as parameters. This is due to the fact that the equation assumed in steady state is now also part of the reduced Jacobian. Using the equation of the quasi steady state for a particular QSS-species and filling it in the formula of the derivative of that same species in the reduced Jacobian will of course result in a zero derivative for that QSS-species. Corrupted results are thus obtained and many other species concentrations are refrained from evolving.

### 3.5.3 Non-linear manifold when including the plasma parameters

It has already been quoted in this text that the matrices used to project onto the manifold and the matrices to project manifold points on the parameter space depend non-linearly on the plasma conditions. These matrices are the direct link to the manifold. But this representation of the manifold is only valid for the particular case of  $\phi_{e^-}, \phi_{p^+}, T_{e^-}, T_{p^+}$ . This means that other plasma conditions, e.g. in the next grid cell, require new matrices and thus a new manifold in the composition space. This also implies that crossing the boundary of a cell requires a projection from the parameter space to the composition space. In the composition space the point lying on the manifold of the previous cell is projected onto the manifold of the new cell. This new point in the composition space then requires a projection back onto the parameter space of the new manifold. This means going from cell 1 to cell 2, having respectively manifold 1 (subscript  $m1$ ) and manifold 2 (subscript  $m2$ ).

$$\vec{\theta}_1 \rightarrow \vec{\tilde{\theta}}_{m1} \xrightarrow{T_1^{-1}} \vec{\phi}_{m1} \xrightarrow{U_2 I_0 U_2^{-1}} \vec{\phi}_{m2} \xrightarrow{T_2} \vec{\tilde{\theta}}_{m2} \rightarrow \vec{\theta}_2 \quad (3.25)$$

$U_2$  is the column matrix of the eigenvectors of the Jacobian at plasma conditions 2. This is how it is implemented in the section on the 1-dimensional problem. The disadvantage is a very CPU-time consuming algorithm.

Fortunately it can be taken care of this non-linearity by a tabulation *in the state space* where also the plasma conditions are used to parameterize the manifold. Instead of working purely in the composition space the manifold is now elaborated with extra parameters. Going from one cell to another is now simpler. The plasma conditions containing parameters change from one cell to the next and by table look-up the correct concentrations and parameter rates can be retrieved, which are now immediately dependent on plasma conditions as well. This is what we recommend to finally implement ILDM in EIRENE.

### 3.6 Reducing the Monte Carlo code Eirene

The ILDM technique seems a good method to automatically reduce the hydrocarbon reaction system. By eliminating movement only in the fastest directions it ensures the best possible approximation for a specified number of parameters. Unfortunately, it is not possible to directly implement the ILDM algorithm as such in the Monte Carlo code EIRENE. This code follows a huge amount of single particles through the spacial grid and does not calculate concentrations until enough particle trajectories have been simulated such that the statistical noise (=error) is reduced down to a certain level. The concentrations are determined at this stage by averaging the residence time of all these particles in the different grid cells. It is clear that EIRENE requires information about the actual reactions that take place, as well as their rates and their chance distribution. Analogously to reducing deterministic codes, reducing the calculation effort in EIRENE can be realized by reducing the number of species/variables and making new reactions in which only these new variables (=parameters) participate. After averaging the many chance experiments with the reduced system, one can then use the reduction equations to calculate the concentrations of the original species from the parameter concentrations. The technique we propose to achieve the reduction is still based on determining the reduced Jacobian of the ILDM parameter space. We will first show that the columns of the Jacobian represent locally a kind of condensed chemical reactions.

#### 3.6.1 Localized reaction mechanism

When translating the reaction scheme into a system of differential equations the various reactions seem to get lost by summation of the reaction rates in the chemical source term (see 2.19). The chemical source term is in general dependent on the plasma temperatures, the particle energy and the plasma densities. It is precisely the **external** dependency of the plasma densities that allows us to linearize the system. Locally the system can be represented by:

$$\frac{\partial \vec{\phi}}{\partial t} = F_{\vec{\phi}}|_{\vec{\psi}_0} \vec{\phi}$$

The elements of the Jacobian  $F_{\vec{\phi}}|_{\vec{\psi}_0}$  are also a sum of different reactions. Nevertheless this can be reinterpreted into a chemical reaction system. Though some information as e.g. the exact reactions is lost when building the Jacobian, it still contains enough information to reconstruct an equivalent reaction scheme and run the Monte Carlo simulation. Likewise from the reduced Jacobian in the parameter space new reactions can be retrieved with the parameters as new species. The parameter concentrations can be calculated from the Monte Carlo simulation. These concentrations will be transformed back onto the basis of the state space by means of the parameter and reduction equations. This technique seems quite simple

but in practice a lot of problems arise. A ‘proof of principle’ follows in the validation of the program.

**Example of localized reaction mechanism**

The easiest way to clarify the significance of the Jacobian matrix is with an example. From the hydrocarbon reaction mechanism the following 5 CH<sub>4</sub> reactions were selected to present a model simple reaction system. As explained in section 2.2.2 the rate of change of each species can be calculated using the reaction matrix, the reaction rate coefficients ( $\omega$ ) and the concentration of all species. Due to the nature of collision reactions and because of the high

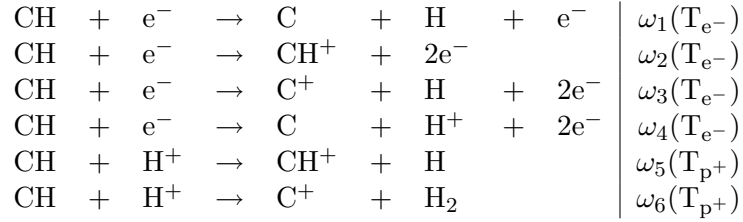
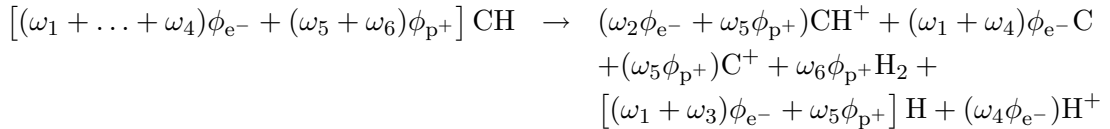


Table 3.1: The CH reactions and their rates

concentration of the background, the rates of change are linear functions of the hydrocarbon species concentrations. Keep in mind that although the Jacobian is independent from the species concentrations, it is nevertheless dependent on the background conditions and the species energies. For the model reaction system (table 3.1) the Jacobian contains all zero columns except for the CH column. The e<sup>-</sup> and p<sup>+</sup> are part of the plasma and are not considered.

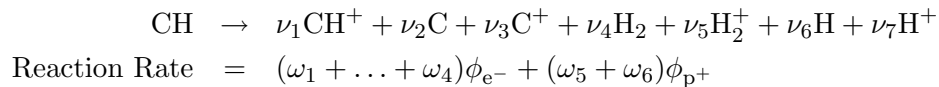
	H	...	CH <sup>+</sup>	CH
H	0		0	$\omega_1 \cdot \phi_{e^-} + \omega_3 \cdot \phi_{e^-} + \omega_5 \cdot \phi_{p^+}$
H <sub>2</sub> <sup>+</sup>	0		0	0
H <sub>2</sub>	0		0	$\omega_6 \cdot \phi_{p^+}$
C <sup>+</sup>	0		0	$\omega_5 \cdot \phi_{p^+}$
C	0		0	$\omega_1 \cdot \phi_{e^-} + \omega_4 \cdot \phi_{e^-}$
CH <sup>+</sup>	0		0	$\omega_2 \cdot \phi_{e^-} + \omega_5 \cdot \phi_{p^+}$
CH	0		0	$\omega_1 \cdot \phi_{e^-} - \omega_2 \cdot \phi_{e^-} - \omega_3 \cdot \phi_{e^-} - \omega_4 \cdot \phi_{e^-} - \omega_5 \cdot \phi_{p^+} - \omega_6 \cdot \phi_{p^+}$

It becomes clear now that all CH<sub>4</sub> reactions are grouped together in the last column of the Jacobian. Locally, for a specified ( $\phi_{e^-}, \phi_{p^+}, T_{e^-}, T_{p^+}$ ), this can be seen as one reaction. This reaction can be used to represent the reaction model of table 3.1. In the next equation  $T_{e^-}$  and  $T_{p^+}$  are not written any more, to simplify the notations. The reaction based on the column of the Jacobian can be written as:



It appears that the coefficient in the Jacobian offer enough information to write down the new reactions and their rates. The diagonal element is always chosen as the reactant and the other coefficients are the product’s coefficients. Although this new reaction conserves elements

and charge, it is not a real chemical reaction, because its coefficients are dependent of  $\phi_{e^-}$ ,  $\phi_{p^+}$ ,  $T_{e^-}$ ,  $T_{p^+}$ , and  $E_s$ . Locally however the coefficients are fixed. And this can be interpreted as a chemical reaction. In this reaction the coefficient of  $\text{CH}_4$  represents the total chance a CH will collide (see equation 2.10), either with a proton or with an electron. Therefore the reaction coefficients of the products should be divided by the coefficient of CH. The reaction then takes the form of a collision reaction and the output can be easily calculated when following one CH particle:

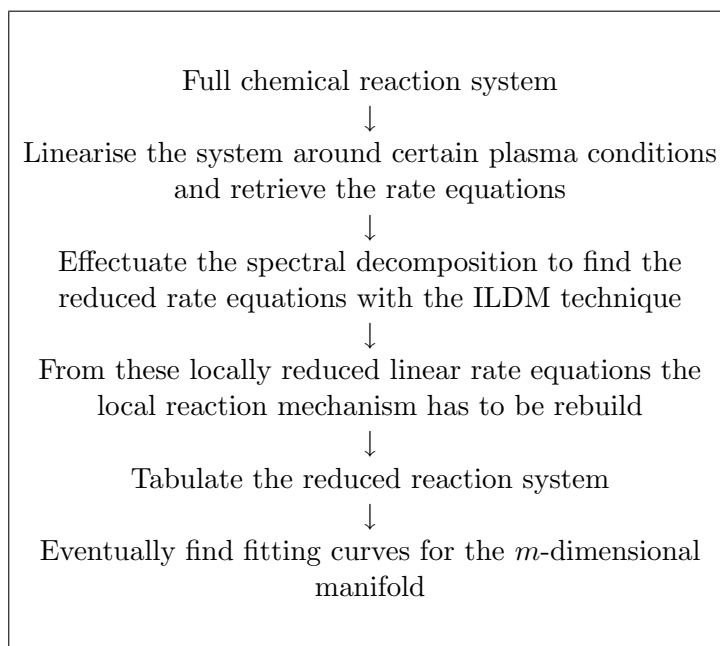


In this example only  $\text{CH}_4$  reacted with the background plasma. If more species react with the background plasma, one localized reaction can be made for every species. The new localized reaction mechanism, based on the local Jacobian thus consists of  $n_s$  reactions and one localized rate for every reaction.

### 3.6.2 Strategy for implementation

The following strategy seems the most appropriate for implementation of the ILDM in EIRENE. The goal is to rebuild a reaction mechanism with a reduced number of variables (chosen by the user) and reactions. This computationally less expensive reaction mechanism can then be used for the Monte Carlo simulations. To achieve this one can start by reducing the local Jacobian. From this reduced Jacobian the reduced reaction mechanism can be set up. What is obtained now is a reaction mechanism valid at the specific plasma conditions  $\phi_{e^-}$ ,  $\phi_{p^+}$ ,  $T_{e^-}$ ,  $T_{p^+}$ , and the species energy  $E_s$ . This has to be elaborated for a range of plasma conditions and parameter energies. Therefore one could tabulate these Jacobian matrices. To avoid the use of excessive memory for tabulation the good option would be to construct a set of fitting curves for the reduced mechanism. These curves can be used analogously as for the full mechanism to run the simulations. Of course once the parameter concentrations have been averaged from the big amount of chance experiments, the concentrations in the full state space can be calculated using the inverse of the matrix that projects the state space onto the parameter space. Notice that this matrix will also depend on plasma conditions.

Schematically the procedure can be represented as:



### 3.6.3 Strange effects in the reduced space

The problem with the reduced space is that the parameters cannot be chosen totally free as the hydrocarbon transport code requires a separate handling of ions and neutrals. Ions are passed to the separate charged particle module in EIRENE or even to the code B2 for motion along the magnetic field lines.

Secondly the new reduced Jacobian can contain reactions that are physically impossible. For example only negative coefficients occur in the column. Do not mistake. These are not wrong results. It is a consequence of the reduction. The real question is: "Is this problematic for EIRENE?" In the Monte Carlo game negative weight coefficients can be attributed to the collision reaction products. A negative weight coefficient means that when averaging the species residence time this time should be subtracted. There is however one disadvantage to this procedure. The noise (error) on the Monte Carlo result increases a lot if sign changes are involved in the contributions to final results.

Thirdly information about the energy that is released or required by the new reactions must be calculated. Also new scattering angles must be determined. Although a solution has only be given for replacing travel lengths and reaction products, the approach can very certainly be extended towards integration of all involved reaction characteristics, including scattering and kinetic energy of the products. This is part of the future work beyond this initial study.

## 3.7 Conclusion

In this chapter the reader was introduced to reduction methods and the wide variety of conventional and more recent approaches to reducing chemical systems. In the first section 3.2 the Quasi Steady State Approximation and the Intrinsic Low Dimensional Manifold, are

elaborated in detail. Their reduction equations defining the manifold are exposed for the linear problem and implemented in an easy to handle matrix structure. The parameter projection matrix can be used to convert manifold points from the state space to the parameter space. Throughout the chapter the example from the chemistry chapter 2 is used to illustrate the concepts. In a second stage it is important to know how to project the state space onto the manifold, for initial conditions do not necessarily lie on the manifold and transport can drive the state away from the manifold. Section 3.4 explains how points ought to be projected from wherever it be onto the manifold. A remark section was added on the delicate subject that the choice of parameter equations is for the implementation. To conclude the ILDM technique is adapted towards integration into the Monte Carlo transport code EIRENE (section 3.6). The concepts of how it can be done are explained based on an interpretation of the local Jacobian matrix. The interpretation of the Jacobian is first explained whereafter the strategy of implementation follows. The strategy has been tested with a simple example and the problems encountered doing the first steps into this new domain are discussed briefly in the last subsection of 3.6. The actual implementation of the scattering angles and energy exchange during the reaction belongs to the future work.



## Chapter 4

# ADMT Fortran Code

### 4.1 Introduction

To study the potential of the existing reduction methods on the hydrocarbon mechanism we developed a numerical tool in Fortran. This program, called ‘ADMT’ is an extended version of a perl program, called Hydkin (REITER, 2006), that simulates the behavior of the hydrocarbon chemistry in a deterministic way. In addition to simulating the ‘full’ behavior of the hydrocarbon chemistry, ADMT extends Hydkin with an ILDM and a QSSA analysis of this behavior, to determine the ‘reduced’ behavior of the chemistry.

ADMT is a tool for investigating the hydrocarbon reaction system, and it allows the user to make several important analysis. First, it can be used to calculate the kinetic coefficients of all the hydrocarbon reactions for different plasma conditions. Secondly, it makes an eigenvalue analysis of the Jacobian matrix for different plasma conditions. This allows to study the decay of the Jacobian’s stiffness and eigenvalues with a changing plasma temperature and species energy. Thirdly, the program can solve the differential equation system that models a closed chemical reactor (0D). By comparing the full solution of this model to an ILDM or a QSSA solution of arbitrary size, the reduction potential of these two methods can be investigated. Finally, the program can simulate a plug reactor (1D). The importance of this one dimensional convective transport model is the possibility to study the behavior of the ILDM or the QSSA solution at the boundary of grid cells, that have a different plasma condition.

The main goal of this chapter is to provide the reader with enough information about the ADMT program We will try to achieve this in consecutive steps: First, the structure of the ADMT program will be discussed and illustrated in section 4.2. Secondly, the results of our program will be validated in section 4.3. Finally, in section 4.4, we will indicate how to use the program and how to predict some results.

### 4.2 ADMT structure

The ADMT program consists of three major parts. First, the user has to specify the setup of the program, next the program calculates all required data and finally, the data are exported to Matlab for postprocessing. Before discussing each of these parts in detail, we will start this section with the general flow diagram of the program.

## 4.2.1 Flow chart of the program

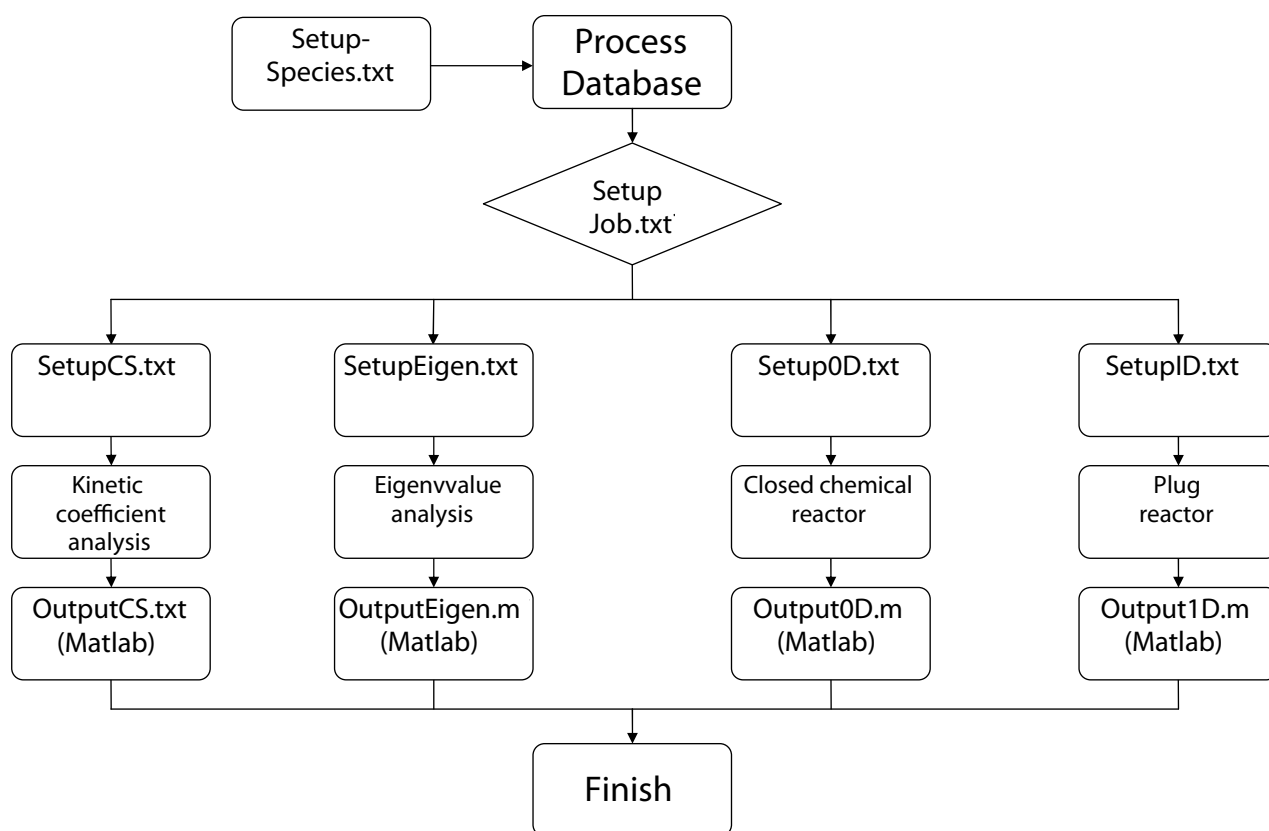


Figure 4.1: General flow diagram of ADMT

## 4.2.2 Preprocessing

Before running the program, the user is required to specify what he or she wants to simulate. To set up ADMT at least three input files must be adapted:

**SetupSpecies.txt** provides ADMT with information about the hydrocarbon reaction mechanism and it consists of two parts. In the first part of SetupSpecies.txt, the user has to specify the text file that contains the names of all reaction files. These files cover the stoichiometry of each reaction, together with the parameters of their rate coefficient formula. In the second part of SetupSpecies.txt, the user has to specify all species, that are present in the reactions. In general SetupSpecies.txt only requires to be adapted when new reactions and/or species are added to the hydrocarbon database.

**SetupJob.txt** specifies which type of analysis will be made. The user can select a certain analysis by setting the corresponding boolean from false ('F') to true ('T'). ADMT allows to make four analyses:

- Kinetic Coeff Analysis (T/F)

- Eigenvalue Analysis (T/F)
- 0-Dim Problem (T/F)
- 1-Dim Problem (T/F)

The setup of these analyses will be discussed next.

Depending on which analyses the user specified in SetupJob.txt, the following text files must be adapted:

**SetupCS.txt** is used when calculating the cross sections and the reaction rate coefficients of the hydrocarbon system for different plasma conditions. It is divided in two parts. In the first part, a vector of background energies is specified for the calculation of the cross sections. In the second part, the user has to specify a vector of background temperatures and a vector of species energies for the calculation of the rate coefficients.

**SetupEigen.txt** specifies the setup when making an eigenvalue analysis of the Jacobian matrix of the chemical source term for different plasma conditions. As the Jacobian depends on the plasma concentration, the plasma temperature and the energy of the species, see section 2.3.3, these conditions must be specified by the user.

**Setup0D.txt** is used when simulating the behavior of a closed chemical reactor. The file consists of three parts. In the first part, the user has to provide information about the number of species in the reactor ('nSpec'), about the type of simulation ('Full', 'QSSA' or 'ILDM') and about the size of the reduced space. In the second part, the time vector must be specified and finally, in the third part, all species which are present in the reactor must be provided with an initial condition and a fixed energy. The concentration and the energy of the electrons and the protons represent the background concentration and the plasma temperature respectively.

**Setup1D.txt** is used when simulating the behavior of a plug reactor. In addition to the variables required in Setup0D.txt, the user has to specify the convective speed, the size of the simulation domain, the number of grid cells and the spatial behavior of the background conditions, which can be constant ('const'), linear ('lin'), exponential ('exp') or a step function ('step').

### 4.2.3 Processing

After completing the input text files, the program can be executed. As the program operates, it passes through subsequent parts. The main goal of this section is to explain how each of these parts works, by relating them to the theory presented in chapters 2 and 3.

#### Reaction and parameter matrix

No matter what the user specified in 'SetupJob.txt' the program will always first process the information specified in 'SetupSpecies.txt'. Reading in the reaction text files, leads to the creation of the stoichiometric coefficient matrix, see equation (2.16) and a reaction parameter

matrix, that stores the parameters of the cross section and the rate coefficient formulas, specified in section 2.2.2. These two matrices represent the hydrocarbon reaction mechanism and form the base of all calculations.

### Cross sections and rate coefficients

If the user specified ‘T’ for ‘Kinetic Coeff Analysis’ in SetupJob.txt, the program will use the parameters in the parameter matrix together with the formulas presented in section 2.2.2, to calculate the cross sections and the rate coefficients of all reactions in the reaction matrix. Because the plasma energy, the plasma temperature and the species energies are specified in the form of arrays in SetupCS.txt, the output of this analysis will be a two dimensional cross section matrix ( $n_{EP} \times n_r$ ) and a three dimensional rate coefficient matrix ( $n_{ES} \times n_{TP} \times n_r$ ). With  $n_{ES}$ ,  $n_{EP}$  and  $n_{TP}$  being the size of the species energy, the plasma energy, and the plasma temperature array respectively and with  $n_r$  being the number of reactions.

### Eigenvalue analysis of the Jacobian matrix

If ‘Eigenvalue Analysis’ is selected in SetupJob.txt, the program makes a spectral decomposition of the Jacobian matrix for each combination of background conditions specified in SetupEigen.txt. The eigenvalues of the Jacobian are easy to determine because they are on its diagonal elements, see section 2.3.3. The Jacobian itself is calculated with the use of equation (2.27). This analysis stores the eigenvalues in a six dimensional eigenvalue matrix ( $n_{T_{e-}} \times n_{T_{p+}} \times n_{\phi_{e-}} \times n_{\phi_{p+}} \times n_{ES} \times n_s$ ). With  $n_s$  being the number of species.

### The closed chemical reactor

If the user specifies to solve the ‘0-Dim Problem’ in SetupJob.txt, the program will numerically solve the homogenous system of linear differential equations that represents the chemical source term or a reduced form of it.

**Equation system** The system of differential equations that models a closed chemical reactor are given by:

$$\frac{\partial \vec{\phi}(t)}{\partial t} = F_{\vec{\phi}} \cdot \vec{\phi}(t) \quad \vec{\phi}(0) = \vec{\phi}_0 \quad \text{Full system} \quad (4.1)$$

$$\frac{\partial \vec{\theta}(t)}{\partial t} = F'_{\vec{\theta}} \cdot \vec{\theta}(t) \quad \vec{\theta}(0) = \vec{\theta}_0 \quad \text{Reduced system} \quad (4.2)$$

with  $F_{\vec{\phi}}$  being the Jacobian matrix of the full system,  $F'_{\vec{\theta}}$  being the Jacobian matrix of the reduced system and  $\vec{\theta}_0$  being the projection of  $\vec{\phi}_0$  onto the manifold. The background conditions are specified as:

$$\begin{aligned} T_{e-}(t) &= T_{e-}(0) \\ T_{p+}(t) &= T_{p+}(0) \\ E(t) &= E(0) \end{aligned}$$

with  $T_{e-}(0)$ ,  $T_{p+}(0)$  and  $E(0)$  being the initial conditions of the electron temperature, the proton temperature and the species energy respectively.

**Components** The Jacobian matrix of the full system can easily be calculated using equation (2.27), whereas the reduced Jacobian depends on the Jacobian of the full system, on the size and the method of reduction and on the parametrization of vector  $\vec{\delta}$ . It is calculated with the use of equation (3.17).

**Initial conditions** The projection  $\vec{\phi}_0$  to  $\vec{\theta}_0$  is implemented as described in section 3.4. The eigenvectors, which are required to project, are calculated with the help of the NAG Fortran subroutine F02EBF (NAG, 2006).

**Numerical solution** The numerical solution of equations (4.1) and (4.2) is different, because of the different structure of both of these matrices. The upper triangular structure and the disparateness of the eigenvalues of  $F_{\vec{\phi}}$  enable the use of an implicit solver with backward substitution, see section 2.3.4, but they prohibit the use of an explicit solver. The reduced Jacobian  $F'_{\vec{\theta}}$  on the contrary, has a much lower stiffness than  $F_{\vec{\phi}}$ , but loses its upper triangular structure for certain parameterizations  $\vec{\delta}$ , which enables the use of an explicit solver but prohibits the use of backward substitution in the implicit solver. For the sake of stability, we also implemented an implicit solver for equation (4.2).

**Output** In case of simulating the full system, the solution can be directly stored into the solution matrix ( $n_s \times n_t$ ), with  $n_t$  being the size of the time vector, whereas in case of simulating the reduced system, the solution must first be transformed back to the composition space, using equation (3.16), before storing it into the solution matrix.

### The plug reactor

If the user selects ‘1-Dim Problem’ in SetupJob.txt, the program will numerically solve the system of linear differential equations that represents the one dimensional convective transport of the hydrocarbon mixture. As the mixture moves through the reactor, it can experience changing background conditions.

**Equation system** The system of differential equations that models a plug chemical reactor are given by:

$$\frac{\partial \vec{\phi}(t, x)}{\partial t} = F_{\vec{\phi}}(x) \cdot \vec{\phi}(t, x) - V(x) \cdot \frac{\partial \vec{\phi}(t, x)}{\partial x} \quad \vec{\phi}(0, x) = \vec{\phi}_0(x) \quad (4.3)$$

$$\frac{\partial \vec{\theta}(t, x)}{\partial t} = F'_{\vec{\theta}}(x) \cdot \vec{\theta}(t, x) - V'(x) \cdot \frac{\partial \vec{\theta}(t, x)}{\partial x} \quad \vec{\theta}(0, x) = \vec{\theta}_0(x) \quad (4.4)$$

with  $F_{\vec{\phi}}(x)$  and  $F'_{\vec{\theta}}(x)$  being the Jacobian matrices for the full and the reduced system respectively at a distance  $x$ , with  $V(x)$  being a diagonal matrix that contains the speed of a species ( $V_{ii} = \sqrt{2E/M_i}$ ) on its diagonal and  $V'(x)$  being the projection of  $V(x)$  onto the manifold at  $x$ . In addition to these partial differential equations, the background conditions must be specified:

$$\begin{aligned} T_{e-}(t, x) &= T_{e-}(0, x) \\ T_{p+}(t, x) &= T_{p+}(0, x) \\ E(t, x) &= E(0, 0) \end{aligned}$$

**Components** The components of the partial differential equations (4.3) and (4.4) must be evaluated in each grid cell ( $x_i$ ). The full and the reduced Jacobian matrices are calculated for each cell as explained in the previous section. The speed matrix is the same for each cell ( $V(x) = V$ ), because we assumed the hydrocarbon particles to have a constant speed. The reduced speed matrix  $V'(x)$  however, is different in each cell, as it depends on the projection matrices, which change from cell to cell.  $V'(x)$  is calculated by using equation (3.24) together with the fact that  $\vec{\phi}(t, x) = T^{-1}(x) \cdot \vec{\theta}(t, x)$ :

$$V'(x) = T(x) \cdot U(x) \cdot \begin{pmatrix} I & 0 \\ 0 & 0 \end{pmatrix} \cdot U^{-1}(x) \cdot V \cdot T^{-1}(x) \quad (4.5)$$

**Initial conditions** In a reduced simulation, the initial condition of each grid cell must be projected onto the cell's manifold. The projection algorithm is identical to the one used for the projection of the initial condition of the closed reactor.

**Boundary conditions** The upwind scheme used to solve equations (4.3) and (4.4), only requires one boundary condition, at the upwind boundary of the domain. We implemented a constant influx  $\vec{J}$  boundary condition, because this represents the constant sputtering of hydrocarbon particles from the divertor plate:

$$\vec{J}(t, x_0) = V \cdot \vec{\phi}(0, x_0)$$

with  $x_0$  being the position of the upwind boundary. The user only has to specify the boundary condition of the full system, because the reduced equation uses the projection of  $\vec{\phi}(0, x_0)$  as its boundary condition.

**Numerical solution** As only convection is present in this transport model, the upwind scheme can be used. It is obtained by using the backward difference formula for the spatial derivative. For an implicit solver, the upwind scheme is given by:

$$\left( I - \Delta t \left( F_{\vec{\phi}}(x_k) - \frac{V}{L_k} \right) \right) \vec{\phi}(t+1, x_k) = \vec{\phi}(t, x_k) + \frac{V \cdot \vec{\phi}(t+1, x_{k-1})}{L_k} \Delta t \quad (4.6)$$

$$\left( I - \Delta t \left( F_{\vec{\theta}}(x_k) - \frac{V'(x_k)}{L_k} \right) \right) \vec{\theta}(t+1, x_k) = \vec{\theta}(t, x_k) + \frac{V'(x_k) \cdot \vec{\theta}'(t+1, x_{k-1})}{L_k} \Delta t \quad (4.7)$$

with  $I$  being the unit matrix,  $x_k$  being the position of the middle point of cell  $k$ ,  $L_k$  being its length and  $x_{k-1}$  being the position of the middle point of the cell upwind from cell  $k$ . Note that the right hand side of equations 4.6 and 4.7 still contains a concentration vector which must be evaluated at  $t+1$ . This is normal because the concentration of the upwind cell at  $t+1$  is already known. When solving the reduced equation, care should be taken not to use the concentration of cell  $k-1$ , but to use its projection on the manifold of cell  $k$ . The projection is made with the help of equation (3.25):

$$\vec{\theta}'(t+1, x_{k-1}) = T_k \cdot U_k \cdot \begin{pmatrix} I & 0 \\ 0 & 0 \end{pmatrix} \cdot U_k^{-1} \cdot T_{k-1}^{-1} \cdot \vec{\theta}(t+1, x_{k-1})$$

As only cells  $k-1$  and  $k$  occur in the algebraic equations (4.6) and (4.7), they require only one boundary condition,  $\vec{\phi}(t, x_0)$  and  $\vec{\theta}(t, x_0)$  respectively, to be solved.

**Output** When simulating the full system, the solution of equation (4.3) can be directly stored into the three dimensional solution matrix ( $n_s \times n_t \times n_{Cells}$ ), with  $n_{Cells}$  being the number of grid cells. In case of simulating the reduced system, the solution of each cell must first be transformed back to the composition space, using equation (3.16), before storing it into the solution matrix.

#### 4.2.4 Postprocessing

Finally, all results of ADMT are exported to Matlab for postprocessing. To help the user we have written m-files in Matlab, which first build the input files, then run the executable of ADMT and finally analyze the output graphically. These standard analyses will be discussed briefly in what follows.

**AnalyseCS.m** commands ADMT to make a kinetic coefficients analysis of the hydrocarbon reaction mechanism. **OutputCS.m** can be used to make plots of the cross sections vs. plasma energy decay and of the reaction rate coefficients in function of the plasma temperature and the species energy.

**AnalyseEigen.m** commands ADMT to run an eigenvalue analysis of the Jacobian matrix for different plasma temperature-species energy combinations. The results are processed by **OutputEigen.m** to plot the Jacobian's stiffness in function of the plasma temperatures and species energies. It also plots all non zero eigenvalues for a range of plasma temperatures at a specified species energy.

**Analyse0D.m** simulates the behavior of the hydrocarbon mixture in a closed reactor for different types and sizes of manifolds. In order to achieve this, **Analyse0D.m** has to run ADMT for each manifold. **Output0D.m** makes plots of the hydrocarbon concentration vs. time and of the concentration of one species in function of another species.

**Analyse1D.m** orders ADMT to simulate the behavior of the hydrocarbon mixture in a slug reactor, again for different types and sizes of manifolds. For each species **Output1D.m** plots the time dependent solutions of all manifolds in function of the distance.

The importance of all of these analyses will become clear in the results chapter 5.

### 4.3 Validation of ADMT

To guaranty the plausibility of the results of the ADMT program, we will validate all of its analyses in this section. First the calculation of the kinetic coefficients, next the implementation of the solvers and finally, the implementation of the reduction techniques will be validated.

#### 4.3.1 Validation of the kinetic coefficients

As already mentioned in the introduction, ADMT is an extended version of the perl program **Hydkin**. Beside simulating the behavior of the hydrocarbon chemistry in a deterministic

way, the latter program also offers the possibility to evaluate the cross sections and the rate coefficients of the hydrocarbon reactions, for different energies and temperatures respectively. Therefore, the calculation of the kinetic coefficients can be validated by comparing the results of both programs. In what follows, first the calculation of the cross sections and then the calculation of the rate coefficients will be validated.

### Cross Sections

Under divertor conditions, the interactions between the hydrocarbons (neutrals and ions) and the main plasma particles (electrons, protons) provoke ionization, dissociative excitation, recombination and charge exchange reactions, that were presented in section 2.2.1. Based on the results of mono-energetic collision experiments, Janev and Reiter derived seven types of analytical fitting formulas for the cross sections ( $\sigma$ ) of all the hydrocarbon reactions. These fitting formulas were presented in section 2.2.2. Table 4.1 illustrates the perfect match between the Hydkin and the ADMT calculation of the cross sections, for equation type five. This is also the case for the other equation types. Their tables can be found in appendix A.

$\sigma$ (cm <sup>2</sup> )		Plasma energy (eV)					
		1eV	205eV	409eV	613eV	817eV	1000eV
r_3966.t_6							
react 1 (a)	<i>Hydkin</i>	4.65E-15	2.79E-15	2.61E-15	2.50E-15	2.42E-15	2.37E-15
	ADMT	4.65E-15	2.79E-15	2.61E-15	2.50E-15	2.42E-15	2.37E-15
react 2 (b)	<i>Hydkin</i>	9.20E-16	2.41E-22	3.03E-23	9.00E-24	3.80E-24	2.07E-24
	ADMT	9.20E-16	2.41E-22	3.03E-23	9.00E-24	3.80E-24	2.07E-24
react 3 (a)	<i>Hydkin</i>	5.13E-15	3.08E-15	2.88E-15	2.77E-15	2.69E-15	2.64E-15
	ADMT	5.13E-15	3.08E-15	2.88E-15	2.77E-15	2.69E-15	2.64E-15
r_4005.t_9							
react 1 (a)	<i>Hydkin</i>	2.12E-15	5.83E-16	7.45E-16	8.57E-16	9.42E-16	1.00E-15
	ADMT	2.12E-15	5.83E-16	7.45E-16	8.57E-16	9.42E-16	1.00E-15
react 2 (b)	<i>Hydkin</i>	3.75E-17	4.58E-24	5.77E-25	1.71E-25	7.24E-26	3.94E-26
	ADMT	3.75E-17	4.58E-24	5.77E-25	1.71E-25	7.24E-26	3.94E-26
react 3 (a)	<i>Hydkin</i>	4.72E-16	1.51E-16	2.48E-16	3.22E-16	3.82E-16	4.27E-16
	ADMT	4.72E-16	1.51E-16	2.48E-16	3.22E-16	3.82E-16	4.27E-16
r_4005.t_16							
react 1 (a)	<i>Hydkin</i>	1.75E-15	7.51E-16	8.77E-16	9.50E-16	9.99E-16	1.03E-15
	ADMT	1.75E-15	7.51E-16	8.77E-16	9.50E-16	9.99E-16	1.03E-15
react 2 (b)	<i>Hydkin</i>	1.69E-17	2.03E-24	2.55E-25	7.58E-26	3.20E-26	1.74E-26
	ADMT	1.69E-17	2.03E-24	2.55E-25	7.58E-26	3.20E-26	1.74E-26
react 3 (b)	<i>Hydkin</i>	1.12E-17	1.35E-24	1.70E-25	5.05E-26	2.13E-26	1.16E-26
	ADMT	1.12E-17	1.35E-24	1.70E-25	5.05E-26	2.13E-26	1.16E-26

Table 4.1: Comparison of the cross sections (cm<sup>2</sup>) for equation type 5

Having a closer look at table 4.1, one can see that the cross sections have been compared for different plasma energies and for different reactions. The reason why we have chosen to compare reactions from files r\_3966.t\_6, r\_4005.t\_9 and r\_4005.t\_16, is twofold. Firstly, we have chosen them because the reaction files contain CH<sub>y</sub>, C<sub>2</sub>H<sub>y</sub> and C<sub>3</sub>H<sub>y</sub>-proton collision reactions respectively, with  $y \leq 2x + 2$ , which allows us to check if ADMT correctly reads in the parameters of the cross section formulas, for different hydrocarbon species. Secondly, we have chosen them, because they offer us the means to check if the cross section formulas for equation type 5 (5a and 5b) are correctly implemented. The cross sections of ADMT match

the ones of Hydkin, for all equation types and for all plasma energies, so, we can conclude that ADMT can be trusted when calculating the cross sections.

### Rate Coefficients

For most of the hydrocarbon reactions the rate coefficient ( $\langle \sigma v \rangle$ ) is calculated by averaging  $\sigma \cdot v$  over the Maxwellian velocity distribution of the plasma particles. For some reactions however, no cross sectional fittings are available. Their rate coefficients are approximated with analytical fittings. The integration and the analytical fitting formulas were presented in section 2.2.2. Before comparing the calculation of the rate coefficients, first a word about the implementation of the integral in equations (2.12) and (2.13).

**The electron collision integral** given by equation (2.12) is numerically integrated using Gauss-Laguerre integration with  $n=32$  abscissas ( $x_k$ ) and weights ( $w(x_k)$ ):

$$\int_0^{\infty} f(x) \cdot dx = \int_0^{\infty} e^{-x} [e^x f(x)] \cdot dx \approx \sum_{k=1}^n w(x_k) e^{x_k} f(x_k)$$

Using this relationship and substituting  $x = (v/u)^2 - (v_{th}/u)^2$  in equation (2.12) the electron collision integral is calculated as:

$$\begin{aligned} \langle \sigma v \rangle_l &= \frac{4}{\pi^{1/2} u^3} \left( e^{-\frac{v_{th}^2}{u^2}} \right) \int_0^{\infty} e^{-x} [v^3 \sigma_l(v)] \cdot dx \\ &\approx \frac{4}{\pi^{1/2} u^3} \left( e^{-\frac{v_{th}^2}{u^2}} \right) \sum_{k=1}^{32} w(x_k) v_k^3 \sigma_l(v_k) \end{aligned}$$

with  $v_k = \sqrt{v_{th}^2 + u^2 x_k}$ . The abscissas ( $x_k$ ) and the weights ( $w(x_k)$ ) can be found in EFUNDA (2006).

**The proton collision integral** presented in equation (2.13) is numerically integrated using a recursive Simpson method (BULTHEEL, 1996). Before applying this method, the infinite upper boundary of equation (2.13) must be approximated. The approximative upper boundary ( $v_{rel}^{max}$ ) is determined by requiring that the integrand of equation (2.13) is zero (if  $i < 1E-317$  then  $i=0$  for the computer):

$$e^{-\frac{(v_{rel}^{max}-V)^2}{u^2}} - e^{-\frac{(v_{rel}^{max}+V)^2}{u^2}} = 0$$

$v_{rel}^{max}$  is calculated iteratively, with an accuracy of 1E-10. After setting the upper boundary, the program uses the recursive Simpson method to evaluate the integral with an accuracy of 1E-8.

For the sake of clarity, only the comparison of the rate coefficients of the charge exchange reactions (equation type 5) is presented below, in table 4.2. The comparison for the hydrocarbon-electron reactions and for the reactions with analytic fittings, can be found in appendix A.

$\langle \sigma v \rangle$ (cm <sup>3</sup> /s)		Plasma temperature (eV)					
		1eV	205eV	409eV	613eV	817eV	1000eV
r_3966_t_6							
react 1 (a)	<i>Hydkin</i>	7.01E-09	6.00E-08	7.88E-08	9.22E-08	1.03E-07	1.11E-07
	ADMT	7.01E-09	6.00E-08	7.88E-08	9.22E-08	1.03E-07	1.11E-07
react 2 (b)	<i>Hydkin</i>	1.12E-09	1.32E-12	4.73E-13	2.59E-13	1.69E-13	1.25E-13
	ADMT	1.12E-09	1.32E-12	4.73E-13	2.59E-13	1.69E-13	1.25E-13
react 3 (a)	<i>Hydkin</i>	7.78E-09	6.63E-08	8.76E-08	1.03E-07	1.16E-07	1.25E-07
	ADMT	7.78E-09	6.63E-08	8.76E-08	1.03E-07	1.16E-07	1.25E-07
r_4005_t_9							
react 1 (a)	<i>Hydkin</i>	2.81E-09	1.57E-08	2.78E-08	3.84E-08	4.79E-08	5.57E-08
	ADMT	2.81E-09	1.57E-08	2.78E-08	3.84E-08	4.79E-08	5.57E-08
react 2 (b)	<i>Hydkin</i>	1.60E-10	9.25E-14	3.29E-14	1.80E-14	1.17E-14	8.63E-15
	ADMT	1.60E-10	9.25E-14	3.29E-14	1.80E-14	1.17E-14	8.63E-15
react 3 (a)	<i>Hydkin</i>	8.63E-15	5.09E-09	1.08E-08	1.62E-08	2.10E-08	2.49E-08
	ADMT	8.63E-15	5.09E-09	1.08E-08	1.62E-08	2.10E-08	2.49E-08
r_4005_t_16							
react 1 (a)	<i>Hydkin</i>	2.34E-09	1.86E-08	2.98E-08	3.85E-08	4.58E-08	5.13E-08
	ADMT	2.34E-09	1.86E-08	2.98E-08	3.85E-08	4.58E-08	5.13E-08
react 2 (b)	<i>Hydkin</i>	8.83E-11	4.82E-14	1.71E-14	9.35E-15	6.08E-15	4.49E-15
	ADMT	8.83E-11	4.82E-14	1.71E-14	9.35E-15	6.08E-15	4.49E-15
react 3 (b)	<i>Hydkin</i>	5.89E-11	3.21E-14	1.14E-14	6.24E-15	4.06E-15	2.99E-15
	ADMT	5.89E-11	3.21E-14	1.14E-14	6.24E-15	4.06E-15	2.99E-15

Table 4.2: Comparison of the rate coefficients (cm<sup>3</sup>/s) for equation type 5 at a species energy E=0.1eV

Having a closer look at table 4.2 one can see that ADMT and Hydkin display identical results for the rate coefficients for different reactions and different plasma temperatures. As this is also the case for the rate coefficients presented in appendix A, ADMT calculates the rate coefficients correctly.

### 4.3.2 Validation of the Jacobian matrix

To reach full agreement between Hydkin and ADMT, their simulation of the hydrocarbon chemistry must be equal. Achieving this means that both programs correctly solve the same model. In this section we will show that ADMT and Hydkin do have the same model, while in the next section we will show that the solver was implemented correctly. Both programs model the hydrocarbon chemistry with equation (2.24):

$$\frac{\partial}{\partial t}(\vec{\phi}) = F_{\vec{\phi}}|_{\vec{\phi}_0} \vec{\phi}$$

The only term that can be different in this equation is the Jacobian matrix  $F_{\vec{\phi}}|_{\vec{\phi}_0}$ . Therefore the goal of this section is to demonstrate that ADMT and Hydkin construct the same Jacobian matrix. In section 2.3.3 the elements of the Jacobian matrix were given by equation (2.27):

$$F_{ij} = \begin{cases} \sum_{l_j} \nu_{il} \langle \sigma v \rangle_l \cdot \phi_{pe} & \text{for } i = 1, \dots, n_s \text{ and } 3 \leq j \leq i \\ 0 & \text{for all other indices} \end{cases}$$

where the sum contains all the reactions  $l_j$  between species  $j$  and the background particles. A Jacobian element is thus dependent on the hydrocarbon reactions, on their stoichiometry and

rate coefficients, and on the background concentration. The calculation of the rate coefficients has already been validated in the previous sections and the background concentration is specified by the user, so they will not induce errors when calculating the Jacobian. Therefore only the stoichiometry and the reaction selection mechanism require further investigation.

**Stoichiometry** With the help of the orthogonal relationship between the reaction- and the element vectors, which is defined in section 2.3.1, we were able to detect certain reactions in the database, that did not conserve charge nor H-atoms due to typing errors. The correction of these reactions led to a new species  $C_2H^{2+}$  and to the conservation of both charge and H-atoms.

**Reaction selection** As  $\nu_{il} = -1$  for each reaction  $l_i$ , element  $F_{ii}$  will contain all reactions between the species  $i$  and the background particles. Therefore, validating the calculation of the Jacobian matrix can be achieved, by comparing only its diagonal elements. The diagonal elements in table 4.3 were evaluated for a plasma temperature of  $1eV$ , a species energy of  $1eV$  and a plasma density of  $1E13/cm^3$ .

		F <sub>ii</sub> (1/s)					
i =1-6	<i>Hydkin</i>	0.00E+00	0.00E+00	0.00E+00	0.00E+00	0.00E+00	0.00E+00
	ADMT	0.00E+00	0.00E+00	0.00E+00	0.00E+00	0.00E+00	0.00E+00
i =7-12	<i>Hydkin</i>	-1.35E+00	-1.68E+05	-1.30E+04	-3.77E+05	-2.93E+04	-2.75E+05
	ADMT	-1.35E+00	-1.68E+05	-1.30E+04	-3.77E+05	-2.93E+04	-2.75E+05
i =13-18	<i>Hydkin</i>	-7.90E+04	-2.33E+05	-8.21E+04	-1.47E+05	-2.95E+04	0.00E+00
	ADMT	-7.90E+04	-2.33E+05	-8.21E+04	-1.47E+05	-2.95E+04	0.00E+00
i =19-24	<i>Hydkin</i>	-3.55E+05	-7.51E+03	0.00E+00	-4.65E+05	-2.89E+04	-5.75E+05
	ADMT	-3.55E+05	-7.51E+03	0.00E+00	-4.65E+05	-2.89E+04	-5.75E+05
i =25-30	<i>Hydkin</i>	-4.39E+04	-6.88E+05	-7.57E+04	0.00E+00	-8.02E+05	-1.56E+05
	ADMT	-4.39E+04	-6.88E+05	-7.57E+04	0.00E+00	-8.02E+05	-1.56E+05
i =31-36	<i>Hydkin</i>	-1.93E+06	-1.21E+05	-2.20E+05	-2.47E+04	-6.19E+05	-1.55E+04
	ADMT	-1.93E+06	-1.21E+05	-2.20E+05	-2.47E+04	-6.19E+05	-1.55E+04
i =37-42	<i>Hydkin</i>	0.00E+00	-7.01E+05	-3.30E+04	0.00E+00	-7.81E+05	-4.42E+04
	ADMT	0.00E+00	-7.01E+05	-3.30E+04	0.00E+00	-7.81E+05	-4.42E+04
i =43-48	<i>Hydkin</i>	0.00E+00	-9.08E+05	-5.48E+04	0.00E+00	-9.78E+05	-1.51E+05
	ADMT	0.00E+00	-9.08E+05	-5.48E+04	0.00E+00	-9.78E+05	-1.51E+05
i =49-54	<i>Hydkin</i>	-1.05E+06	-1.47E+05	-1.21E+06	-2.29E+05	-8.65E+06	-1.89E+05
	ADMT	-1.05E+06	-1.47E+05	-1.21E+06	-2.29E+05	-8.65E+06	-1.89E+05

Table 4.3: Comparison of the diagonal elements of the Jacobian matrix for a plasma temperature of  $1eV$ , a species energy of  $1eV$  and a plasma density of  $1E13/cm^3$

### 4.3.3 Validation of the implicit solvers

In the previous section we demonstrated that Hydkin and ADMT do model the same chemical system. In this section we will validate its simulation. First, we will explain that ADMT correctly simulates the behavior of the hydrocarbon mixture in a closed chemical reactor, while in the second part, we will validate the simulation of its behavior in a plug reactor.

### Solver for the closed chemical reactor equations

To prove that the 0D implicit solver, given by equation (2.29), is implemented correctly, we will make use of the hydrocarbon reaction mechanism that was presented in section 2.2.3, in table 2.1. Figure 4.2 represents the behavior of this reaction mechanism, at a plasma temperature of  $10eV$ , a plasma density of  $1E13/cm^3$  and a species energy of  $1eV$ .

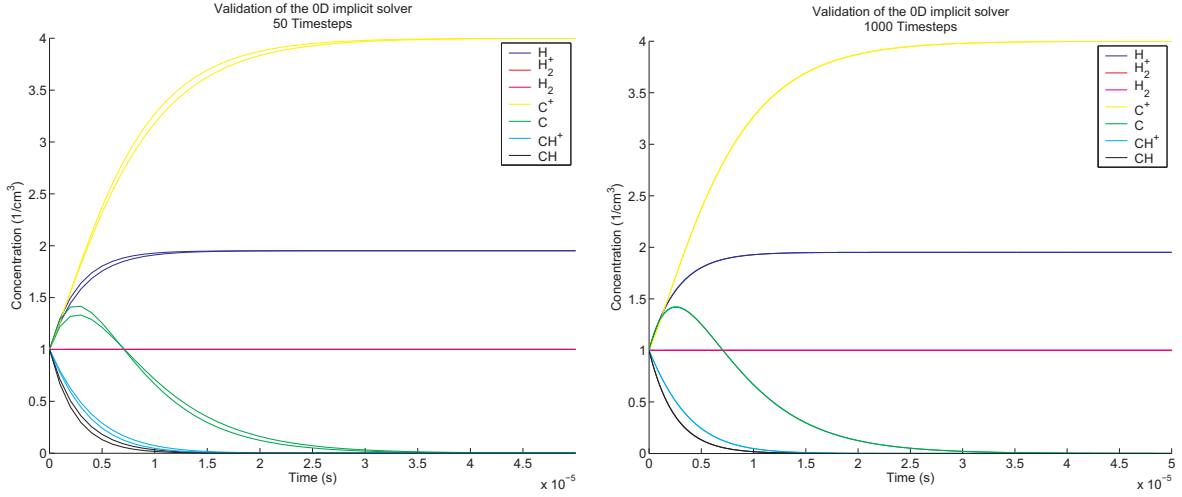


Figure 4.2: Closed reactor with species up to CH at a plasma temperature of  $10eV$ , a plasma density of  $1E13/cm^3$  and a species energy of  $1eV$ . Comparison between the solution of the 0D implicit solver and the exact solution for a different number of time-steps

Because equation (4.1) is a linear system of differential equations, it can be solved analytically (DIERCKX and PIESSENS, 2003):

$$\frac{\partial \vec{\phi}}{\partial t} = \exp\left(F_{\vec{\phi}} \cdot t\right) \cdot \vec{\phi}_0$$

Therefore the implementation of the numerical solver can be tested, by comparing its solution with the exact one. Figure 4.2 illustrates this comparison for a discretization of 50 and 1000 time steps. Because the numerical solution for a simulation with 1000 time steps lies on the exact solution, the error noticed when simulation with only 50 time steps is due to discretization. Thus, we can conclude that the 0D implicit solver is implemented correctly.

### Solver for the plug reactor equations

To prove that the 1D implicit solver is correctly implemented, is more difficult. Because in general, the system of differential equations which model the plug reactor (4.3) is non-linear in  $x$ . If however, the plasma conditions are constant over the domain, the steady state system resembles the model of a 0D reactor (4.1):

$$\begin{aligned} V(x) \cdot \frac{\partial \vec{\phi}(\infty, x)}{\partial x} &= F_{\vec{\phi}}(x) \cdot \vec{\phi}(\infty, x) & \vec{\phi}(0, x) &= \vec{\phi}_0(x) \\ \frac{\partial \vec{\phi}(\infty, vt)}{\partial t} &= F_{\vec{\phi}}(vt) \cdot \vec{\phi}(\infty, vt) & \vec{\phi}(0, vt) &= \vec{\phi}_0(vt) \end{aligned}$$

with  $x = vt$  and  $v$  being the uniform velocity of all hydrocarbons. This result is normal, because for constant plasma conditions, the plug reactor represent a closed chemical reactor moving through space, with a certain velocity  $v$ . Therefore, with these plasma conditions, the solution of the 0D problem can be scaled to the steady state 1D solution by multiplying the time axis with  $v$ . Figure 4.3 represents both the steady state 1D and the scaled 0D solution. The plasma conditions are equal to the ones used in the previous section.

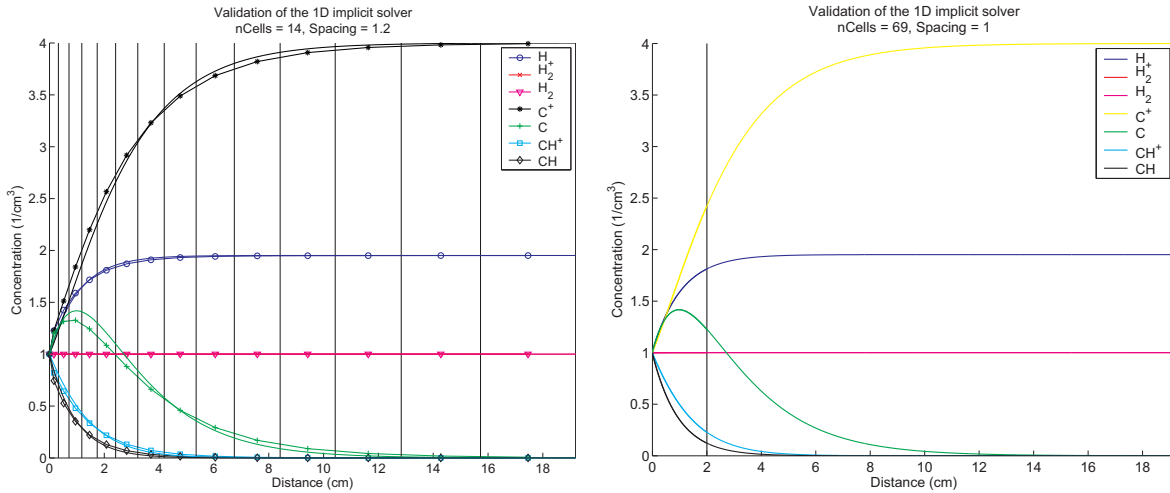


Figure 4.3: Plug reactor with species up to CH at a plasma temperature of  $10eV$ , a plasma density of  $1E13/cm^3$  and a species energy of  $1eV$ . The species move with a constant velocity of  $3.8387e5 cm/s$  through a reactor of  $19.1935 cm$ . Comparison between the steady state solution of the 1D implicit solver and the scaled exact 0D solution

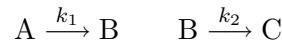
The left plot of figure 4.3 represents the comparison between the steady state 1D and the scaled 0D solution for a coarse grid, of which the cell boundaries are represented by the vertical lines. Due to the use of a spacing coefficient the approximation of the exact scaled 0D solution is quite ok, even close to the divertor plate ( $x=0$ ). For the reacting species, the largest error can be noted for C, because its production rate is a function of the concentration of all the reacting species (C,  $CH^+$  and CH), while the production rate of the other reacting species is independent of the concentration of C. To test if the error arises from discretisation, a finer grid has been used in the right plot of figure 4.3. To make a finer grid, we have increased the number of cells to 69, instead of 14, and decreased the domain length to  $2cm$ , instead of  $19.1935cm$ . For the sake of visibility only the cell boundary of the last cell is represented in the right plot. With this finer grid the error between the numerical and the exact solution is invisible. We can therefore conclude that the implementation of the 1D implicit solver is correct for constant plasma conditions. As this implementation is independent of the plasma conditions, it will also be correct for changing plasma conditions.

#### 4.3.4 Validation of the reduction techniques

Now that we are sure that the program correctly simulates the behavior of the hydrocarbon mixture in a closed or a plug reactor, we can finally start validating the implementation of the reduction techniques. In this section, will first assure that the QSSA method is correctly implemented. Next we will validate the implementation of the ILDM method.

### QSSA Validation

To validate the implementation of the QSSA method, we used an example from literature (RAWLINGS and EKERDT, 2004). The example is the following:



The initial concentrations in a closed, isothermal, reactor are  $\phi_A = \phi_{A0}$ ,  $\phi_B = \phi_C = 0$ . For these conditions, the exact full solution and the exact solution for the quasi steady state approximation of species B ( $\phi_B = k_1/k_2\phi_A$ ), are given by:

Full Solution		QSSA Solution	
$\phi_A(t)$	$= \phi_{A0}e^{-k_1t}$	$\phi_A(t)$	$= \phi_{A0}e^{-k_1t}$
$\phi_B(t)$	$= \phi_{A0}\frac{k_1}{k_2-k_1}(e^{-k_1t} - e^{-k_2t})$	$\phi_B(t)$	$= \frac{k_1}{k_2}(\phi_{A0}e^{-k_1t})$
$\phi_C(t)$	$= \phi_{A0}\frac{1}{k_2-k_1}(k_2(1 - e^{-k_1t}) - k_1(1 - e^{-k_2t}))$	$\phi_C(t)$	$= \phi_{A0}(1 - e^{-k_1t})$

Table 4.4: Exact Full and QSSA solution of the example of RAWLINGS and EKERDT (2004)

To be able to calculate the QSSA solution of this example with ADMT, we created a new reaction file of equation type 1, with the two reactions of the example. Because ADMT only works with hydrocarbon species, we chose species A= $H_2$ , species B= $H_2^+$  and species C=H.

Reactions	Parameters for Equation Type 1			
e + H <sub>2</sub> -> H <sub>2</sub> <sup>+</sup> + e	1.1300E + 01	1.4439E + 00	-1.2724E + 00	-2.2221E + 00
	9.2822E + 00	-1.5506E + 01	8.2778E + 00	
e + H <sub>2</sub> <sup>+</sup> -> H + e	1.1260E + 01	2.5E + 00	-1.9647E + 00	-0.6084E + 00

Table 4.5: Implementation of the example of RAWLINGS and EKERDT (2004) in ADMT. The parameters of the reactions are the ones required to calculate the cross sections for reactions of equation type 1

Also electrons are present in these reactions, because ADMT requires the reactions to be of the collision type. However, they do not influence the results because their overall stoichiometric coefficient is zero. After running ADMT with this example, for a plasma temperature of 10eV, a plasma density of 1E13/cm and a species energy of 1eV,  $k_1$  and  $k_2$  were found to be 0.7667/s and 3.764/s respectively. The comparison between the exact QSSA solution of table 4.4 and the QSSA solution of ADMT is presented in figure 4.4

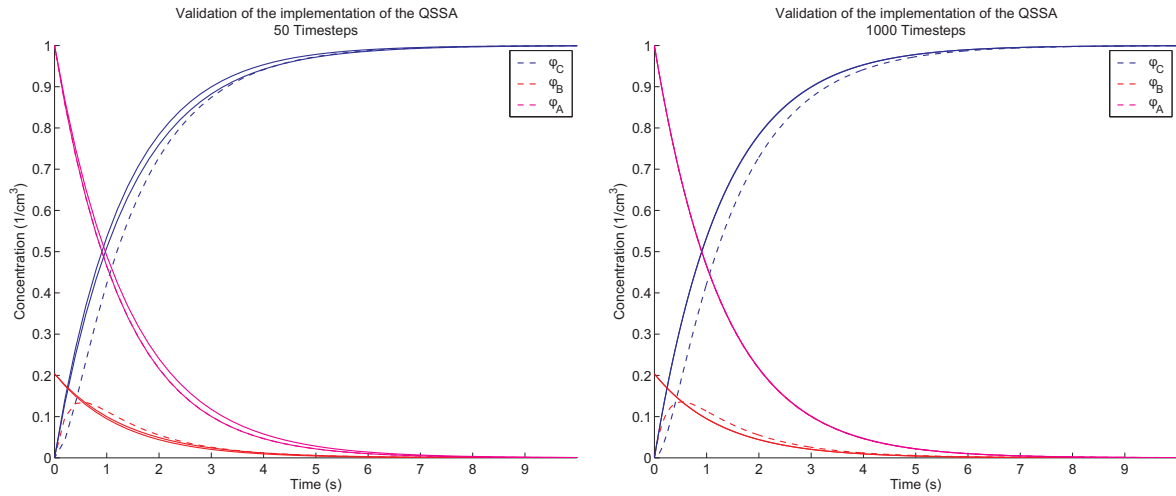


Figure 4.4: Comparison between the exact and the numerical QSSA solution of the example, for  $k_1 = 0.7667/s$  and  $k_2 = 3.764/s$  and  $\phi_{A0} = 1/cm^3$ . The exact full solution is presented by the dashed lines

The dashed lines in the figure represent the exact full solution, while the full lines represent the numerical and the exact QSSA solution. Comparing the two plots of figure 4.4, one can see that as the number of time-steps is raised from 50 to 1000, the discretisation error disappears. The numerical QSSA solution then equals the analytical QSSA solution. We can therefore conclude that the QSSA method has been correctly implemented in ADMT.

**Remark** If QSSA with projection, see section 3.2.3 and 3.5.2 at page 53, is used to simulate this example, the results are a lot better than the normal QSSA solution. This can be seen in figure 4.5. As we developed this model ourselves, we can not validate it with a solution found in literature.

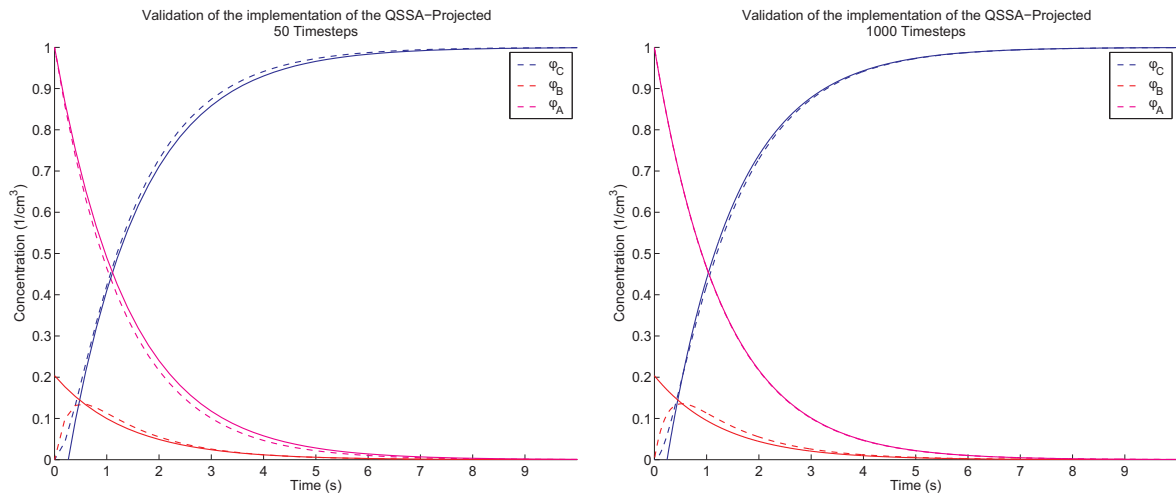


Figure 4.5: The QSSA with projection solution of the example, for  $k_1 = 0.7667/s$  and  $k_2 = 3.764/s$  and  $\phi_{A0} = 1/cm^3$ . The exact full solution is presented by the dashed lines

### ILDM Validation

The implementation of the ILDM method in ADMT, can be validated using the same example as for the validation of the QSSA. The exact ILDM solution is determined by neglecting the influence of the fast eigenvector on the full solution. In this case this can be achieved by setting  $e^{-k_2 t} = 0$  in the full solution, presented in table 4.4:

ILDM Solution	
$\phi_A(t)$	$= \phi_{A0} e^{-k_1 t}$
$\phi_B(t)$	$= \phi_{A0} \frac{k_1}{k_2 - k_1} e^{-k_1 t}$
$\phi_C(t)$	$= \phi_{A0} \frac{1}{k_2 - k_1} (k_2(1 - e^{-k_1 t}) - k_1)$

Table 4.6: ILDM solution of the example of RAWLINGS and EKERDT (2004)

To prove that the ILDM method is correctly implemented in ADMT, both the exact ILDM solution of table 4.6 and the ILDM solution of ADMT are presented in figure 4.6. The dashed lines in the figure represent the exact full solution, while the full lines represent the numerical and the exact ILDM solution.

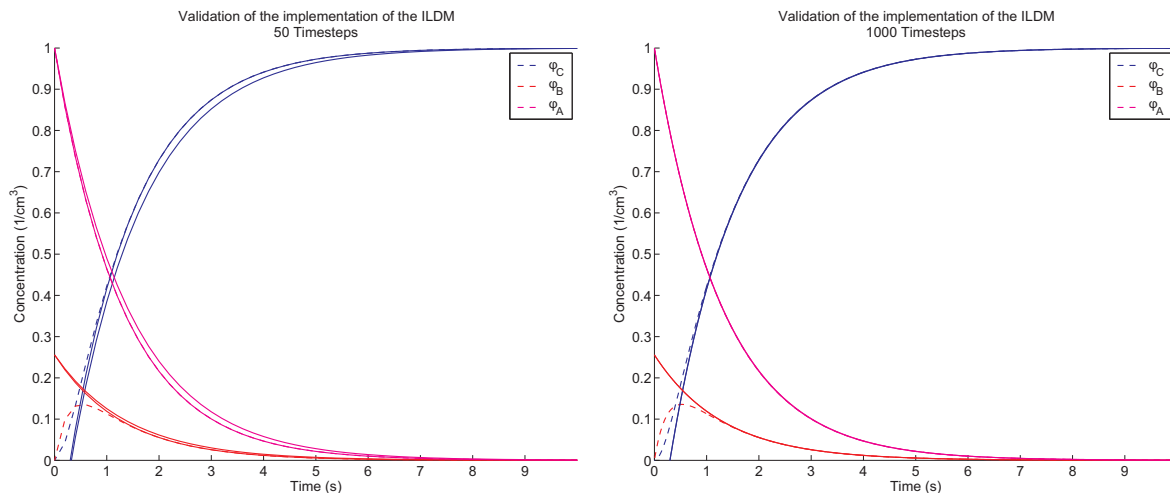


Figure 4.6: Comparison between the exact and the numerical ILDM solution of the example, for  $k_1 = 0.7667/s$  and  $k_2 = 3.764/s$  and  $\phi_{A0} = 1/cm^3$ . The exact full solution is presented by the dashed lines

Because no difference can be noticed between the numerical and the analytical ILDM solution for 1000 time steps, we can conclude that the ILDM method has been correctly implemented in ADMT.

**Remark** The ILDM solution approaches the full solution a lot faster than the QSSA solution does.

#### 4.3.5 Validation of the reduction techniques in EIRENE

Recall that the ultimate goal of reducing the hydrocarbon chemistry in the plasma edge, is to fully implement the reduction techniques into EIRENE. In this section we will illustrate that

the first steps of this ambitious goal have been reached, by testing the adapted QSSA and ILDM method, see section 3.6, in EIRENE, for constant background conditions. To validate our adapted methods, the results of EIRENE will be compared to the ones of ADMT, for a test case based on the exemplary CH reaction mechanism of chapter 2, specified in section 2.2.3.

### Test Case

The test consists of the simulation of the chemical sputtering of CH molecules into a divertor with constant plasma conditions. As the goal of this example is merely to illustrate some basic concepts, we additionally assume all produced hydrocarbons to move in one dimension with a uniform velocity. Figure 4.7 represents the full simulation of both ADMT and EIRENE, for a plasma temperature of 1eV, a plasma density of  $1E13/cm^3$  and an influx characterized by a concentration  $\phi_{CH}=8.14E10/cm^3$  and a velocity  $v=3.8387E5cm/s$ .

(These numbers result from an assumption of a mono-energetic influx of 1 Amp CH molecules at  $x=0$  into the computational domain, with an energy of 1 eV. Neutral particle fluxes are expressed also in Amp in EIRENE, by artificially assigning one elementary charge to each particle. The spatial coordinate  $x$  in EIRENE can be converted into a time  $t$ , for this one-speed problem. The influx at  $x=0$  in EIRENE is translated into an equivalent initial condition at  $t=0$  for ADMT.)

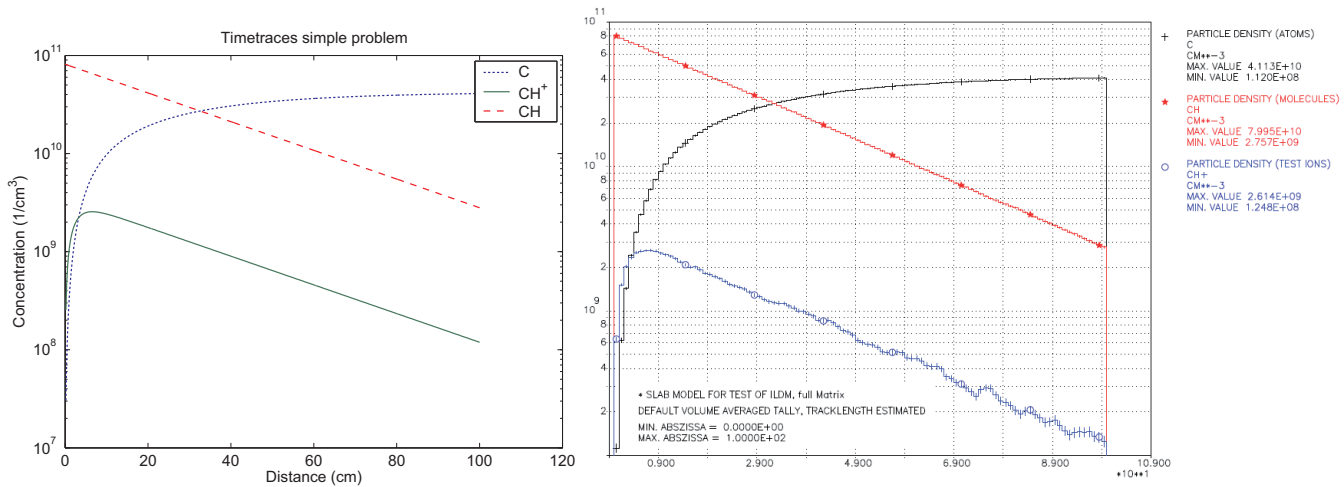


Figure 4.7: Comparison between the full solution of ADMT and EIRENE, for a plasma temperature of 1eV, a plasma density of  $1E13/cm^3$  and an influx characterized by a concentration  $\phi_{CH}=8.14E10/cm^3$  and a velocity  $v=3.8387E5cm/s$

Beside the statistical noise on the EIRENE solution the two time traces are identical. Now that we can be sure that both programs simulate the same full model, the QSSA and ILDM solution of ADMT can be used to validate the adapted QSSA and ILDM method in EIRENE.

**Remark** The full EIRENE simulation was reported to take 10 minutes of CPU-time.

### QSSA in EIRENE

The QSSA option already exists in EIRENE, so it could readily be applied on the test case. Using the same setup as for the full system, the EIRENE simulation for the quasi steady state of  $\text{CH}^+$  is presented in the rightmost plot of figure 4.8, while the ADMT simulation of the QSSA is presented in the left plot. One can notice in the ADMT simulation that the QSSA solution for  $\text{CH}^+$  does not seem to fall on the exact solution. This is merely a side effect of the use of a logarithmic concentration axis. So the error between the QSSA and the full solution is not constant, but decreases exponentially with the travel distance.

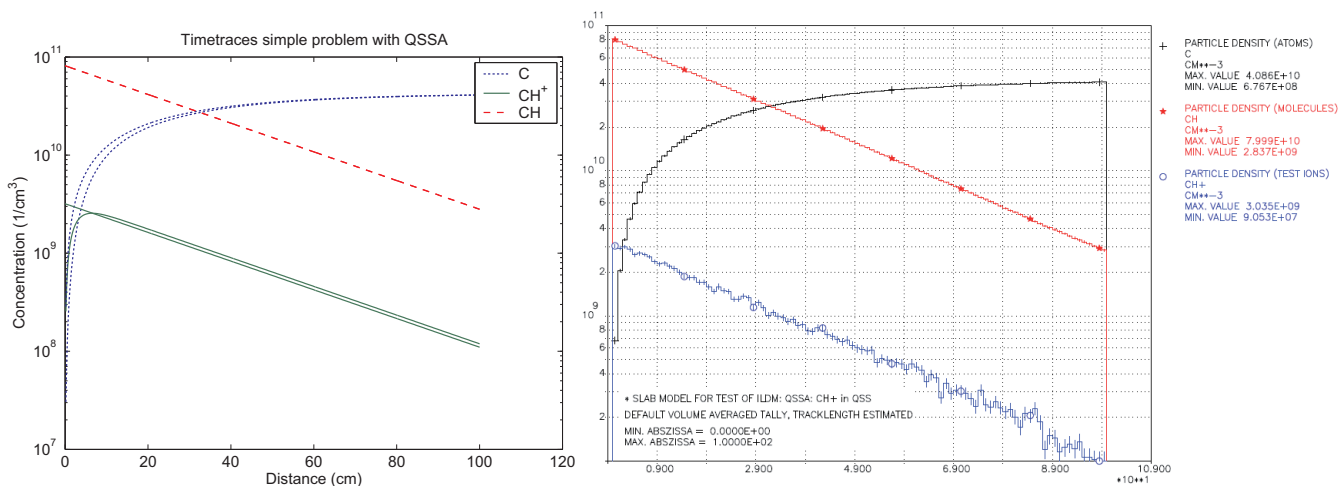


Figure 4.8: Comparison between the QSSA solution of ADMT and EIRENE, for a plasma temperature of 1eV, a plasma density of  $1\text{E}13/\text{cm}^3$  and an influx characterized by a concentration  $\phi_{\text{CH}}=8.14\text{E}10/\text{cm}^3$  and a velocity  $v=3.8387\text{E}5\text{cm}/\text{s}$

Within the unavoidable statistical noise still present in the EIRENE solution, meticulous examination of both plots and the raw data allows us to conclude that both solutions are identical.

**Remark** The QSSA EIRENE simulation for the statistical precision as indicated in the figure (see error bars on  $\text{CH}^+$  profile) required a simulation time of nearly 10 minutes.

### ILDm in EIRENE

The ILDM method has not been fully implemented yet into EIRENE. For this first trial, we wanted to avoid some of the strange effects of the reduced Jacobian, see section 3.6.3. Therefore we chose the eigenvector space itself to be the parameter space. This space has the advantage of decoupling the dynamical behavior of the variables and of producing a diagonal reduced Jacobian matrix. Physically such a diagonal matrix represents a chemical system in which a species  $i$  is destroyed after a time  $\tau_i = -1/\lambda_i$ , without the production of any other species.

$$\vec{U}_i^L \xrightarrow{-\lambda_i} 0 \quad i = 1 \dots m \quad (4.8)$$

with  $m$  being the dimension of the manifold (in the test case  $m=2$ ). In addition to representing extremely simple chemical reactions, the lack of off-diagonal elements in the reduced Jacobian,

filters all statistical noise out of the EIRENE solution. Consequently, in this parameter space, the ILDM solution of EIRENE is obtained within a few milliseconds. In statistical terms: the random walks from the corresponding diagonal effective reaction matrix are all identical, hence producing zero statistical Monte Carlo error. The new chemical parameter reactions of equation (4.8), with their rates  $\lambda_i$ , can be directly integrated into EIRENE for ILDM simulation. After running this parameter simulation, the solution was transformed back to the composition space, using the normal ILDM technique. Both the ILDM solutions of EIRENE and the ADMT are presented in figure 4.9

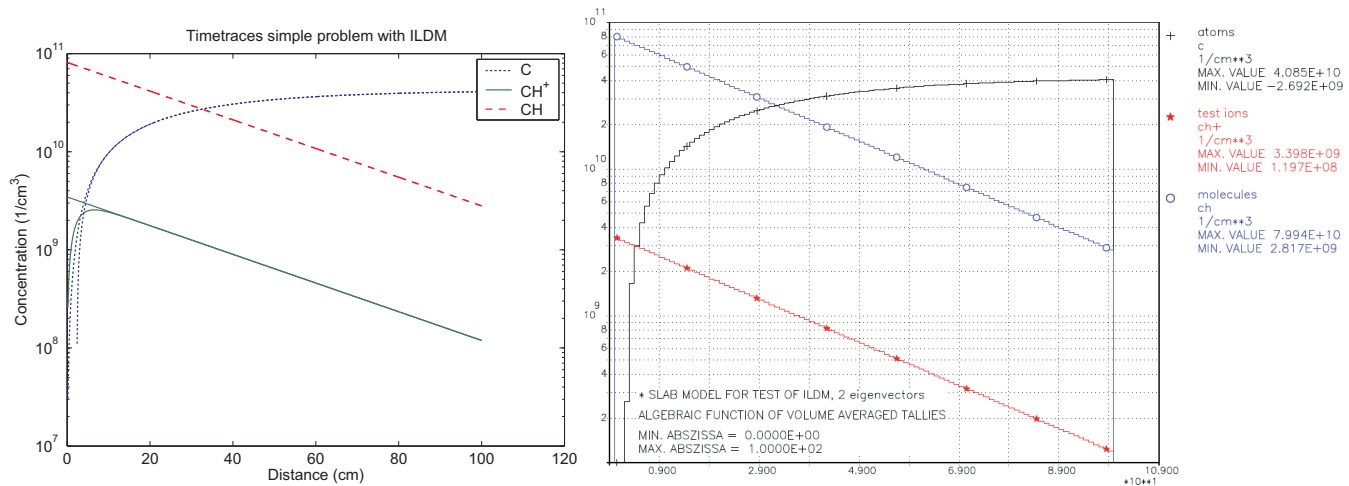


Figure 4.9: Comparison between the ILDM solution of ADMT and EIRENE, for a plasma temperature of 1eV, a plasma density of  $1E13/cm^3$  and an influx characterized by a concentration  $\phi_{CH}=8.14E10/cm^3$  and a velocity  $v=3.8387E5cm/s$

Having a closer look at figure 4.9 allows to conclude that both plots are identical. These results are of great importance, because they validate a first trial of the adapted ILDM method within the EIRENE code. Each entry in the reduced Jacobian translates into a process to be simulated by random numbers in the Monte Carlo scheme. It seems therefore to be beneficial for Monte Carlo procedures to use a reduced Jacobian which is “as diagonal as possible” in order to eliminate statistical noise from the sampling. In our simple model case this elimination was even perfect.

**Remark** In future applications of ILDM in EIRENE, the eigenvector space of the Jacobian matrix can not be so easily used, because this space changes with the background conditions and with the species energy. There is thus no possibility to choose one set of parameters that decouples the hydrocarbon system for the whole divertor domain. Therefore, future works lies in either finding the optimal parameter space(s) for the divertor, or in adding multiple projections to the new manifolds as Monte Carlo particles enter new cells.

This latter method would retain some aspects of the great computational (statistical) advantages observed in our simple test case, which results from the decoupling of Monte Carlo species (Eigenmodes) by diagonalizing the reaction matrix.

## 4.4 Using ADMT

The purpose of the last section of this chapter is twofold. Firstly, we want to provide the user of ADMT, with typical divertor conditions, which allow him or her to run realistic simulations of the closed and of the plug reactor. Secondly, we will present results that can help the user to predict some of the simulation results. To achieve this purpose, we will first present simulations of the typical divertor plasma conditions at ITER. Next, we will help the user to set up a typical hydrocarbon close reactor model and finally, we will do the same for the plug reactor.

### 4.4.1 Typical Divertor Conditions

In this subsection typical divertor plasma and hydrocarbon conditions will be presented.

#### Plasma conditions

The divertor plasma conditions are typically characterized by the temperature and the density of the electrons and the protons. In general, the proton density equals the electron density, because the plasma is globally neutral. For the hot plasmas of fusion devices, the difference between the proton and the temperature in the plasma edge is typically about factor two. The protons are usually hotter, because they are cooled less by the collision reactions. Figures 4.10 and 4.11 present a B2-EIRENE simulation of the electron density and temperature, respectively, in ITER. The proton density and temperature are not presented in the figures, but can be estimated from the electron density and temperature, respectively ( $\phi_{p+} \approx \phi_{e-}$  and  $T_{e-} \leq T_{p+} \leq 2T_{e-}$ ).

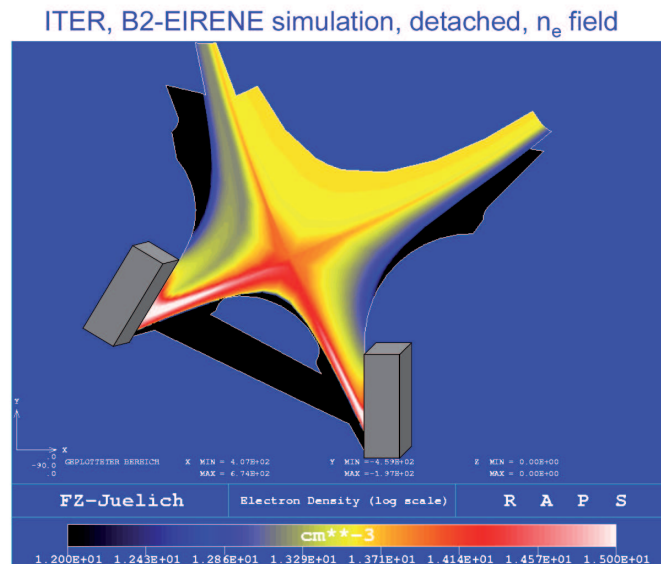


Figure 4.10: Simulation of the distribution of electron densities in the ITER divertor (REITER and Kotov, 2006)

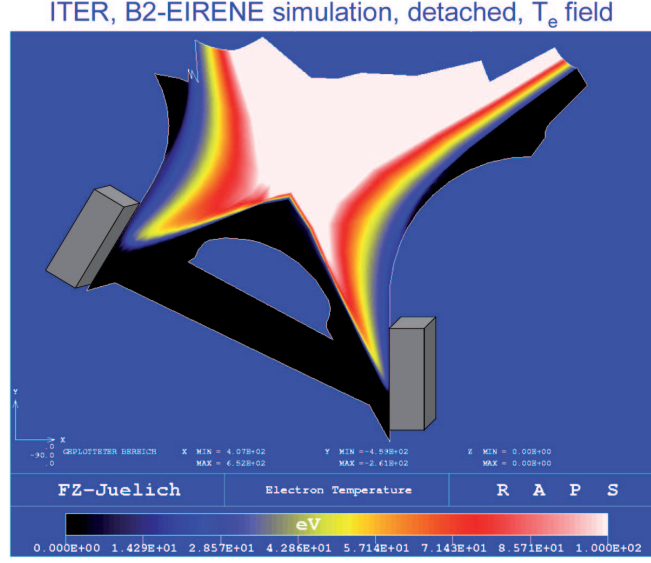


Figure 4.11: Simulation of the distribution of electron temperature in the ITER divertor (REITER and Kotov, 2006)

As could be suspected, figures 4.10 and 4.11 show that the electrons have a high density and a low temperature near the divertor plates,  $\phi_{e^-} \approx 10E15/cm^3$  and  $T_{e^-} \approx 1eV$ . Moving away for the divertor plates increases the plasma temperature ( $T_{e^-max} \approx 100eV$ ) and decreases the plasma density ( $\phi_{e^-min} \approx 10E13/cm^3$ ).

### Hydrocarbon conditions

Experiments (JANEV and REITER, 2002b) show that the main hydrocarbon fluxes into the divertor are mostly due to the sputtering of  $CH_3$ ,  $CH_4$ ,  $C_2H_2$ ,  $C_2H_4$ ,  $C_2H_6$ ,  $C_3H_4$ ,  $C_3H_6$  and  $C_3H_8$ . In general, the total rate of this process is about 1 or 2% of the incoming proton flux. Knowing that the hydrocarbons are released at thermal energies ( $E_{HC} \approx T_{Wall}$ ), their initial concentration can be calculated as:

$$\phi_{HC} \approx \frac{0.01 \cdot x_{HC} \cdot \phi_{p^+} \cdot v_{p^+}}{V_{HC}} = \frac{0.01 \cdot x_{HC} \cdot \phi_{p^+} \cdot \sqrt{2T_{p^+}/m_{p^+}}}{\sqrt{2E_{HC}/M_{HC}}}$$

with  $\phi_{HC}$  and  $\phi_{p^+}$  being the concentration of the sputtered hydrocarbon species and of the protons, respectively.  $x_{HC}$  represents the sputtering yield of the hydrocarbon species HC. For  $T_{p^+}=0.1eV$ ,  $\phi_{p^+}=1E13/cm^3$ ,  $E_{HC}=0.1eV$  and  $x_{HC} = 1$ , only  $C_3H_8$  is sputtered, with an initial concentration of approximately:

$$\phi_{C_3H_8} \approx 6.6E11/cm^3$$

Practically, the hydrocarbons are supposed to sputter with an initial speed  $V_{HC}$ , based on the wall temperature  $T_{Wall}$  and an initial density  $\phi_{HC} \approx 10^{-2}\phi_{p^+}$ .

### 4.4.2 Predicting the results of a closed chemical reactor simulation

In the last section, we have provided data to select the plasma and the hydrocarbon conditions inside the divertor. Now, in this section, we will explain how to use these data to predict the time to steady state and to choose the possible dimension reduction in advance.

### Time to steady state

To estimate the time to steady state of the system, the eigenvalue spectrum of the Jacobian can be used:

$$t_{SS} = -3/\lambda_{min}$$

with  $t_{SS}$  being the time to steady state and  $\lambda_{min}$  being the least negative of the non-zero eigenvalues. Based on this criterion, we have made figure 4.12, which can readily be used to approximate the time to steady state.

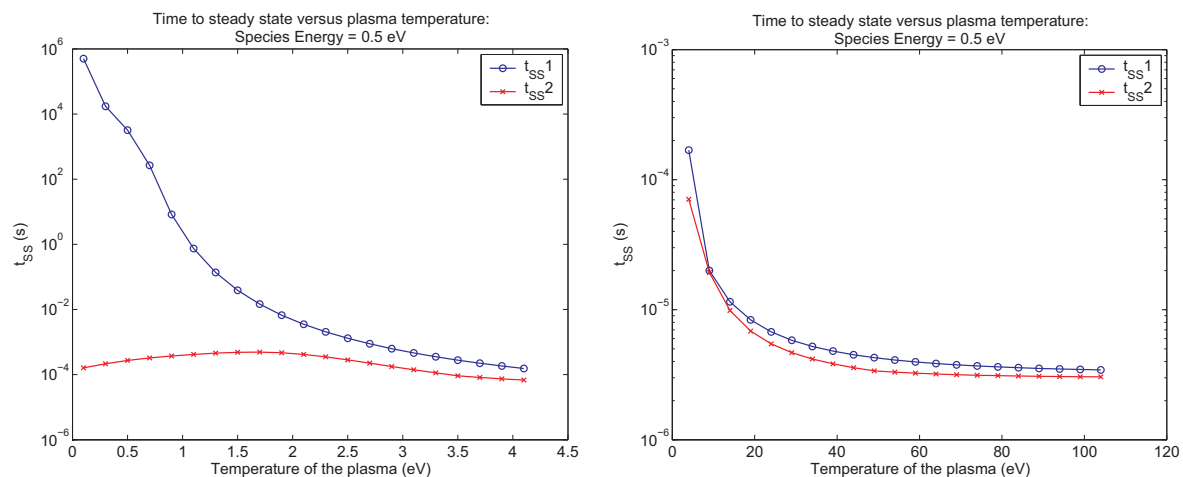


Figure 4.12: Time to steady state for plasma conditions  $T_{e-}=T_{p+}=E$  and  $\phi_{e-}=\phi_{p+}=1E13/cm^3$

The time to steady state,  $t_{SS}^1$  in figure 4.12, provides an upper boundary of the time vector, when simulating the behavior of the closed chemical reactor. When one is interested to study the fast hydrocarbon reactions, the upper time boundary is determined by  $t_{SS}^2$  instead of  $t_{SS}^1$ .

**Remark** Figure 4.12 can also be used to approximate the time to steady state, for different species energies and for different plasma densities. For the latter however, the time to steady state must be scaled, because the system behaves linear with the plasma density:

$$t_{SSNew} = \left( \frac{\phi_{peNew}}{\phi_{peFig}} \right)^{-1} \cdot t_{SSFig}$$

### Expected reduction with ILDM

The main issue when reducing chemical systems, is to know how much information can be neglected, without losing a certain degree of accuracy. To help the user to predict how many dimensions can be cut off, we have made dimension reduction charts. These charts expose the dimension reduction potential of the ILDM for different plasma conditions at a fixed decay time ( $t_{decay}$ ). Four of these charts are presented in figures 4.13 and 4.14.

The charts give the highest number of dimensions that can be reduced for the full hydrocarbon chemistry ( $n_f = n_s - m = 54 - m$ ), and they must be interpreted as follows. After the decay time, for which the figure was made, the influence of the slowest fast eigenvector on the

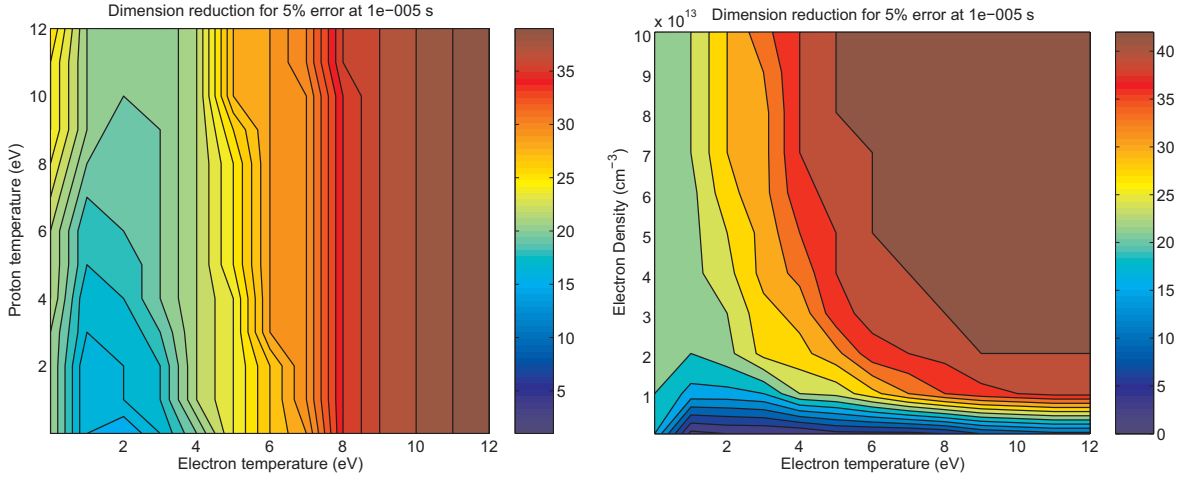


Figure 4.13: Dimension reduction for 5% relative error at a decay time  $t_{\text{decay}}=1\text{E}-5\text{s}$ . Left,  $\phi_{e^-}=\phi_{p^+}=1\text{E}13/\text{cm}^3$  and  $E=1\text{eV}$ . Right,  $T_{p^+}=1\text{eV}$ ,  $\phi_{p^+}=1\text{E}13/\text{cm}^3$  and  $E=1\text{eV}$

solution, will be 5% of its original influence. Therefore, when simulating the closed reactor problem, the full solution will fall on the  $m$ -dimensional ILDM after a time  $t \approx t_{\text{decay}}$ .

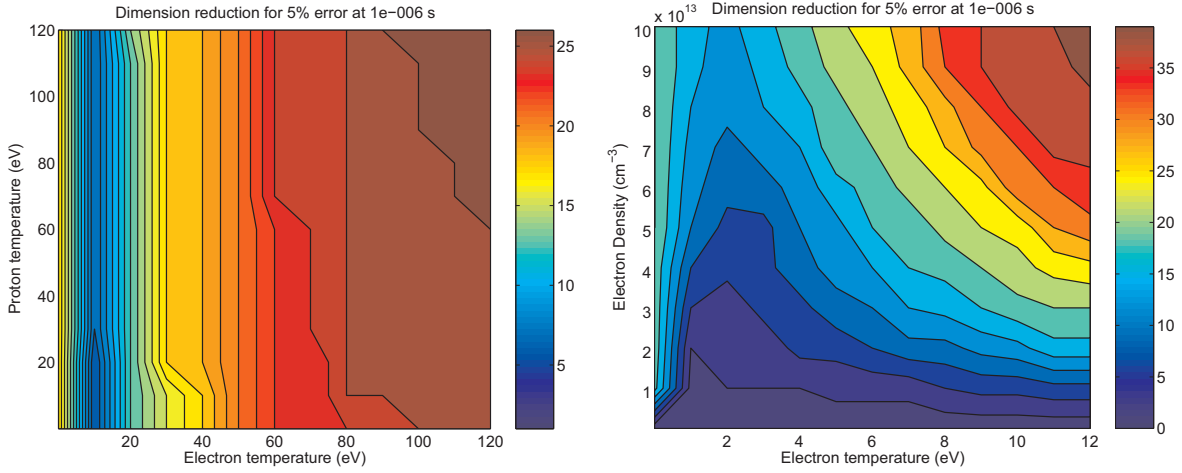


Figure 4.14: Dimension reduction for 5% relative error at a decay time  $t_{\text{decay}}=1\text{E}-6\text{s}$ . Left,  $\phi_{e^-}=\phi_{p^+}=1\text{E}13/\text{cm}^3$  and  $E=1\text{eV}$ . Right,  $T_{p^+}=1\text{eV}$ ,  $\phi_{p^+}=1\text{E}13/\text{cm}^3$  and  $E=1\text{eV}$

To illustrate the use of these charts, let's take a plasma temperature  $T_{e^-}=T_{p^+}=12\text{eV}$ , a plasma density  $\phi_{e^-}=\phi_{p^+}=1\text{E}13/\text{cm}^3$  and a species energy  $E=1\text{eV}$ . If we want to know the solution of the closed reactor after a time of  $1\text{E}-05\text{s}$ , the left chart of figure 4.13, states that approximately 40 dimensions can be neglected. After a time of  $1\text{E}-05\text{s}$  the system can thus be completely represented by a  $54-40=14$  dimensional ILDM. Recalling that the full hydrocarbon system has 13 non-reacting species, 13 algebraic conservation equation reduce the system even further, to only 1 differential equation. Analogously, using figure 4.14, after a time of  $1\text{E}-06\text{s}$ , the same system can only be reduced about 5 dimensions, instead of 40 for  $1\text{E}-05\text{s}$ . Plots for other decay times can be found in section 5.3 in chapter 5.

**Remark** Because the influence of the energy of the species on the eigenvalues of the Jacobian matrix can be neglected, the reduction potential exposed in figures 4.13 and 4.14 can also be used for other species energies.

### 4.4.3 Predicting the results of a plug reactor simulation

In this section, we will explain how to use the information about the divertor conditions, to predict some properties of the plug reactor model. First, we will explain how to predict the time to steady state. Next, we will show how to select the length of the reactor.

#### Time to steady state

The deterministic model of a transient plug reactor, see equation (4.3), contains both a chemical and a physical source term. The reactor is in steady state if:

$$\frac{\partial \vec{\phi}(\infty, x)}{\partial t} = F_{\vec{\phi}}(x) \cdot \vec{\phi}(\infty, x) - V(x) \cdot \frac{\partial \vec{\phi}(\infty, x)}{\partial x} = 0$$

The global time to steady state, can be determined by finding the largest time to steady state of these two terms. For the transport term, the time to steady state of the full reactor, is determined by the time required for a particle to reach its end:

$$t_{SS\text{Transp}} = \frac{L}{v_{\min}}$$

with  $L$  being the length of the reactor and  $v_{\min}$  being the speed of the slowest hydrocarbon particle. For the chemical term, the time to steady state can be determined as the maximum of the time to steady state of each cell:

$$t_{SS\text{Chem}} = \max(t_{SS\text{Chem}}(1), t_{SS\text{Chem}}(2), \dots, t_{SS\text{Chem}}(\text{nCells}))$$

with  $t_{SS\text{Chem}}(i)$  being the chemical time to steady state of cell  $i$ , which can be determined in figure 4.12. Finally, the global time to steady state can be determined as:

$$t_{SS\text{Total}} \approx \max(t_{SS\text{Chem}}, t_{SS\text{Transp}})$$

#### Selecting the length plug reactor

Normally, the geometry of the plug reactor is a known value. For example, in ITER, the distances the hydrocarbons travel in the divertor, in the poloidal direction, range from a few centimeters to about 1 meter. If the length of the reactor is unknown, its length can be estimated with the following formula:

$$L \approx \bar{v} \cdot t_{SS\text{fig}}$$

where  $L$  is the reactor length,  $\bar{v}$  is the average speed of the hydrocarbons and  $t_{SS\text{fig}}$  is the time to steady state of figure 4.12, evaluated at the plasma conditions of the first cell. The formula can be derived, by assuming that  $L$  is the position at which the steady state solution for a homogenous plug reactor stops varying in the direction of the flow.

## 4.5 Conclusion

From the first part of this chapter the structure and functioning of the program ADMT should be clear. More important, the validation of the different components of ADMT confirms that investigations on the full hydrocarbon mechanism as is done in chapter 5 can be done with this numerical tool in a highly reliable way. It has been assured that results of HYDKIN and ADMT correspond to each other. The reduction methods ILDM and QSSA in ADMT have been checked with examples from literature. Moreover the suggested implementation of ILDM in EIRENE has been checked with a small test case. This produces the ‘proof of validity’ for the approach. Given a set of typical divertor conditions from ITER which the user can also find in this chapter, it is possible to analyze correctly the influence of the reduction methods on the full hydrocarbon mechanism. This will be done explicitly in the next chapter 5. A short user guide has been written in the last part of the chapter.



## Chapter 5

# Study of the full hydrocarbon chemistry with ADMT

### 5.1 Introduction

This chapter combines the knowledge of the previous chapters to investigate the potentiality of ILDM on the full hydrocarbon reaction mechanism with 54 species. The chapter is build up of a few sections each discussing a different aspect of the ILDM reduction. First the significance of the eigenvalues is explained in section 5.2. Section 5.3 describes how much the system can be reduced for given background conditions based on the criteria imposed on the eigenvalues. The effect of plasma conditions and species energy is examined here on the number of reduction dimensions. The stiffness is exposed in section 5.4. Section 5.5 gives another approach on the criterion for the determination of a good dimension reduction. In addition the eigenvectors also constitute an interesting subject of investigation (section 5.6). Section 5.7 gives the full solution, the ILDM solution and the QSSA solution of different species in a comparative time frame. The behavior of the reduction of the full reaction system becomes clear. Finally section 5.8 shows the solution of a 1-dimensional transient experiment with the hydrocarbon reaction mechanism. This model tells us how the grid size influences the results when applying the ILDM or the QSSA reduction methods.

### 5.2 Significance of the Eigenvalues

Because the eigenvalues play an important role in the dynamical behavior of the reaction system it is worth to thoroughly examine them. They influence the rate of change of the uncoupled species (the eigenvectors), they determine the speed at which the chemical system reacts on perturbations and their disparateness determines the stiffness, which is important for stability during numerical calculations. The analytical solution helps with the understanding of the their impact.

$$\vec{\phi}(t) = c_1 \cdot \exp(\lambda_1 t) \cdot \vec{u}_1 + c_2 \cdot \exp(\lambda_2 t) \cdot \vec{u}_2 + \dots + c_{n-1} \cdot \exp(\lambda_{n-1} t) \cdot \vec{u}_{n-1} + c_n \cdot \exp(\lambda_n t) \cdot \vec{u}_n$$

The amplitude of the respective eigenvectors is  $c_i \cdot \exp(\lambda_i t)$  where the  $c_i$ 's are defined by the initial conditions. This means an eigenvalue is exactly the inverse decay time of its associated mode or eigenvector: ( $\tau = |\frac{1}{\lambda}|$ ). The relative influence of a timescale on a species is directly related with the component of that species in the eigenvector. More important, the ILDM

algorithm now precisely uses the eigenvalues to determine and relax the fastest uncoupled processes. It is obvious to see in the analytical solution that as the time reaches a multiple of  $\tau = \left|\frac{1}{\lambda}\right|$ , the contribution of the corresponding fast eigenvector will be negligible.

From another point of view, when the ILDM directly relaxes the fast eigenvector at time  $t = 0$ , the ILDM solution will approximate the real solution at a time of around  $3 \cdot \tau = \left|\frac{3}{\lambda}\right|$ . To obtain a good approximation in systems with transport, the ILDM solution must lie on the real solutions before the fastest transport processes can occur or if the dimension of the ILDM is  $m$ ,  $|\lambda_{n+1}| > |\lambda_{transp}|_{max}$ . In this case analyzing the spectrum of the eigenvalues allows a determination of the dimension of the ILDM. In contrast, if no external cut-off timescale is known or imposed, the gaps between the succeeding eigenvalues can be used. If the gap between the fast eigenvalue  $m + 1$  and the slower eigenvalue  $m$  is big in comparison with the gap between eigenvalue  $m + 1$  and the fastest eigenvalue  $n$ ,  $m$  is a good choice for the ILDM dimension. Analyzing the eigenvalues of the reaction mechanism therefore makes it possible to determine the dimension of the ILDM.

### 5.3 Dimension reduction

Based on the significance of the eigenvalues one can define the number of dimensions that should be reduced. In order to do so it is handy to know the time scales of transport. If one compels the influence of an eigenmode to a certain percentage, a decay of that eigenvector can be imposed at that certain moment in time:  $e^{\lambda\tau} < 5\% \approx e^{-3}$ . Knowing the cut off timescale  $\tau$ , for example from transport, it is now possible to determine which eigenmodes do not comply this condition:  $\lambda_i < \frac{-3}{\tau}$ . The number  $n_f$  of eigenmodes that can be assumed relaxed within 5% of their initial deviation at time  $t_{decay} = 1E - 05$  is given in figure 5.1 as a function of electron and proton temperature in the left figure and as a function of the electron temperature and the electron density in the right graph. The influence of the species

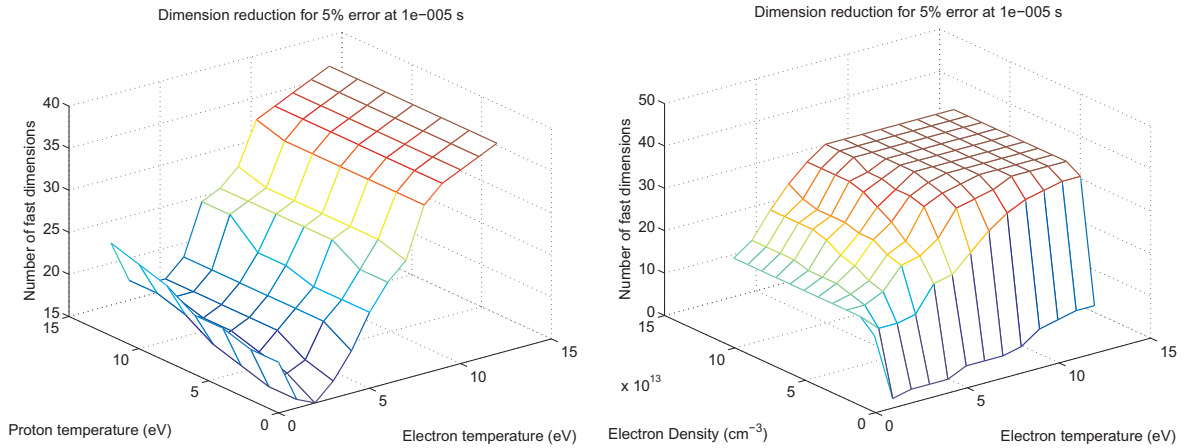


Figure 5.1: Proposed number of fast modes to relax at  $T_{p+} = 1\text{eV}$ ,  $\phi_{e-} = \phi_{p+} = 1\text{E}13\text{cm}^{-3}$  and  $E = 1\text{eV}$  for 5% error at  $\tau = 1E - 05$

energy is negligible and thus not given. Generally the electron temperature and the proton temperature are not more different than an order of magnitude of 100. The electron and ions density on the other side are always practically identical. Otherwise the plasma edge would

have a net charge. The proton temperature seems to have little influence on the eigenvalues. It is mainly the electron temperature that determines the reducibility of the system. On the other hand the electron density is in the usual range, above  $1E13$  not much of importance. If the timescales of transport are more stringent, the time to convergence ( $t_{\text{decay}}$ ) should be

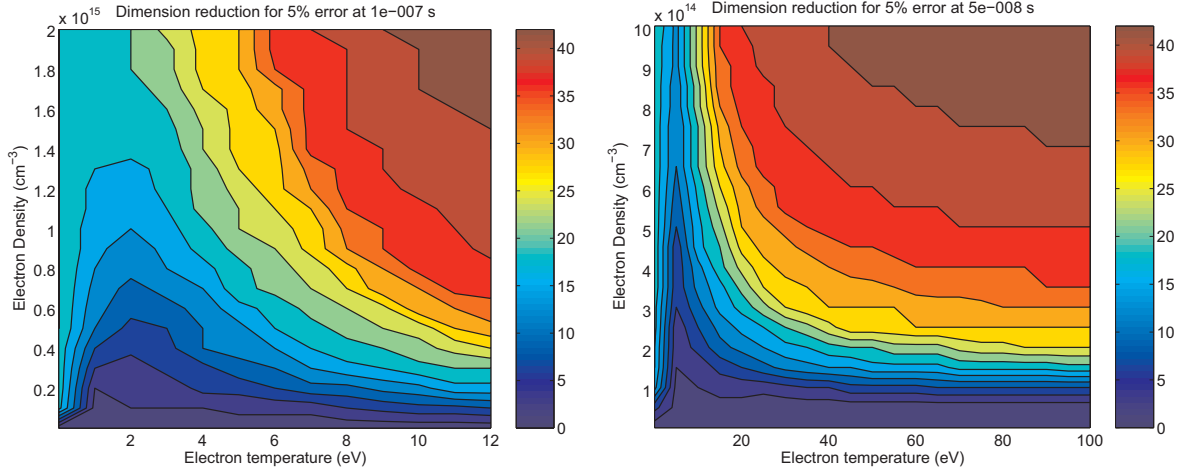


Figure 5.2: Proposed number of fast modes to relax at  $T_{p+} = 5\text{eV}$ ,  $\phi_{p+} = 1E14\text{cm}^{-3}$  and  $E = 1\text{eV}$  for 5% error at  $\tau = 1E - 07$  or  $\tau = 1E - 08$

reduced. This is given in the left plot of figure 5.2 for  $\tau = 1E - 07$  and proton temperatures around 5eV. Also for higher plasma temperatures and higher densities it is interesting to know the reduction potential. This is presented in 5.2 right. The practical use of these dimension reduction charts is however not yet optimized. For more realistic charts the dependency of the transport timescale has to be taken into account. The transport timescale is proportional to  $\frac{L}{v}$  where  $v$  is the velocity of the hydrocarbons. This velocity is first related to the sputtering process. But as the particle interacts with the warmer background it generally increases its speed. In low temperature backgrounds the particle will move slower and its timescale will be bigger, whereas in high temperature ranges the particles will have shorter transport timescales. The length in the formula is typically a grid cell length. Because in each grid cell the user expects the ILDM solution to be as close to the full solution as possible. The researcher has to consider all these restrictions when he efficiently wants to implement the ILDM method in a 2 or 3 dimensional simulation model.

## 5.4 Stiffness

Together with its order and its convergence, the domain of stability is an important property that determines the usefulness of a numerical method. In Monte Carlo methods the stiffness has a direct influence on the noise in the solution. As explained in the appendix, the stiffness of an ODE plays a key role to determine this domain. To calculate and plot the stiffness of the hydrocarbon system the definition from the appendix is used. It is represented in figure (5.3) left for a background concentration that is quite common in the divertor region, respectively  $\frac{1e^{13}}{\text{cm}^3}$ . Some of the eigenvalues of the Jacobian of the hydrocarbon system are zero, because of the system's conservation laws. Therefore the stiffness is calculated after cutting away the zero eigenvalues. Although the stiffness varies strongly with the plasma

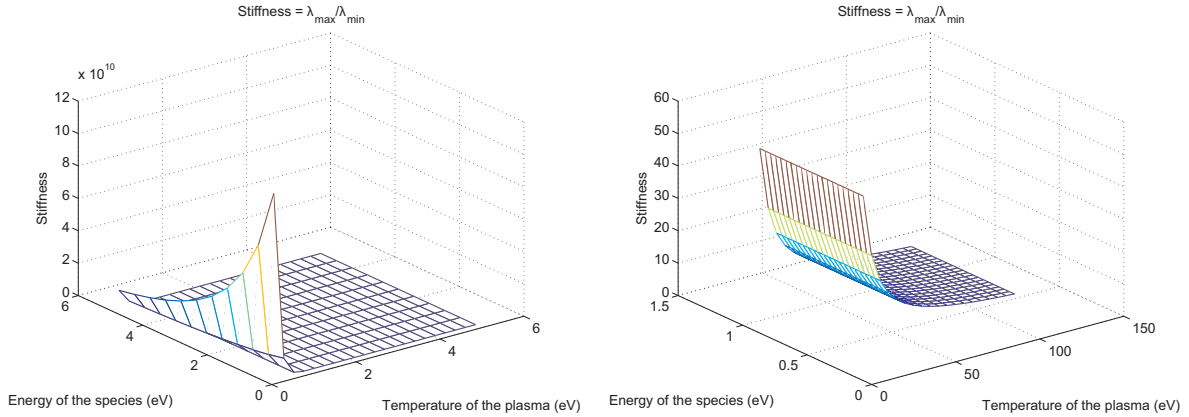


Figure 5.3: Stiffness of the full hydrocarbon reaction system in function the temperature of the plasma and the energy of the species, for an electron and proton concentration of  $1e13 \frac{1}{cm^3}$

temperature for the whole range energies, the species energy only changes the stiffness at the lowest plasma temperatures. This can be explained by studying the reaction rates of the processes. The rates of the electron collision reactions are only dependent on the speed of the electrons. Because of their low mass, for the same amount of energy the electrons will move extremely fast compared to the species they collide with, so species can be supposed to have no speed at all. In proton collision reactions, the higher mass of the protons, and thus the lower speed, does not allow to neglect the speed of the species. Therefore these reaction rates are calculated with a relative speed  $v_r = |\vec{u} - \vec{V}|$ ,  $u$  and  $V$  being respectively the speed of the proton and the speed of the species. Only at low energies of the plasma particles this relative speed is influenced by the speed of the species. So only at low plasma energies the reaction rates and thus also the stiffness are influenced by the species energy. The reason why

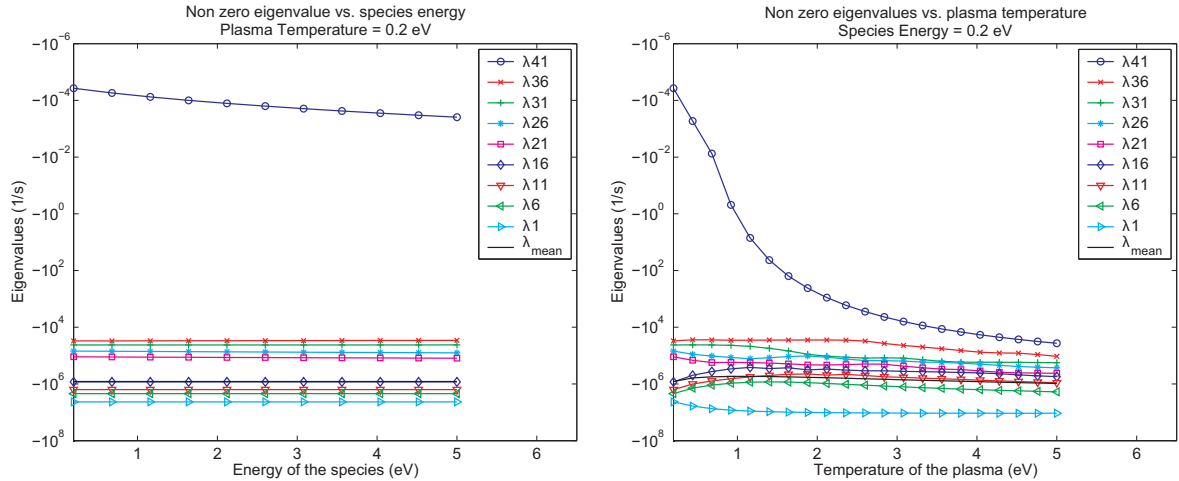


Figure 5.4: The dependency and grouping of the eigenvalues for plasma concentrations of  $1e13 \frac{1}{cm^3}$

the stiffness keeps decreasing with increasing plasma temperature is difficult to explain from

figure 5.3. To better understand why and how the stiffness changes, new figures 5.4 of some non-zero timescales between the fastest ( $\tau_1 = \frac{-1}{\lambda_1}$ ) and the slowest timescale ( $\tau_{41} = \frac{-1}{\lambda_{41}}$ ) of the hydrocarbon system are plot with a logarithmic scale.  $\lambda_{mean}$  represents the mean value of the non-zero eigenvalues. In this scaling of the y axis the logarithm of the stiffness is equivalent with the gap between the two extreme timescales. The left plot shows that the eigenvalues are barely dependent on the energy of the species. At these low plasma temperatures they even tend to group into 3 zones. In the right plot the eigenvalues are presented with changing background temperature. Apparently, especially the slowest timescale is sensitive to a change in plasma temperature, while the fastest timescale stay relatively constant. It is thus possible to reduce the stiffness by cutting some of the fastest timescales but the influence of the plasma temperature cannot be removed. Above some 5 to 10eV plasma temperature the stiffness remains in the orders of 1E+02. At lower plasma temperatures however the stiffness shoots upward to values as high as 1E+10 at 0.1eV. The reason for these high values is the very low reactivity of C and C<sup>+</sup> at these low temperature ranges. Many processes involving these species are inactive or extremely slow at these low plasma temperatures. This could also be seen from the cross sections and reaction rates calculated in chapter 2 section 2.2.3.

Figure 5.3 shows that even though the stiffness of the hydrocarbon system decreases with increasing plasma temperature, it will never fall below  $\approx 10$  in the limiter temperature range (up to 100eV for TEXTOR). The numerical solver will thus experience stability problems especially at low plasma energies, where small time steps will make the solver inefficient. As can be seen from figure 5.4 the time step for the explicit solver is almost independent of the plasma temperature and should be smaller than the fast timescale ( $\Delta t < 10^{-7}$ ). Applying the ILDM algorithm allows to eliminate a specified number of fast eigenvalues, which automatically decreases the stiffness and increases the stability or the time step. The influence of the dimensionality of the ILDM on the stability will be studied in the next subsection.

## 5.5 Eigenvalue spectrum

The present hydrocarbon reaction mechanism contains 54 species and thus 54 eigenvalues. Because of the conservation of elements and the presence of non reacting species, 13 eigenvalues are 0. This leaves 41 non-zero negative eigenvalues or thus 41 dynamical variables in the system. Figures 5.5 and 5.6 plot a selection of eigenvalues, with  $\lambda_1$  being the fastest (most negative) and  $\lambda_{41}$  being the slowest (the least negative) of the system.

As explained in the last subsection, all eigenvalues are almost independent of the energy of the species. When plotted in function of the temperature of the plasma, the eigenvalues display a much more interesting behavior. At low temperatures ( $< 0.5\text{eV}$ ) is close to zero as can be seen from the left graph of figure 5.5. This was related to the reactiveness of the carbon species (C). It is not before conditions of 3eV that this eigenvalue joins the others and falls below  $-1\text{E}+04 \text{ s}^{-1}$ . The approximation for the ITER simulations thus seems unsatisfactory for higher temperatures. C cannot be representative for the transport of the hydrocarbons in these conditions. Additionally at low temperatures it can be noticed that the faster eigenvalues tend to group into 2 distinct group. This is illustrated in the left graph of figure 5.6 were the slowest dynamical timescale  $\lambda_{41}$  was left out. The groups are interesting for cut off. Let us explain how. Recall that a gap between two eigenvalues means a great reduction in stiffness can be achieved when the gap is taken as last dimension to reduce. On the other hand this jump is a big loss in accuracy because the convergence with the full

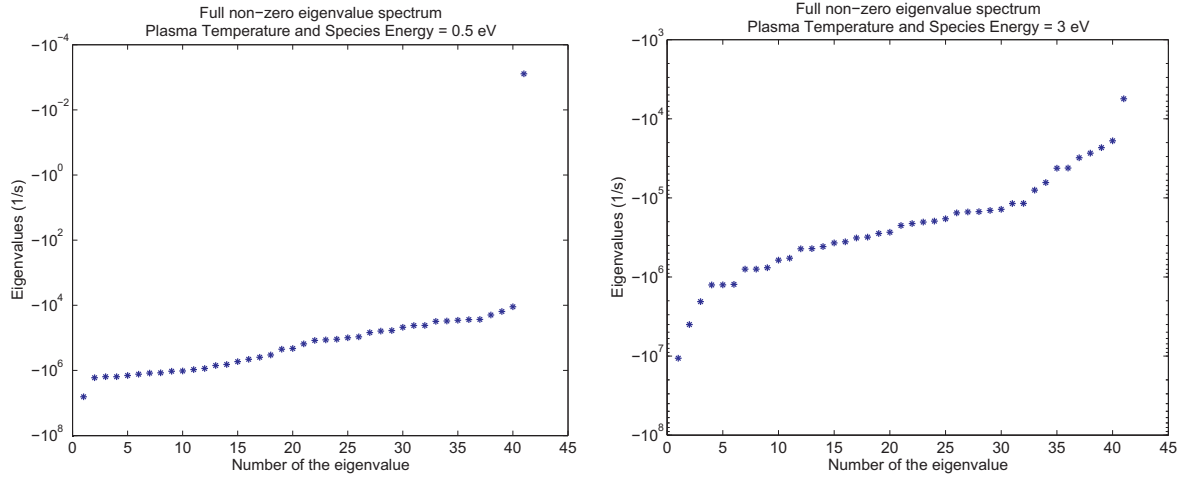


Figure 5.5: Eigenvalue spectrum of the hydrocarbon reaction mechanism, for an electron and proton concentration of  $1e13 \frac{1}{cm^3}$  and plasma temperatures being 0.5 and 3eV

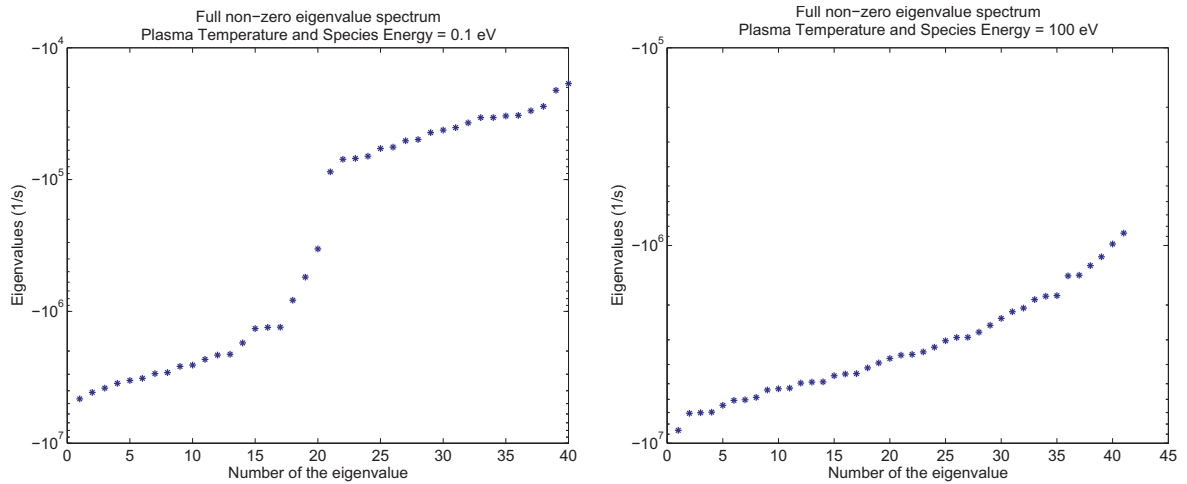


Figure 5.6: Eigenvalue spectrum of the hydrocarbon reaction mechanism, for an electron and proton concentration of  $1e13 \frac{1}{cm^3}$

solution will suddenly happen much later. So in comparison with leaving out all the previous eigenmodes requiring only smaller steps from one to another, this last step over a big time gap is disadvantageous for the ILDM approximation.

Taking a closer look at the left graph of figure 5.6, the gap between two consecutive eigenvalues stay relatively small until eigenvalue  $\lambda_{17}$ . Including this eigenvalue into the ILDM gives the manifold dimension  $m = 54 - 17 = 37$ . Reducing the dimensionality of the ILDM by one ( $m = 36$ ), will decrease the stiffness of the system, but it will imply a big loss in the convergence time of the ILDM solution and the full chemical kinetics. The convergence time associated with the 36-dimensional ILDM dynamics is  $t_{37} < \left| \frac{1}{\lambda_{17}} \right| \approx 3 \times 10^{-6} s$ . Therefore a good ILDM dimension, being one with a small number of parameters and a good accuracy, should be based on the least negative eigenvalue of a relatively flat decay in figure 5.6. At low

temperatures of around 0.1eV good choice for ILDM dimensions are  $m = 37, \lambda_{17}, m = 34, \lambda_{20}$  and  $m = 16, \lambda_{38}$ .

At intermediate energies (0.5 – 5eV) the eigenvalues stay quite constant except for the exotic behavior of the slowest one. The grouping is lost somewhere just below 1eV. At increasing plasma temperatures one would expect the eigenvalues to drop even further because the chemical processes should fully activated. However, up to a hundred eV the eigenvalues do not tend to fall below 1E-07eV. It is difficult to decern bigger jumps between the eigenvalues as they tend to smoothly distribute themselves between 9E-06 and 8E-05. One can notice an isolated gap in the slower eigenvalues between  $\lambda_{35}$  and  $\lambda_{36}$  which would result in a manifold of dimension 19.

A last theme to study, is the domain of the eigenvalues. Figures 5.5 through 5.6 show that the size of the domain of the eigenvalues decreases with increasing temperature and that the eigenvalues become faster.

Normally, the ILDM dimension is determined by the timescales of a perturbation e.g. transport. If these are well defined they can be directly used to cut off any eigenvalue that is too fast. This cut-off time then defines the dimension of the ILDM.

## 5.6 Eigenvector analysis

For homogenous linear systems  $\frac{\partial \vec{\psi}}{\partial t} = F_{\psi} \vec{\psi}$  the left eigenvectors of the system are equivalent with the ILDM equations of that system (see 3.5.2). Table 5.1 represents the left eigenvectors (= the rows of the inverse eigenvector matrix) of a system with 15 species at an temperature of 5eV, an energy of 1eV and a background concentration of  $1e13 \frac{1}{cm^3}$ . The left eigenvectors are ordered, with  $\vec{u}_{15}^L$  being the fastest eigenvector. As the dimension of the ILDM decreases, more and more fast eigenvectors constitute an equation and their vector product with the species concentrations are set to zero, starting with  $\vec{u}_{15}^L$ .

	$e$	$p$	$H$	$H_2$	$H_2^+$	$C^+$	$C$	$CH^+$	$CH$	$CH_2^+$	$CH_2$	$CH_3^+$	$CH_3$	$CH_4^+$	$CH_4$
$\vec{u}_1^L$	1	0	0	0	0	0	1	0.582	1.08	0.598	1.03	0.557	0.861	0.608	0.849
$\vec{u}_2^L$	0	1	0	0	0	0	-5.51E-05	0.582	0.076	0.587	0.0227	0.520	-0.165	0.533	-0.206
$\vec{u}_3^L$	0	0	1	0	0	0	5.51E-05	0.418	0.904	1.22	1.77	1.75	2.49	2.26	3.06
$\vec{u}_4^L$	0	0	0	1	0	0	0	0	0	0.0113	0.00664	0.0362	0.0266	0.0750	0.0544
$\vec{u}_5^L$	0	0	0	0	1	0	0	0	0.0101	0.086	0.0967	0.328	0.309	0.527	0.52
$\vec{u}_6^L$	0	0	0	0	0	1	1	1	1	1	1	1	1	1	1
$\vec{u}_7^L$	0	0	0	0	0	0	-1.73E+00	-1.96	-2.44	-2.38	-3.07	-3.01	-3.42	-3.02	-3.6
$\vec{u}_8^L$	0	0	0	0	0	0	0	0	-2.54	-2.6	-12.7	-15.2	-25.9	-17.6	-37
$\vec{u}_9^L$	0	0	0	0	0	0	0	0	0	0	11.9	17.5	35.9	22.5	61.2
$\vec{u}_{10}^L$	0	0	0	0	0	0	0	-1.76	0.722	0.772	-1.51	-15.5	-65.8	-34.6	-244
$\vec{u}_{11}^L$	0	0	0	0	0	0	0	0	0	0	0	-12.7	-66.3	-33.7	-310
$\vec{u}_{12}^L$	0	0	0	0	0	0	0	0	0	0	0	0	0	0	-3370
$\vec{u}_{13}^L$	0	0	0	0	0	0	0	0	0	0	0	0	-75.9	-32.8	4660
$\vec{u}_{14}^L$	0	0	0	0	0	0	0	0	0	-1.62	1.18	-1.48	60.8	25.4	-1410
$\vec{u}_{15}^L$	0	0	0	0	0	0	0	0	0	0	0	0	0	1.27	-0.415

Table 5.1: Left eigenvectors of the system at  $E_p = E_e = 1eV$  and  $E_s = 1eV$  and a plasma concentration of  $1e13 \frac{1}{cm^3}$

Putting  $\vec{u}_{15}^L$  on zero relaxes eigenvector 15 and gives an algebraic equation to reduce the dimension of the system to 14. Continuing relaxing eigenvectors more algebraic equations are created and the dimension of the dynamical systems keeps decreasing.  $\vec{u}_{10}^L$  (see table 5.1) is an eigenvector that directly represents species number 15 or  $CH_4$ . Relaxing this eigenvector

not only puts the concentration of  $CH_4$  to zero ( $-6,7CH_4 = 0$ ), but also the concentrations of  $CH_4^+$ ,  $CH_3$  and  $CH_3^+$ . This arises from the fact that some eigenvectors span exactly the same space as the species. This can be reasoned out of the corresponding left eigenvectors. The answer to the question why an eigenvector directly contains only one species, is given by the nature of the cascade reactions. The rate of change of the heaviest species in such a system will always only depend on its own concentration, so it will also represent a direction of a left eigenvector. The second question, why also other species are set to zero, can again be answered by the cascade nature of the system. An ILDM of dimension 10 differs however from a quasi steady state assumption of species, because the left eigenvectors 12 and 15 still represent combinations of species, even with the concentration of  $CH_4$ ,  $CH_4^+$ ,  $CH_3$  and  $CH_3^+$  set to zero. It is certain that as ILDM passes from dimension 11 to dimension 10 the approximation of the true solution will get a lot worse, especially for species  $CH_4$ ,  $CH_4^+$ ,  $CH_3$  and  $CH_3^+$ .

It makes no sense to expose here the full left eigenvalue matrix of the 54 species. A quick check however at  $T_{e^-} = T_{p^+} = 5\text{eV}$ ,  $E = 1\text{eV}$  and  $1\text{E}13\text{ cm}^{-3}$  shows us that reducing according to the ILDM-technique with 12 fast timescales contains the QSS assumptions for the following species  $C_3H_5^+$ ,  $C_3H_5$ ,  $C_3H_6^+$ ,  $C_3H_6$ ,  $C_3H_7^+$ ,  $C_3H_7$ ,  $C_3H_8^+$  and  $C_3H_8$ . If one only reduces 9 dimensions, 4 of the reduction equations can be replaced by the QSSA for the first for species of the previous case. To know if the ILDM assumptions holds some QSSA assumptions the more general way is to search for common subspaces. If part of the ILDM equation vectors can be spanned by species vectors then these QSSA assumptions can replace some of the ILDM assumptions. This exercise is however not of great interest. Its purpose is rather to point out the similarities between QSSA and ILDM, which could be useful in future investigations of the system.

## 5.7 Closed chemical reactor

This section compares the time traces of the two reduction methods at different grades of reduction. This pure observation of the temporal behavior of the chemical kinetics is done in the theoretical model of a closed chemical reactor with a homogeneous mixture and where no other process can disturb the chemistry. The time traces are an illustrative way to understand the systems behavior and the influence of the reduction. Many properties of the reduction methods themselves can be explained with these plots. They directly show the time needed for a reduction method to comply with the full solution for the plotted species. In this section the loss of information about the chemical kinetics can be perceived. We demonstrate the influence of gap size between the timescale when reducing the system.

In the figures 5.7 and 5.8 the time traces of some species are plotted for the given background conditions. The initial conditions were chosen  $1\text{cm}^{-3}$  for all hydrocarbon species. The plasma temperature was set to  $1\text{eV}$  because the eigenvalue spectrum showed a remarkable gap for which we now want to demonstrate the influence on the reduction. The type and the dimension of the manifold is written in the legend. The manifolds of higher dimensions take more time scales into account and are thus normally more accurate. The ILDM 33 and 32 falls onto the full solution already between  $1.5E-02$  and  $2E-02$ , whereas the other ILDM's take more time to converge. The  $C_2H_4^+$  and  $C_2H_3$  time traces typically show this property of ILDM manifolds. When this behavior can not be observed this is often due to the components of the species in the concerned eigenvectors. This can cause the ILDM of a higher dimension

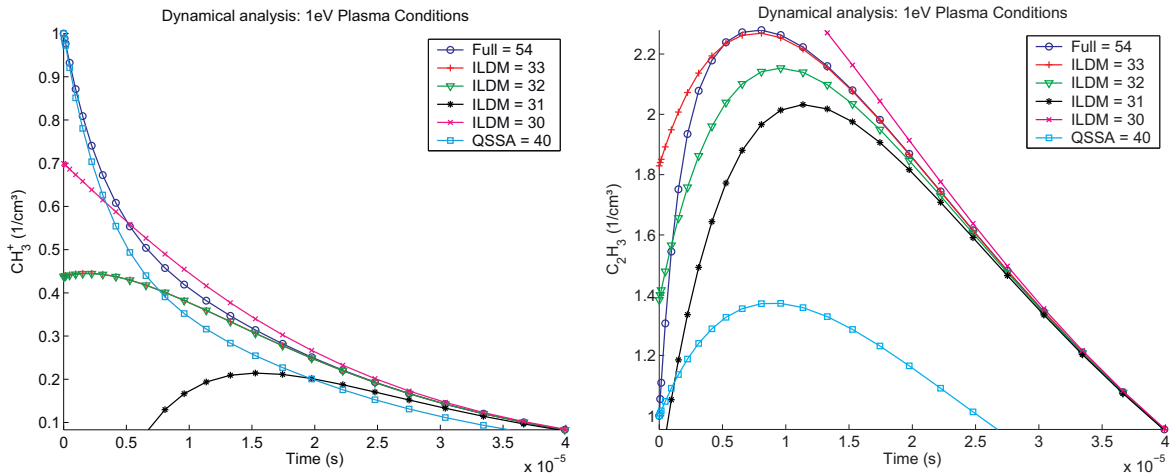


Figure 5.7: Time traces of  $\text{CH}_3^+$  and  $\text{C}_2\text{H}_3$  for a temperature of 1eV, an energy of 1eV and a background concentration  $1e13 \frac{1}{\text{cm}^3}$

to sometimes converge later with the full solution. Nevertheless as a general rule the higher dimensional manifolds are more accurate!

In figure 5.7 left it is irrefutable that the difference between ILDM 33 and 32 is much smaller than the one between 32 and 31 where the bigger gap takes away a lot of the precision of the approximation. The consequences of this bigger than usual gap in the eigenvalue spacing can also be observed in the the time traces of figure 5.7 right and the left figure of 5.8. When taking away still one more degree of freedom going from 31 to 30, it is observed that the approximation stays in comparison pretty good. Once the big jump has been taken, it doesn't really matter anymore wether a next, close, timescale is cut off or not.

The QSSA solution on the other hand has been given a much higher dimension because of two reasons. Firstly it cannot be reduced much further as there are only a certain number of ions present in the system and we assumed that only ions could be seen as reactive 'radical' species in quasi steady state. The QSSA manifolds have thus a minimal dimension of  $54 - 30 = 24$  whereas the ILDM has been given more freedom and we notice that in general using ILDM the system can be reduced with a maximum of  $54 - 13 = 41$  dimensions. This is only limited by the conservation of elements. Secondly the QSSA is a worse approximation, even with higher dimensional manifolds the QSSA doesn't seem to beat the ILDM approximation. Remember that we are exposing the QSSA with conservation of equilibrium in these plots. This variant is generally a better approximation than the variant proposed in literature. Although the QSSA solution starts in the same initial condition for  $\text{CH}_3^+$  and  $\text{C}_2\text{H}_3$  it immediately takes distance from the full solution and is attracted towards it only much further when steady state is achieved and the system attains its equilibrium.

A peculiarity of the the ILDM approximation is that it can sometimes coincide partly with the QSSA approximation. The reason for this has been explained in the section about the left eigenvectors 5.6. This can be easily observed in the time trace of  $\text{C}_3\text{H}_8^+$  of figure 5.8. The ILDM solutions for this species stay on zero because of the structure of the left eigenvectors. In general problems this coincidence doesn't occur very often, but for the hydrocarbon mechanism the upper triangular Jacobian structure results frequently in short left eigenvectors containing only a few elements at the end. Therefore in many cases there

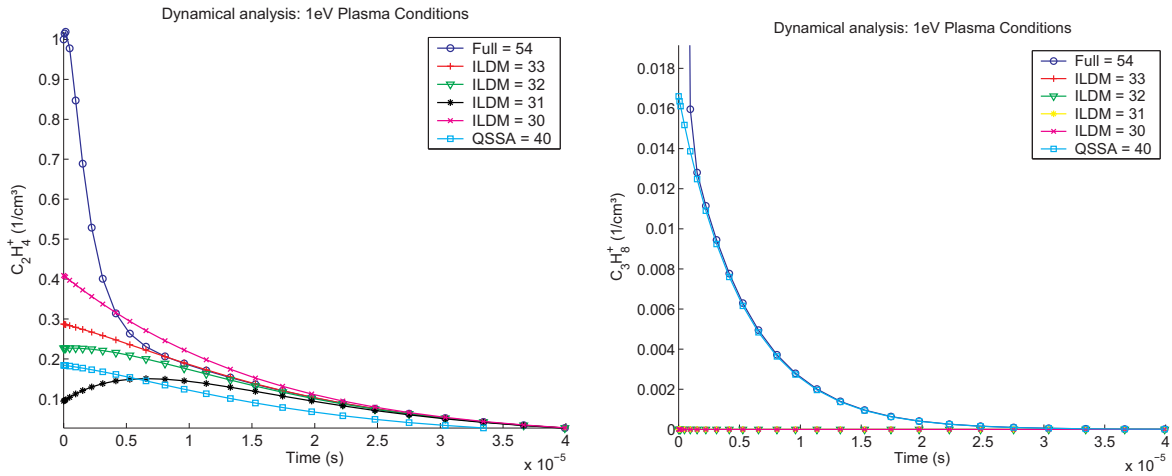


Figure 5.8: Time traces of  $C_2H_4^+$  and  $C_3H_8^+$  for a temperature of 1eV, an energy of 1eV and a background concentration  $1e13 \frac{1}{cm^3}$

is an overlap between the QSSA of some species (not necessarily ions) and the ILDM. This doesn't mean that QSSA is a good reduction method but it implies that some species can be chosen for quasi steady state rather than letting the user pick the species for the QSS assumption. It is exactly here that lies the advantage of ILDM it detects automatically the modes to relax!

## 5.8 Chemical plug reactor

A chemical plug reactor is characterized by the convective transport of a chemical mixture in one dimension. On its way through the reactor, the mixture is subject to changing background conditions, that influence its reactivity. In fusion research, this simple one dimensional model, provides a first step to simulate the reduced transport of the sputtered hydrocarbons, with ILDM. Applying the ILDM technique on the plug reactor model, means: solving its projected transport equation (4.4) in a low dimensional parameter space. A consequence of the projection, is that both the chemical and the physical source term can only produce composition changes within the manifold. Therefore, for each grid cell, the ILDM solution will always lie on the manifold of the cell. It is important to keep this in mind, when seeking the cell conditions (chemical timescales, velocity and cell length) for which the full solution can be approximated by the ILDM solution.

This section consists of two subsections. First, the effects of the projection at the cell boundaries is investigated and illustrated for the CH-example of section 2.2.3. And the ILDM method will be applied on the full hydrocarbon chemistry.

### Investigation of the effect of the projection at the cell boundaries

The implicit solver of the plug reactor model, presented in section 4.2.3, contains both the concentration of cell  $k$  and its upwind neighbor  $k-1$ . Because the concentrations of cell  $k-1$  are not necessarily on the manifold of cell  $k$ , they must be projected when used in the solver, see equation 4.5. Not projecting results in a diverging solution, if the spatial distribution

of plasma conditions in the reactor is non-uniform, see figure 3.4 in section 3.4.3. In this subsection, the effects of the projection on the ILDM solution will be investigated, by first focussing on the cell boundary and then elaborating the effect for multiple cells.

**Closer look on the cell boundary** To solve the model of the plug reactor numerically, the geometry is discretized into a large number of grid cells which can be seen as small homogeneous open, because this time transport is allowed, chemical reactors. At a specific moment in time, each of these cells has some kind of averaged uniform mixture condition (energy, temperature and concentrations), depending on the type of discretisation. In what follows, we will study the response of a cell on the projection, by assuming that the global cell concentrations are a function of their spatial distribution in the cell. For simplicity, we study a cell in steady state. Then, the spatial distribution of its concentrations is given by:

$$V \cdot \frac{\partial \vec{\phi}(\infty, x)}{\partial x} = F_{\vec{\phi}} \cdot \vec{\phi}(\infty, x) \quad (5.1)$$

which was derived from equation (4.3). Because the plasma conditions are constant in the cell, the diagonal speed matrix ( $V$ ) and the Jacobian matrix ( $F_{\vec{\phi}}$ ) are independent of the position in the cell ( $x$ ). Assuming that the hydrocarbons have a uniform speed ( $v$ ), equation 5.1, can be transformed into the model equation of a closed chemical reactor by substituting  $x = vt$ .

$$\frac{\partial \vec{\phi}(\infty, x)}{\partial t} = F_{\vec{\phi}} \cdot \vec{\phi}(\infty, x)$$

Under these assumptions, the timescales of the Jacobian matrix can be used to predict the relaxation distance  $x_{\text{relaxf}}$  needed for the reduced system and the full system to converge:

$$x_{\text{relaxf}} = v \cdot t_{\text{decay}} \quad (5.2)$$

with  $t_{\text{decay}}$  being for example three times the slowest of the fast timescales, which are decoupled for reduction, of the Jacobian matrix. If the full hydrocarbon system is used  $t_{\text{decay}}$  can in this case directly be determined with figures 4.13 and 4.14.

Figure 5.9 illustrates a two cell model for the CH-example of section 2.2.3, with a temperature jump between both cells (from 0.1 to 7 eV). The influx conditions were chosen to be on the manifold of the left cell, to observe only the effect of the projection when entering the right cell. The left plot in figure 5.9 illustrates the spatial distribution of the concentrations, while the right plot illustrates the global concentrations in both cells. The cell centres can be found at  $x=2.5\text{cm}$  and  $x=7.5\text{cm}$ . Both the one dimensional ILDM and the full solution are plot. The ILDM solution is represented by the solid lines, while the full solution is represented by the dashed lines.

In what follows next, we want to show that the relaxation distance can be used to approximate the error between the ILDM and the full solution of the cell. This error is also dependent on the way the spatial distribution of the concentration within the cell is used to determine the homogeneous concentration of the cell. For the plug reactor model, figure 5.9 shows that the concentration is more an averaged value of the spatial distribution of the concentration than it is the concentration at the end of the cell. Therefore, the error between the ILDM and the FULL solution will, due to the projection, only be small, if the spatial

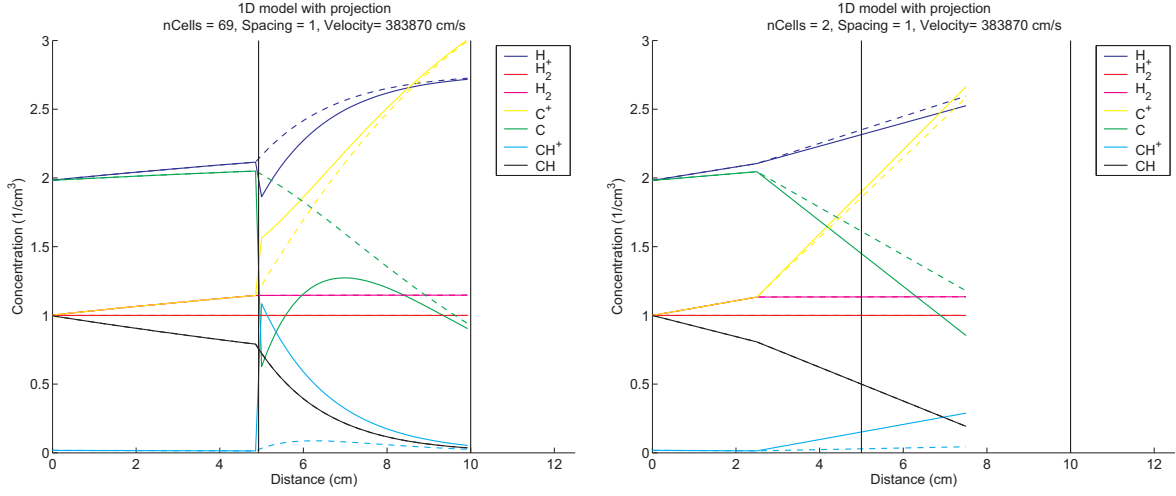


Figure 5.9: Left: The spatial behavior of the concentrations of the molecules in the CH-example, for a two cell model, with a temperature jump between both cells from 0.1 to 7 eV. Right: The global concentrations of the molecules of the CH-example for the same conditions. The plasma density is 1E13eV

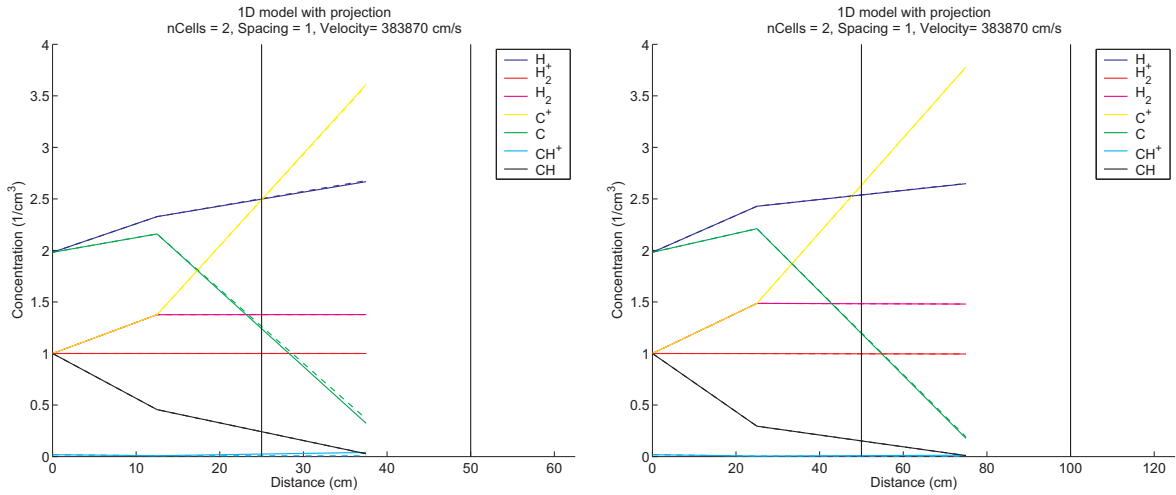


Figure 5.10: The global concentrations of the molecules of the CH-example for the same conditions, for a two cell model, with a temperature jump between both cells from 0.1 to 7 eV. Left:  $L_{\text{Cell}} = 5x_{\text{relax}}$ . Right:  $L_{\text{Cell}} = 10x_{\text{relax}}$ . The plasma density is 1E13eV

distribution of the ILDM and the full solution are equal for most of the cell. This means that if  $L_{\text{Cell}} \gg x_{\text{relaxf}}$  the projection will not be noticed in the solution.

For figure 5.9 the second cell has a chemical timescale of 0.41s. Because the relaxation distance ( $x_{\text{relaxf}} = 4.7\text{cm}$ ) equals the cell length, the error between the ILDM and the full solution of that cell is still significant. If the cell length is increased to  $L_{\text{Cell}} = 10x_{\text{relaxf}}$ , the error disappears. This can be verified in figure 5.10.

**Multiple cells** At each cell boundary, the ILDM solution of the upwind cell is projected onto the manifold of the cell. These projections introduce jumps at the cell boundaries, that are attenuated by the chemistry in the cell, see figure 5.9. As explained in the previous paragraph, the cell's capacity to attenuate, depends on its size, on the hydrocarbon speed and on the chemical timescales. If the cell is incapable of attenuating a jump, an ILDM solution different from the full solution will be projected on the next cell. In general, the manifolds of these cells are close together, so the projection will only introduce a small extra jump onto the error. If the cell can attenuate more than this extra jump, the ILDM solution will start approaching the full solution again.

The size of the extra jumps at subsequent cell boundaries will thus be dependent on the projection distance of the concentrations of the upwind cell to the manifold of the actual cell. In a plug reactor, the distance from the manifold is dependent on two factors. First, on the temperature, because the fast eigenvectors change with temperature. Secondly, on the travelled distance through the reactor, because the chemical equilibrium lies on all manifolds.

We can thus conclude that close to the wall, the ILDM solution will not lie on the full solution and that strong manifold changes due to temperature, will also bring the ILDM solution away from the full solution, if the mixture is far from chemical equilibrium. These conclusions are illustrated in figure 5.11.

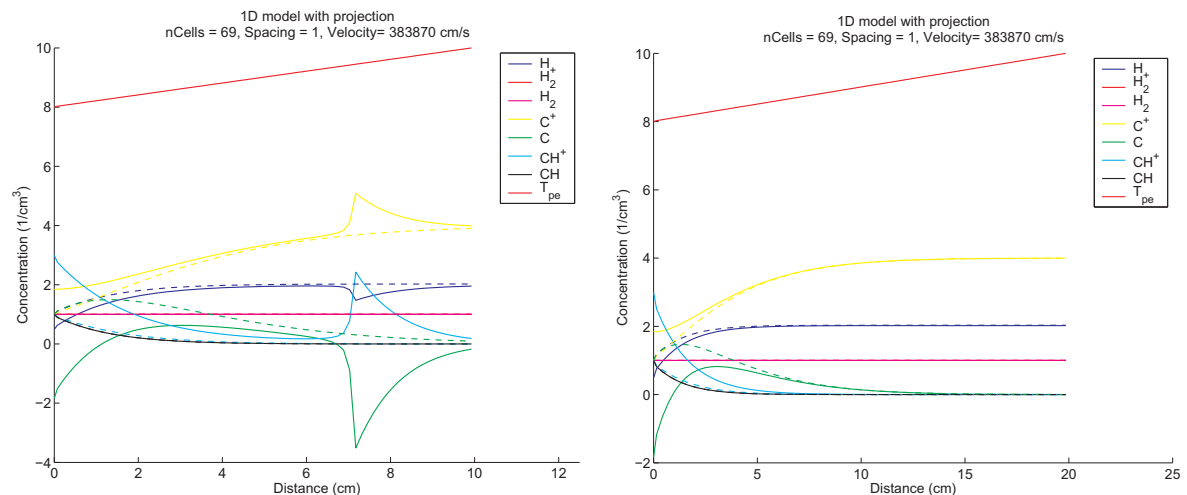


Figure 5.11: The behavior of the CH-example in a plug reactor with a linear temperature rise, from 8 to 10 eV. The plasma density is  $1E13eV$

The left plot of this figure illustrates the behavior of the hydrocarbon mixture in a plug reactor, if the temperature rises from 8 to 10 eV. One can readily notice that at about 9.5 eV the ILDM solution and the full solution seem to diverge. The big jump arises because from one cell to another the manifold changes suddenly. This is due to the phenomenon of crossing eigenvalues. If the eigenvalues cross, a slower eigenvector suddenly becomes fast. This changes the equations of the manifold. After this jump the ILDM solution in the coming cells converges with the full solution again. The right plot of this figure illustrates the influence of the initial projection. In this plot a same overall temperature decay was used, but for a larger reactor. In this case, the crossing eigenvalues have no more effect on the ILDM solution, because the mixture is in chemical equilibrium before the temperature reaches 9 eV.

9.420eV	C	CH <sup>+</sup>	CH
C	-1.633E+05	3.365E+05	2.191E+05
CH <sup>+</sup>	0	-3.753E+05	1.340E+05
CH	0	0	-3.748E+05

9.478eV	C	CH <sup>+</sup>	CH
C	-1.6508E+005	3.3791E+05	2.206E+05
CH <sup>+</sup>	0	-3.771E+05	1.364E+05
CH	0	0	-3.780E+05

Table 5.2: Jacobian matrices for  $T_{pe}=9.420eV$  and  $T_{pe}=9.478eV$ , the other background conditions are:  $\phi_{pe}=1E13/cm^3$ ,  $E=1eV$ . Note that the two fastest eigenvalues of the Jacobian matrices cross

### Simulation of the full hydrocarbon system

In this last section the full capabilities of ADMT are used to expose the behavior of the complete hydrocarbon system in a 1 dimensional transport model. With the help of section 4.4.1 a set of initial conditions and background conditions was chosen that comes close to the conditions in the ITER divertor. A varying plasma energy  $T_{pe}$  from 0.1eV at the divertor plate (0cm) up to 10eV deeper into the plasma edge ( $L = 10cm$ ) was applied throughout the grid together with a spatially uniform density of  $\phi_{pe} = 1E13cm^{-3}$ . The sputtering yield from this plasma flux was assumed to come for 100% from the  $C_3H_8$  molecule resulting in an initial density of  $6.6E11cm^{-3}$  and velocity of  $6.6E4cm/s$ . The sputtering velocity is calculated here from its energy  $E_{HC} = 0.1eV$  with  $v = \sqrt{\frac{2E}{m}}$ .

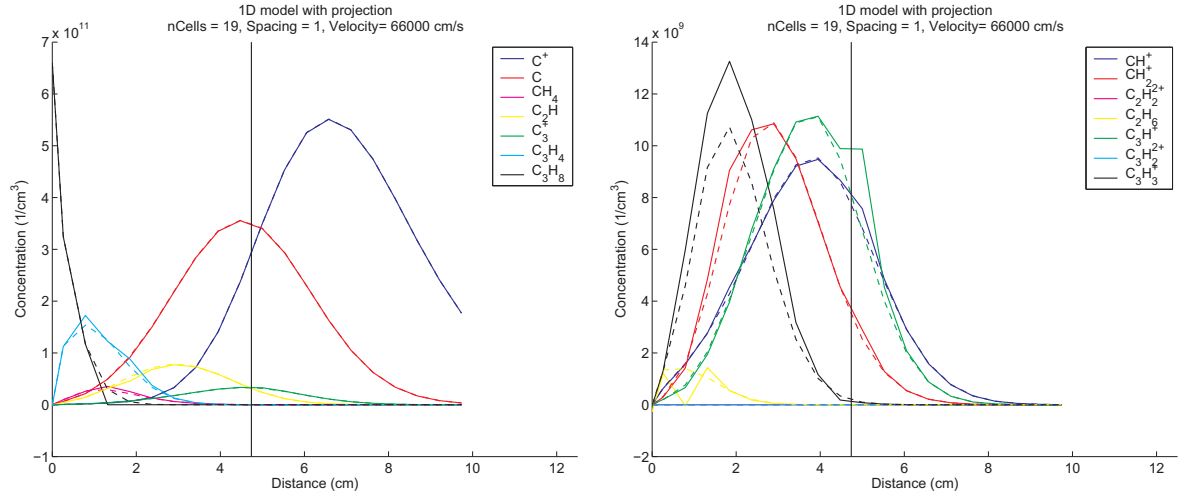


Figure 5.12: The global concentrations of the molecules of the CH-example for the same conditions, for a two cell model, with a linearly increasing temperature from 0.1 to 10 eV.  $L_{Grid} = 10cm$  and  $nCells = 19$ . The plasma density is  $1E13eV$

The results from the ADMT run for the 1-dimensional plug reactor at time  $1E - 04s$  are illustrated in figure 5.12. Note that steady state is not yet reached at this time. For later times steps the spatial distribution of  $C^+$  should rise and become a monotonously increasing function that reaches an equilibrium of about  $3 \times 6.6E11cm^{-3}$ . As it is not possible to show all species concentrations in one plot only a few are selected. The dimension of the ILDM has been chosen to 38 and only 16 fast time scales were decoupled from the dynamics. It seems that for lower dimensions of the manifold the ILDM approximations with projection at the cell boundary get suddenly a lot worse.

From the species of interest  $\text{CH}_3$ ,  $\text{C}_2\text{H}$ ,  $\text{C}_2\text{H}_3$  and  $\text{C}_2\text{H}_5$  only  $\text{C}_2\text{H}$  is given in 5.12, but it can be told that the others occur in quite big amounts as well. It can thus easily be understood from this model that these radicals contribute to the deposition in the remote areas of the reactor.

The (2+)-ions in figure 5.12 right are all close to zero concentration. Therefore the ILDM approximates them by assuming them zero. This corresponds to a QSSA for these species. In the behavior of  $\text{C}_2\text{H}_6$  one can notice oscillations. There is a jump downward followed by an upward jump after which it converges with the full solution again. This is to be explained because two eigenvalues are crossing each other twice. Another species shows this behavior too. Of course when eigenvalues cross other species will show this defect too.

An important general remark is to be made about the ILDM and its applicability on the different species. As the error of a single species resulting from the approximation is not only dependent on the eigenvalues but also on the contribution the eigenvectors make to that species. It can be said that generally the heavy species are faster and more reacting than the ones with lower mass. As from the catabolic structure of the reactions, they are thus more readily broken down and have in general lower concentrations partly due to their higher content of elements. This lower concentration makes them more sensitive to cutting of eigenvectors which is clearly visible in the difference between the left and the right plot of 5.12.

## 5.9 Conclusion

This chapter has combined the knowledge of all the previous ones to thoroughly investigate the properties and potentiality of reduction methods on the full hydrocarbon reaction mechanism including all 54 species. The eigenvalues appear to be correct estimates for the accuracy of the reduced solution. In ILDM approximations the big gap between two consecutive eigenvalues is a good place for cutting off the faster eigenmodes. This has been demonstrated in the 0-D model. It is thus always interesting to get an overview of the eigenvalues in the in the desired domain of plasma conditions. On the other hand dimension reduction charts are convenient tools to determine the optimum reduction for a range of plasma conditions. These charts are based on a convergence time retrieved from the transport processes and a required accuracy. It is also clear from these results that the stiffness of the system can be reduced with the ILDM reduction technique. The analysis of the 1-dimensional plug reactor model gives very interesting results about the choice of grid cell width and the importance of the projection at the cell boundaries.



## Chapter 6

# Conclusion

We close this work by summarizing the main results (next section) and by providing an outlook to future work, in particular on the remaining open issues of implementation of ILDM techniques into Monte Carlo kinetic transport codes such as EIRENE and for the particular hydrocarbon transport-chemistry issue studied in the present work.

### 6.1 Summary

The summary of the most significant results of the FORTRAN program are:

#### Cross Sections and Reaction Rates

- Thanks to the detailed comparison of HYDKIN (PERL) and an independently written FORTRAN program ‘ADMT’ we discovered a significant number of programming errors, data inconsistencies, etc. in both codes.

The resulting modifications in HYDKIN in July 2006 have now led to simulations which match the experimental observations (C, C2 and CH light emission from controlled gas puff experiments of CH<sub>4</sub>, C<sub>2</sub>H<sub>6</sub> and C<sub>3</sub>H<sub>8</sub> into the hydrogen plasma) from the TEXTOR tokamak at FZ-Juelich much better than before.

- This code verification program allows now to conclude that the cross sections and reaction rates of the full hydrocarbon mechanism for the species up to C<sub>3</sub>H<sub>8</sub> are calculated correctly in both ADMT and HYDKIN and this in the complete range of plasma conditions and species energies.
- This independent duplication of code development has increased considerably the credibility and reliability of both codes, in particular also because not only the programming language but also the method of solution for the ODE’s in both codes is completely different.

#### Spectral decomposition of the Jacobian

- It has been discovered that the hydrocarbon catabolism generate an upper triangular Jacobian matrix.

- Consequently the eigenvalues of the Jacobian lie on its diagonal which is computationally very beneficial because special efficient routines exist to calculate the eigenvectors of these types of matrices.
- Future expansion of the reaction system will include radiative recombination rates. This will give the Jacobian a Hessenberg form, for which an eigenvalue-eigenvector determination still has significant computational advantages.
- The stiffness of the chemical source term decreases with increasing plasma temperature and is almost independent from the hydrocarbon species energy.
- The stiffness is only influenced by the slowest eigenvalue, because the fastest eigenvalues stays almost constant. The slowest eigenvalue is basically influenced by the C and C<sup>+</sup> species which are barely reactive at low plasma temperatures.
- The steps between succeeding eigenvalues are almost constant in a logarithmic scale. Only at low plasma energies ( $< 0.5 \text{ eV}$ ) the eigenvalues group themselves into 3 zones.
- It can be deduced from the eigenvalue analysis how many eigenvectors can be assumed relaxed. The charts presented in section 4.4.2 for dimension reduction in different plasma conditions are a useful tool for the reduced hydrocarbon simulations. They show, furthermore, that the present treatment of this problem in ITER design studies is obtained as limiting case, which is correct only at very low plasma temperatures. We have been able to evaluate the boundaries in plasma parameter space, at which the present ITER divertor simulation codes loose their accuracy and more complex schemes, e.g. the ILDM concept discussed in this work, have to be implemented.
- The problem with the microscopical way to simulate the hydrocarbon transport is that the timescale of the transport processes are directly associated with the timescales of the chemistry. Therefore cutting in the dynamics of the chemistry often implies a loss in the transport dynamics as well. Therefore it is important to look at big gaps and groupings of the eigenvalues and make a trade off to efficiently reduce the mechanism.

### 0-Dimensional reactive model

- It is a property of the real solution to be attracted towards the ILDM manifold. The timescales are the inverse of the eigenvalue. The time to convergence between the full solution and the ILDM solution is thus directly dependent on the eigenvalues. This is why it serves as a criterion for the determination of the number of dimensions to reduce.
- It is observed in the time traces of section 5.7 that at low plasma temperatures ( $< 0.5 \text{ eV}$ ), where the eigenvalues are grouped together in three groups, the least negative eigenvalue of a group is a good ILDM dimension. Further reducing the dimension of the ILDM produces a big jump in timescales.
- With the same amount of reduction in number of species, an ILDM approximation is much better than a QSS Approximation of the hydrocarbon ions.
- ILDM does in any case reduce the stiffness of the problem, so the explicit solvers stays stable, even for bigger time steps. This is strongly in contrast with the QSSA where it

is dependent on the choice of QSS-species whether the stiffness is reduced or not. In a Monte Carlo solver reducing the stiffness implies a reduction of the statistical noise for a given CPU effort, because in stiff cases trajectories are more frequently interrupted than in non-stiff cases. In this sense the ILDM reduction technique is thus also beneficial for EIRENE.

- The QSSA applied in the thesis is a modified version of the QSSA found in literature. In contrast with the original method our method is forced to conserve the conservation variables from the original Jacobian. This results in a better approximation than the classical QSSA and is more close to what happens in the EIRENE implementation of QSSA. It is however still less good than ILDM.

### 1-Dimensional reactive flow model

- ILDM provides good results if the time interval is big enough. With known speed of the hydrocarbon particle, the length at which the full solution lies on the manifold can thus be determined with the most negative ILDM eigenvalue. As a consequence the grid cells closest to an initial flux which is not on the manifold will always give wrong compositions.
- With spatially changing background temperatures the system should not be solved directly in the parameter space over the different grid cells. Cell boundaries require a projection onto the new manifold. If this is not done the ILDM solution gives poor results, but the same applies, for course, to the QSSA method.
- For explicit solvers calculating the ILDM solution is computationally more expensive than calculating the full solution because of the required projections at the cell boundaries.

### General conclusions

1. The ILDM reduction method can be applied on deterministic as well as stochastic (Monte Carlo) methods of solution. The proof of principle has been given here, although a number of details had to be left for future work. In particular the statistical noise in Monte Carlo procedures may be negatively affected in model cases that are more complex than the ones investigated here. On the other hand the freedom of choices of “parameters” for the ILDM can perhaps be used to optimize Monte Carlo ILDM schemes.
2. The dimension of the ILDM can be chosen based on the timescale and the required accuracy.
3. The ILDM approximation offers better results than the QSSA of the ions.
4. Changing background concentrations require projections onto the new manifold at each cell boundary. We believe that finding an efficient method to achieve this in a Monte Carlo procedure will be essential for the applicability of ILDM in this context.

## 6.2 Future Work

As already mentioned, the nature of the EIRENE code makes it impossible to apply the ILDM algorithm without modifications. As no solution strategy for these modifications exists yet, in this work an implementation of the ILDM algorithm for the EIRENE program was proposed and carried out in a first simple prototypical application. The approach is based on the relation between the Jacobian matrix and the ‘local’ reaction system.

This approach can be used to reduce the current database and the complexity of the problem. The locally reduced Jacobian can be translated into an “efficient” local reaction mechanism. A *tabulation* of this reduced reaction mechanism for the different plasma conditions and species energy will offer the possibility to more efficiently calculate the hydrocarbon transport processes. To use this reduced database efficiently, new *fitting curves* can be constructed. Probably the formulas of these curves will have similar forms as the formulas from the original database, at least if some universal features of the hydrocarbon collision mechanisms (which have already been pointed out by Janev and Reiter in their databases) are retained in the reduced system.

Beside the reduction of the number of reaction rates, it is also necessary to convert the *scattering angles* and *energy* exchanges associated with the collision reactions. The same principle as for the reaction rates is probably applicable for these reaction properties. Although this method seems bullet proof, at first seemingly strange effects arise in the reduced mechanism. Some reaction coefficients become negative. This is however not necessarily inevitable. The real work might then lie in finding a *parametrization* which produces positive coefficients over a wide range of plasma conditions and species’ energies, using in this way the property that ILDM’s are insensitive to the choice of parameters.

A physical peculiarity of the present combined chemistry - transport problem is that some of the species are neutral, and others are ionized. In the strong magnetic fields in fusion experiments (2-10 Tesla) the transport of these ions is essentially restricted to motion parallel to the B-field, whereas the neutral fragments are free to move in all three spatial directions. In order to account for this within the ILDM scheme it would be desirable (perhaps even mandatory) to find a parametrization which keeps neutral and ionized species separate.

If this is possible together with the previous requirement to retain positive coefficients remains to be studied.

An important issue to be solved is the projection at the cell boundaries. It should still be investigated what the results would be when ignoring the shift in species concentration when the plasma conditions change from one cell to another. It might be a characteristic of the ILDM that perturbations automatically decay and that nevertheless the full solution is reached after some time. If this time is short compared to the free flight time of a particle across a grid cell, then the projections may be avoidable.

But in this respect the QSSA method has identical drawbacks.

There are a few extensions that could be added in the future which make the database more accurate. At first introducing a few ‘backward’ (radiative recombination) reactions into the database would make the Jacobian matrix loose its upper diagonal form. A more general way of finding the eigenvalues of this Hessenberg matrix can be found here. Moreover if all possible collision reactions not only between hydrocarbons and the plasma, but also amongst the hydrocarbons themselves, are taken into account the system would be of the second order Riccati type. To handle these and other non-linear problems a numerical calculation of the Jacobian was tested in the ADMT program which works fine. The future investigator of the

hydrocarbon reaction mechanism might have to implement this again in order to reduce the general non-linear systems. This however still seems far ahead.



# Bibliography

- BODENSTEIN, M., LIND, S.C., Geschwindigkeit der Bildung des Bromwasserstoffs aus seinen Elementen, *Zeitschrift für physikalische Chemie, Stochiometrie und Verwandtschaftslehre*, volume 57, (1906), pp. 168–192.
- BRAAMS, B.J., Computational Studies in Tokamak Equilibrium and Transport, Ph.d. thesis, Rijksuniversiteit Utrecht (1986).
- BULTHEEL, A., Inleiding tot de numerieke wiskunde, Deel II: Iteratieve methodes, Wouters (1996).
- DEUFLHARD, P., HEROTH, J., Dynamic dimension reduction in ODE models (1995), URL [citeseer.ist.psu.edu/deuflhard95dynamic.html](http://citeseer.ist.psu.edu/deuflhard95dynamic.html).
- DIERCKX, P., PIESSENS, R., *Analyse II*, Wouters (2003).
- EFUNDA, Engineering Fundamentals, <http://www.efunda.com/> (2006).
- FEDERICI, G., TIVEY, R., ISELI, M., Workshop In-Vessel T Inventory (2003).
- Glassmaker, N., Intrinsic Low-Dimensional Manifold Method for Rational Simplification of Chemical Kinetics.
- GORBAN, A.N., KARLIN, I.V., Coarse-grained quasi-equilibrium approximations for kinetic equations, *Adv. Model. and Analysis C*, volume 35(1), (1992a), pp. 17–27.
- GORBAN, A.N., KARLIN, I.V., The constructing of invariant manifolds for the Boltzmann equation, *Adv. Model. and Analysis C*, volume 33(3), (1992b), pp. 39–54.
- GORISSEN, D.A., *Natuur en Techniek* (1995).
- HENDRICKS, J.S., A Monte Carlo code for particle transport, Los Alamos Science, volume 22.
- ITER, International Thermonuclear Experimental Reactor, Fusion Basics, <http://www.iter.org/> (2005).
- JANEV, R.K., REITER, D., Collision Processes of Hydrocarbon Species in Hydrogen Plasmas: I. The Methane Family, report 3966, Forschungszentrum Jülich (2002a).
- JANEV, R.K., REITER, D., Collision Processes of Hydrocarbon Species in Hydrogen Plasmas: II. The Ethane and Propane Families, report 4005, Forschungszentrum Jülich (2002b).

- JET, Joint European Torus, Fusion Basics, <http://www.jet.efda.org/> (2005).
- LAM, S.H., Using CSP to Understand Complex Chemical Kinetics, *Combustion Science and Technology*, volume 89(5–6).
- LAM, S.H., GOUSSIS, D.A., Understanding Complex Chemical Kinetics with Computational Singular Perturbation, *Symposium (International) on Combustion/The Combustion Institute*, volume 22, (1988), pp. 931–941.
- LAM, S.H., GOUSSIS, D.A., A study of homogenous methanol oxidation kinetics using CSP, *Symposium (International) on Combustion/The Combustion Institute*, volume 24, (1992), pp. 113–120.
- LAMARSH, J.R., BARATTA, A.J., *Introduction to Nuclear Engineering*, Prentice Hall, 3rd edition (2001).
- MAAS, U., POPE, S.B., Implementation of Simplified Chemical Kinetics Based on Intrinsic Low-Dimensional Manifolds, *Symposium (International) on Combustion/The Combustion Institute*, volume 24, (1992a), pp. 103–112.
- MAAS, U., POPE, S.B., Simplifying chemical kinetics: Intrinsic low-dimensional manifolds in composition space, *Combustion and Flame*, volume 88, (1992b), pp. 239–264.
- NAG, Numerical Algorithms Group, Fortran Routines, <http://www.nag.co.uk/> (2006).
- POPE, S.B., Computationally efficient implementation of combustion chemistry using in situ adaptive tabulation, *Combustion Theory and Modelling*, volume 1, (1997), p. 41.
- RAWLINGS, J.B., EKERDT, J.G., *Chemical Kinetics*, Nob Hill Publishing (2004).
- REITER, D., Eirene-A monte carlo linear solver, <http://www.eirene.de/> (2006).
- REITER, D., Kotov, V., *Progress in Divertor Modelling for ITER and future Devices*, Forschungszentrum Jülich (2006).
- REITER, D., *The EIRENE Code User Manual* (1995).
- ROUSSEL, M.R., FRASER, S.J., Accurate steady-state approximations: Implications for kinetics experiments and mechanism, *J. Phys. Chem.*, volume 95, (1991), pp. 8762–8770.
- SAJDA, P., *Computational Neural Modeling and Neuroengineering*, Columbia University (2001).
- SAMM, U., Controlled thermonuclear fusion enters with ITER into a new era.
- SCHMIDT, D., Modellierung reaktiver Strömungen unter Verwendung automatisch reduzierter Reaktionsmechanismen, Ph.d. thesis, Universität Stuttgart (1995).
- Turanyi, T., T.A.S., Philling, M.J., On the Error of the Quasi-Steady-State Approximation, volume 97, (1993), pp. 163–172.
- Tzafiriri, R.A., Edelman, E.R., On the validity of the quasi-steady state approximation of bimolecular reactions in solution, volume 97, (1993), pp. 163–172.
- Wikipedia, Encyclopedia, <http://www.wikipedia.com/> (2006).

# Appendix A

## Comparison ADMT-HYDKIN

### A.1 The hydrocarbon species

		Species i				
i =1-6	e	H <sup>+</sup>	H	H <sub>2</sub> <sup>+</sup>	H <sub>2</sub>	C <sup>+</sup>
i =7-12	C	CH <sup>+</sup>	CH	CH <sub>2</sub> <sup>+</sup>	CH <sub>2</sub>	CH <sub>3</sub> <sup>+</sup>
i =13-18	CH <sub>3</sub>	CH <sub>4</sub> <sup>+</sup>	CH <sub>4</sub>	C <sub>2</sub> <sup>+</sup>	C <sub>2</sub>	C <sub>2</sub> H <sup>2+</sup>
i =19-24	C <sub>2</sub> H <sup>+</sup>	C <sub>2</sub> H	C <sub>2</sub> H <sub>2</sub> <sup>2+</sup>	C <sub>2</sub> H <sub>2</sub> <sup>+</sup>	C <sub>2</sub> H <sub>2</sub>	C <sub>2</sub> H <sub>3</sub> <sup>+</sup>
i =25-30	C <sub>2</sub> H <sub>3</sub>	C <sub>2</sub> H <sub>4</sub> <sup>+</sup>	C <sub>2</sub> H <sub>4</sub>	C <sub>2</sub> H <sub>5</sub> <sup>2+</sup>	C <sub>2</sub> H <sub>5</sub> <sup>+</sup>	C <sub>2</sub> H <sub>5</sub>
i =31-36	C <sub>2</sub> H <sub>6</sub> <sup>+</sup>	C <sub>2</sub> H <sub>6</sub>	C <sub>3</sub> <sup>+</sup>	C <sub>3</sub>	C <sub>3</sub> H <sup>+</sup>	C <sub>3</sub> H
i =37-42	C <sub>3</sub> H <sub>2</sub> <sup>2+</sup>	C <sub>3</sub> H <sub>2</sub> <sup>+</sup>	C <sub>3</sub> H <sub>2</sub>	C <sub>3</sub> H <sub>3</sub> <sup>2+</sup>	C <sub>3</sub> H <sub>3</sub> <sup>+</sup>	C <sub>3</sub> H <sub>3</sub>
i =43-48	C <sub>3</sub> H <sub>4</sub> <sup>2+</sup>	C <sub>3</sub> H <sub>4</sub> <sup>+</sup>	C <sub>3</sub> H <sub>4</sub>	C <sub>3</sub> H <sub>5</sub> <sup>2+</sup>	C <sub>3</sub> H <sub>5</sub> <sup>+</sup>	C <sub>3</sub> H <sub>5</sub>
i =49-54	C <sub>3</sub> H <sub>6</sub> <sup>+</sup>	C <sub>3</sub> H <sub>6</sub>	C <sub>3</sub> H <sub>7</sub> <sup>+</sup>	C <sub>3</sub> H <sub>7</sub>	C <sub>3</sub> H <sub>8</sub> <sup>+</sup>	C <sub>3</sub> H <sub>8</sub>

Table A.1: The 54 species in the hydrocarbon reaction mechanism

## A.2 Cross Sections

$\sigma$ (cm <sup>2</sup> )		Plasma energy (eV)					
		1eV	205eV	409eV	613eV	817eV	1000eV
r_3966.t_7.3							
react 1	HYDKIN	0.00E+00	1.17E-16	8.03E-17	6.21E-17	5.12E-17	4.44E-17
	ADMT	0.00E+00	1.17E-16	8.03E-17	6.21E-17	5.12E-17	4.44E-17
react 2	HYDKIN	0.00E+00	3.49E-17	2.36E-17	1.79E-17	1.46E-17	1.26E-17
	ADMT	0.00E+00	3.49E-17	2.36E-17	1.79E-17	1.46E-17	1.26E-17
react 3	HYDKIN	0.00E+00	1.15E-17	7.64E-18	5.64E-18	4.47E-18	3.77E-18
	ADMT	0.00E+00	1.15E-17	7.64E-18	5.64E-18	4.47E-18	3.77E-18
r_4005.t_A1.1b							
react 1	HYDKIN	0.00E+00	3.68E-16	2.43E-16	1.83E-16	1.48E-16	1.27E-16
	ADMT	0.00E+00	3.68E-16	2.43E-16	1.83E-16	1.48E-16	1.27E-16
react 2	HYDKIN	0.00E+00	3.14E-17	1.98E-17	1.45E-17	1.15E-17	9.73E-18
	ADMT	0.00E+00	3.14E-17	1.98E-17	1.45E-17	1.15E-17	9.73E-18
react 3	HYDKIN	0.00E+00	1.49E-17	9.21E-18	6.68E-18	5.27E-18	4.44E-18
	ADMT	0.00E+00	1.49E-17	9.21E-18	6.68E-18	5.27E-18	4.44E-18
r_4005.t_A2.b.1							
react 1	HYDKIN	0.00E+00	4.56E-17	3.42E-17	2.76E-17	2.34E-17	2.06E-17
	ADMT	0.00E+00	4.56E-17	3.42E-17	2.76E-17	2.34E-17	2.06E-17
react 2	HYDKIN	0.00E+00	3.55E-17	2.70E-17	2.21E-17	1.88E-17	1.67E-17
	ADMT	0.00E+00	3.55E-17	2.70E-17	2.21E-17	1.88E-17	1.67E-17
react 4	HYDKIN	0.00E+00	2.43E-17	1.78E-17	1.43E-17	1.21E-17	1.06E-17
	ADMT	0.00E+00	2.43E-17	1.78E-17	1.43E-17	1.21E-17	1.06E-17

Table A.2: Comparison of the cross sections (cm<sup>2</sup>) between ADMT and HYDKIN for equation type 1

$\sigma$ (cm <sup>2</sup> )		Plasma energy (eV)					
		1eV	205eV	409eV	613eV	817eV	1000eV
r_4005.t_11.0-7							
react 1	HYDKIN	0.00E+00	3.77E-16	2.51E-16	1.91E-16	1.55E-16	1.34E-16
	ADMT	0.00E+00	3.77E-16	2.51E-16	1.91E-16	1.55E-16	1.34E-16
react 2	HYDKIN	0.00E+00	3.68E-17	2.45E-17	1.86E-17	1.51E-17	1.30E-17
	ADMT	0.00E+00	3.68E-17	2.45E-17	1.86E-17	1.51E-17	1.30E-17
react 3	HYDKIN	0.00E+00	4.60E-17	3.06E-17	2.33E-17	1.89E-17	1.63E-17
	ADMT	0.00E+00	4.60E-17	3.06E-17	2.33E-17	1.89E-17	1.63E-17

Table A.3: Comparison of the cross sections (cm<sup>2</sup>) between ADMT and HYDKIN for equation type 8

$\sigma$ (cm <sup>2</sup> )		Plasma energy (eV)					
		1eV	205eV	409eV	613eV	817eV	1000eV
r_3966.t_6							
react 1 (a)	<i>HYDKIN</i>	<i>4.65E-15</i>	<i>2.79E-15</i>	<i>2.61E-15</i>	<i>2.50E-15</i>	<i>2.42E-15</i>	<i>2.37E-15</i>
	ADMT	4.65E-15	2.79E-15	2.61E-15	2.50E-15	2.42E-15	2.37E-15
react 2 (b)	<i>HYDKIN</i>	<i>9.20E-16</i>	<i>2.41E-22</i>	<i>3.03E-23</i>	<i>9.00E-24</i>	<i>3.80E-24</i>	<i>2.07E-24</i>
	ADMT	9.20E-16	2.41E-22	3.03E-23	9.00E-24	3.80E-24	2.07E-24
react 3 (a)	<i>HYDKIN</i>	<i>5.13E-15</i>	<i>3.08E-15</i>	<i>2.88E-15</i>	<i>2.77E-15</i>	<i>2.69E-15</i>	<i>2.64E-15</i>
	ADMT	5.13E-15	3.08E-15	2.88E-15	2.77E-15	2.69E-15	2.64E-15
r_4005.t_9							
react 1 (a)	<i>HYDKIN</i>	<i>2.12E-15</i>	<i>5.83E-16</i>	<i>7.45E-16</i>	<i>8.57E-16</i>	<i>9.42E-16</i>	<i>1.00E-15</i>
	ADMT	2.12E-15	5.83E-16	7.45E-16	8.57E-16	9.42E-16	1.00E-15
react 2 (b)	<i>HYDKIN</i>	<i>3.75E-17</i>	<i>4.58E-24</i>	<i>5.77E-25</i>	<i>1.71E-25</i>	<i>7.24E-26</i>	<i>3.94E-26</i>
	ADMT	3.75E-17	4.58E-24	5.77E-25	1.71E-25	7.24E-26	3.94E-26
react 3 (a)	<i>HYDKIN</i>	<i>4.72E-16</i>	<i>1.51E-16</i>	<i>2.48E-16</i>	<i>3.22E-16</i>	<i>3.82E-16</i>	<i>4.27E-16</i>
	ADMT	4.72E-16	1.51E-16	2.48E-16	3.22E-16	3.82E-16	4.27E-16
r_4005.t_16							
react 1 (a)	<i>HYDKIN</i>	<i>1.75E-15</i>	<i>7.51E-16</i>	<i>8.77E-16</i>	<i>9.50E-16</i>	<i>9.99E-16</i>	<i>1.03E-15</i>
	ADMT	1.75E-15	7.51E-16	8.77E-16	9.50E-16	9.99E-16	1.03E-15
react 2 (b)	<i>HYDKIN</i>	<i>1.69E-17</i>	<i>2.03E-24</i>	<i>2.55E-25</i>	<i>7.58E-26</i>	<i>3.20E-26</i>	<i>1.74E-26</i>
	ADMT	1.69E-17	2.03E-24	2.55E-25	7.58E-26	3.20E-26	1.74E-26
react 3 (b)	<i>HYDKIN</i>	<i>1.12E-17</i>	<i>1.35E-24</i>	<i>1.70E-25</i>	<i>5.05E-26</i>	<i>2.13E-26</i>	<i>1.16E-26</i>
	ADMT	1.12E-17	1.35E-24	1.70E-25	5.05E-26	2.13E-26	1.16E-26

Table A.4: Comparison of the cross sections (cm<sup>2</sup>) between ADMT and HYDKIN for equation type 5

$\sigma$ (cm <sup>2</sup> )		Plasma energy (eV)					
		1eV	205eV	409eV	613eV	817eV	1000eV
r_3966.t_5							
react 1	<i>HYDKIN</i>	<i>5.73E-17</i>	<i>3.78E-21</i>	<i>8.19E-22</i>	<i>3.32E-22</i>	<i>1.75E-22</i>	<i>1.11E-22</i>
	ADMT	5.73E-17	3.78E-21	8.19E-22	3.32E-22	1.75E-22	1.11E-22
react 2	<i>HYDKIN</i>	<i>2.45E-17</i>	<i>1.62E-21</i>	<i>3.51E-22</i>	<i>1.42E-22</i>	<i>7.48E-23</i>	<i>4.75E-23</i>
	ADMT	2.45E-17	1.62E-21	3.51E-22	1.42E-22	7.48E-23	4.75E-23
react 3	<i>HYDKIN</i>	<i>1.17E-16</i>	<i>7.75E-21</i>	<i>1.68E-21</i>	<i>6.80E-22</i>	<i>3.58E-22</i>	<i>2.27E-22</i>
	ADMT	1.17E-16	7.75E-21	1.68E-21	6.80E-22	3.58E-22	2.27E-22

Table A.5: Comparison of the cross sections (cm<sup>2</sup>) between ADMT and HYDKIN for equation type 6

$\sigma$ (cm <sup>2</sup> )		Plasma energy (eV)					
		1eV	205eV	409eV	613eV	817eV	1000eV
r_3966_t_2							
reac 1	<i>HYDKIN</i>	<i>0.00E+00</i>	<i>8.82E-17</i>	<i>5.50E-17</i>	<i>4.08E-17</i>	<i>3.28E-17</i>	<i>2.80E-17</i>
	ADMT	0.00E+00	8.82E-17	5.50E-17	4.08E-17	3.28E-17	2.80E-17
reac 2	<i>HYDKIN</i>	<i>0.00E+00</i>	<i>1.67E-17</i>	<i>1.04E-17</i>	<i>7.74E-18</i>	<i>6.21E-18</i>	<i>5.31E-18</i>
	ADMT	0.00E+00	1.67E-17	1.04E-17	7.74E-18	6.21E-18	5.31E-18
reac 3	<i>HYDKIN</i>	<i>0.00E+00</i>	<i>8.47E-18</i>	<i>5.29E-18</i>	<i>3.92E-18</i>	<i>3.15E-18</i>	<i>2.69E-18</i>
	ADMT	0.00E+00	8.47E-18	5.29E-18	3.92E-18	3.15E-18	2.69E-18
r_4005_t_5							
reac 1	<i>HYDKIN</i>	<i>0.00E+00</i>	<i>5.79E-17</i>	<i>3.68E-17</i>	<i>2.74E-17</i>	<i>2.21E-17</i>	<i>1.89E-17</i>
	ADMT	0.00E+00	5.79E-17	3.68E-17	2.74E-17	2.21E-17	1.89E-17
reac 2	<i>HYDKIN</i>	<i>0.00E+00</i>	<i>2.14E-17</i>	<i>1.36E-17</i>	<i>1.01E-17</i>	<i>8.17E-18</i>	<i>6.99E-18</i>
	ADMT	0.00E+00	2.14E-17	1.36E-17	1.01E-17	8.17E-18	6.99E-18
reac 3	<i>HYDKIN</i>	<i>0.00E+00</i>	<i>4.61E-17</i>	<i>2.89E-17</i>	<i>2.15E-17</i>	<i>1.73E-17</i>	<i>1.48E-17</i>
	ADMT	0.00E+00	4.61E-17	2.89E-17	2.15E-17	1.73E-17	1.48E-17
r_4005_t_12							
reac 1	<i>HYDKIN</i>	<i>0.00E+00</i>	<i>8.35E-17</i>	<i>5.29E-17</i>	<i>3.94E-17</i>	<i>3.17E-17</i>	<i>2.71E-17</i>
	ADMT	0.00E+00	8.35E-17	5.29E-17	3.94E-17	3.17E-17	2.71E-17
reac 2	<i>HYDKIN</i>	<i>0.00E+00</i>	<i>1.37E-17</i>	<i>8.68E-18</i>	<i>6.47E-18</i>	<i>5.21E-18</i>	<i>4.46E-18</i>
	ADMT	0.00E+00	1.37E-17	8.68E-18	6.47E-18	5.21E-18	4.46E-18
reac 3	<i>HYDKIN</i>	<i>0.00E+00</i>	<i>2.74E-17</i>	<i>1.74E-17</i>	<i>1.29E-17</i>	<i>1.04E-17</i>	<i>8.91E-18</i>
	ADMT	0.00E+00	2.74E-17	1.74E-17	1.29E-17	1.04E-17	8.91E-18

Table A.6: Comparison of the cross sections (cm<sup>2</sup>) between ADMT and HYDKIN for equation type 2

## A.3 Rate Coefficients

$\langle \sigma v \rangle$ (cm <sup>3</sup> /s)		Plasma temperature (eV)					
		1eV	205eV	409eV	613eV	817eV	1000eV
r_3966_t_7_3							
react 1	<i>HYDKIN</i>	<i>7.67E-14</i>	<i>8.88E-08</i>	<i>8.84E-08</i>	<i>8.51E-08</i>	<i>8.19E-08</i>	<i>7.93E-08</i>
	ADMT	7.67E-14	8.88E-08	8.84E-08	8.51E-08	8.19E-08	7.93E-08
react 2	<i>HYDKIN</i>	<i>2.05E-16</i>	<i>2.59E-08</i>	<i>2.56E-08</i>	<i>2.44E-08</i>	<i>2.33E-08</i>	<i>2.25E-08</i>
	ADMT	2.05E-16	2.59E-08	2.56E-08	2.44E-08	2.33E-08	2.25E-08
react 3	<i>HYDKIN</i>	<i>7.71E-18</i>	<i>8.17E-09</i>	<i>8.00E-09</i>	<i>7.50E-09</i>	<i>7.04E-09</i>	<i>6.69E-09</i>
	ADMT	7.71E-18	8.17E-09	8.00E-09	7.50E-09	7.04E-09	6.69E-09
r_4005_t_A1_1b							
react 1	<i>HYDKIN</i>	<i>2.08E-13</i>	<i>2.72E-07</i>	<i>2.64E-07</i>	<i>2.50E-07</i>	<i>2.38E-07</i>	<i>2.28E-07</i>
	ADMT	2.08E-13	2.72E-07	2.64E-07	2.50E-07	2.38E-07	2.28E-07
react 2	<i>HYDKIN</i>	<i>1.18E-16</i>	<i>2.29E-08</i>	<i>2.15E-08</i>	<i>1.99E-08</i>	<i>1.86E-08</i>	<i>1.76E-08</i>
	ADMT	1.18E-16	2.29E-08	2.15E-08	1.99E-08	1.86E-08	1.76E-08
react 3	<i>HYDKIN</i>	<i>5.76E-19</i>	<i>1.06E-08</i>	<i>9.93E-09</i>	<i>9.17E-09</i>	<i>8.55E-09</i>	<i>8.10E-09</i>
	ADMT	5.76E-19	1.06E-08	9.93E-09	9.17E-09	8.55E-09	8.10E-09
r_4005_t_A2_b_1							
react 1	<i>HYDKIN</i>	<i>6.68E-15</i>	<i>3.56E-08</i>	<i>3.77E-08</i>	<i>3.75E-08</i>	<i>3.69E-08</i>	<i>3.62E-08</i>
	ADMT	6.68E-15	3.56E-08	3.77E-08	3.75E-08	3.69E-08	3.62E-08
react 2	<i>HYDKIN</i>	<i>1.48E-15</i>	<i>2.80E-08</i>	<i>3.00E-08</i>	<i>3.01E-08</i>	<i>2.97E-08</i>	<i>2.93E-08</i>
	ADMT	1.48E-15	2.80E-08	3.00E-08	3.01E-08	2.97E-08	2.93E-08
react 4	<i>HYDKIN</i>	<i>2.90E-16</i>	<i>1.88E-08</i>	<i>1.97E-08</i>	<i>1.95E-08</i>	<i>1.91E-08</i>	<i>1.88E-08</i>
	ADMT	2.90E-16	1.88E-08	1.97E-08	1.95E-08	1.91E-08	1.88E-08

Table A.7: Comparison of the rate coefficients (cm<sup>3</sup>/s) between ADMT and HYDKIN for equation type 1

$\langle \sigma v \rangle$ (cm <sup>3</sup> /s)		Plasma temperature (eV)					
		1eV	205eV	409eV	613eV	817eV	1000eV
r_3966.t_6							
react 1 (a)	<i>Hydkin</i>	7.01E-09	6.00E-08	7.88E-08	9.22E-08	1.03E-07	1.11E-07
	ADMT	7.01E-09	6.00E-08	7.88E-08	9.22E-08	1.03E-07	1.11E-07
react 2 (b)	<i>Hydkin</i>	1.12E-09	1.32E-12	4.73E-13	2.59E-13	1.69E-13	1.25E-13
	ADMT	1.12E-09	1.32E-12	4.73E-13	2.59E-13	1.69E-13	1.25E-13
react 3 (a)	<i>Hydkin</i>	7.78E-09	6.63E-08	8.76E-08	1.03E-07	1.16E-07	1.25E-07
	ADMT	7.78E-09	6.63E-08	8.76E-08	1.03E-07	1.16E-07	1.25E-07
r_4005.t_9							
react 1 (a)	<i>Hydkin</i>	2.81E-09	1.57E-08	2.78E-08	3.84E-08	4.79E-08	5.57E-08
	ADMT	2.81E-09	1.57E-08	2.78E-08	3.84E-08	4.79E-08	5.57E-08
react 2 (b)	<i>Hydkin</i>	1.60E-10	9.25E-14	3.29E-14	1.80E-14	1.17E-14	8.63E-15
	ADMT	1.60E-10	9.25E-14	3.29E-14	1.80E-14	1.17E-14	8.63E-15
react 3 (a)	<i>Hydkin</i>	8.63E-15	5.09E-09	1.08E-08	1.62E-08	2.10E-08	2.49E-08
	ADMT	8.63E-15	5.09E-09	1.08E-08	1.62E-08	2.10E-08	2.49E-08
r_4005.t_16							
react 1 (a)	<i>Hydkin</i>	2.34E-09	1.86E-08	2.98E-08	3.85E-08	4.58E-08	5.13E-08
	ADMT	2.34E-09	1.86E-08	2.98E-08	3.85E-08	4.58E-08	5.13E-08
react 2 (b)	<i>Hydkin</i>	8.83E-11	4.82E-14	1.71E-14	9.35E-15	6.08E-15	4.49E-15
	ADMT	8.83E-11	4.82E-14	1.71E-14	9.35E-15	6.08E-15	4.49E-15
react 3 (b)	<i>Hydkin</i>	5.89E-11	3.21E-14	1.14E-14	6.24E-15	4.06E-15	2.99E-15
	ADMT	5.89E-11	3.21E-14	1.14E-14	6.24E-15	4.06E-15	2.99E-15

Table A.8: Comparison of the rate coefficients (cm<sup>3</sup>/s) for equation type 5 at a species energy E=0.1eV

$\langle \sigma v \rangle$ (cm <sup>3</sup> /s)		Plasma temperature (eV)					
		1eV	205eV	409eV	613eV	817eV	1000eV
r_4005.t_8							
react 1	<i>HYDKIN</i>	1.47E-08	2.16E-10	1.10E-10	7.40E-11	5.55E-11	4.53E-11
	ADMT	1.47E-08	2.16E-10	1.10E-10	7.40E-11	5.55E-11	4.53E-11
react 2	<i>HYDKIN</i>	3.01E-08	4.42E-10	2.26E-10	1.51E-10	1.14E-10	9.27E-11
	ADMT	3.01E-08	4.42E-10	2.26E-10	1.51E-10	1.14E-10	9.27E-11
react 3	<i>HYDKIN</i>	5.32E-09	7.81E-11	3.99E-11	2.67E-11	2.00E-11	1.64E-11
	ADMT	5.32E-09	7.81E-11	3.99E-11	2.67E-11	2.00E-11	1.64E-11
r_4005.t_15							
react 1	<i>HYDKIN</i>	2.20E-08	3.24E-10	1.65E-10	1.11E-10	8.31E-11	6.78E-11
	ADMT	2.20E-08	3.24E-10	1.65E-10	1.11E-10	8.31E-11	6.78E-11
react 2	<i>HYDKIN</i>	4.65E-08	6.82E-10	3.48E-10	2.33E-10	1.75E-10	1.43E-10
	ADMT	4.65E-08	6.82E-10	3.48E-10	2.33E-10	1.75E-10	1.43E-10
react 3	<i>HYDKIN</i>	9.29E-09	1.36E-10	6.97E-11	4.67E-11	3.50E-11	2.86E-11
	ADMT	9.29E-09	1.36E-10	6.97E-11	4.67E-11	3.50E-11	2.86E-11

Table A.9: Comparison of the rate coefficients (cm<sup>3</sup>/s) between ADMT and HYDKIN for equation type 7

## Appendix B

# Solution methods and stiffness

### B.1 Numerical solution methods for a system of differential equation

#### Forward Euler Method

$$\frac{\partial \vec{\psi}}{\partial t} = \frac{\vec{\psi}^{n+1} - \vec{\psi}^n}{\Delta t} = \vec{F}(\vec{\psi}^n, t^n) \quad \vec{\psi}^{n+1} = \vec{\psi}^n + \Delta t \vec{F}(\vec{\psi}^n, t^n)$$

where  $t^n = n\Delta t$ . This equation is easily evaluated to get  $\vec{\psi}^{n+1}$ .

#### Backward Euler Method

$$\frac{\partial \vec{\psi}}{\partial t} = \frac{\vec{\psi}^{n+1} - \vec{\psi}^n}{\Delta t} = \vec{F}(\vec{\psi}^{n+1}, t^{n+1}) \quad \vec{\psi}^{n+1} - \Delta t \vec{F}(\vec{\psi}^{n+1}, t^{n+1}) = \vec{\psi}^n$$

where  $t^{n+1} = (n+1)\Delta t$ . This equation can not be simply evaluated to get  $\vec{\psi}^{n+1}$ .

### B.2 Stiffness

The discussion of the stiffness presented below is based on a script of P.Sajda SAJDA (2001). Sajda characterizes the stiffness as follows:

- Stiffness measures the difficulty of numerically solving a system of ODE's
- Stiff systems are characterized by disparate time scales e.g. for a system with two time scales of duration  $g$  and  $t$  with  $g \gg t$ , a  $\Delta t$  small enough to resolve matters on the  $t$  time scale will take  $g/t$  steps to resolve matters on the  $g$  time scale
- This is OK if you are interested in matters on the slow time scale, but otherwise one would like  $\Delta t$  to be closer to  $g$  but to do so using explicit numerical methods will cause catastrophic instabilities due to oscillations resulting from the faster component of the system
- Stiff systems require implicit solution methods

The influence of the stiffness can best be illustrated by an example of a 1-dimensional system ( $\vec{\psi} = \psi_1$ ):

$$\frac{\partial \psi_1}{\partial t} = \lambda_1 \psi_1 \quad \Rightarrow \quad \psi_1(t) = \psi_1(0) \exp(\lambda_1 t)$$

The analytic solution demonstrates monotonic, exponential decay from  $\psi_1(0)$  to zero for  $\lambda_1 < 0$ . Solving this system numerically with a forward Euler method (see section B.1) only shows the same behavior if:

$$0 < \psi_1^{n+1} < \psi_1^n \quad \Rightarrow \quad 0 < 1 + \lambda_1 \Delta t < 1 \quad \Rightarrow \quad 0 < \Delta t < \frac{-1}{\lambda_1}$$

with  $\lambda_1 < 0$ . If  $|\lambda_1|$  is big, the forward Euler method is only stable for a very small time step. In contrast, the backward Euler method (see section B.1) does not restrict the choice of the time step:

$$0 < \psi_1^{n+1} < \psi_1^n \quad \Rightarrow \quad 0 < \frac{1}{1 - \lambda_1 \Delta t} < 1$$

with  $\lambda_1 < 0$  and  $\Delta t > 0$  this equation is fulfilled.

Higher order homogenous systems, with dimension  $n$  have an analytical solution based on the eigenvalues ( $\lambda_i$ ) and the corresponding eigenvectors  $\vec{u}_i$  of the Jacobian of the system:

$$\vec{\psi}(t) = a_1 \vec{u}_1 \exp \lambda_1 t + a_2 \vec{u}_2 \exp \lambda_2 t + \dots + a_n \vec{u}_n \exp \lambda_n t$$

with  $\vec{a} = (a_1, \dots, a_n)^T$  being the coefficients that assure a correct initial condition. In this solution, the terms that have a big negative eigenvalue will quickly stop influencing the solution as their decay to zero is much faster than the terms with small negative eigenvalues.

In a forward Euler method, the time step is limited by the most negative eigenvalue ( $\Delta t > \frac{-1}{\lambda_{big}}$ ). If small eigenvalues are present, this leads to using a very small time step to calculate the solution in a long range of time, which is not efficient at all.

As the backward Euler method does not limit the time step, the time step can be based on the slower, but more important processes. This will lead to an inaccurate decay of the fast processes, but the overall error of the solution will be small. Compared to the forward Euler method, the backward however has the disadvantage to be slow.

If the eigenvalues of the Jacobian of a system are ordered in a descending way, the local stiffness of an  $n$  dimensional system can be defined as:

$$\text{Stiffness} \sim \frac{\lambda_n}{\lambda_1}$$